Fluxes of Energy and Carbon Dioxide Over a Suburban Area of Vancouver, BC

by

Cindy Jennifer Walsh

B.Sc., Simon Fraser University, 2001

A THESIS SUBMITTED IN PARTIAL FULFILLMENT OF
THE REQUIREMENTS FOR THE DEGREE OF

MASTER OF SCIENCE
in

THE FACULTY OF GRADUATE STUDIES
(Geography)

UNIVERSITY OF BRITISH COLUMBIA
December 2005

Abstract

In this study, a relatively long-term (August 2001 - December 2002) measurement campaign of radiation, energy and atmospheric CO_2 fluxes was conducted in a fairly homogeneous suburb of Vancouver, British Columbia (Sunset site).

Examination of radiative flux densities revealed that the incoming and outgoing short and longwave radiation followed expected patterns throughout the year, and at the diurnal time scale. Energy fluxes demonstrated more complex patterns. Sensible heat dominated throughout the year. Latent heat was lower than expected. The reasons for this are difficult to determine with confidence but are thought to be at least partially related to low data coverage during the winter. The Sunset site has also become more built over the years with natural surfaces transformed into impervious surfaces that more readily accept heat. The role of heat storage played an important role in the energy balance at the diurnal time scale.

The annual pattern of CO_2 followed expected seasonal trends, with the lowest concentrations recorded in the summer corresponding to the peak in photosynthesis. Diurnal trends of CO_2 concentrations appear to be at least partly linked to the pattern of fossil fuel consumption. A characteristic peak in concentrations at the diurnal time scale was seen in the morning that coincided with the morning rush hour. The pattern of CO_2 fluxes proved more difficult to interpret. Examination of annual CO_2 flux patterns revealed few negative fluxes indicating that the site was a source for CO_2 for most of the year. The diurnal pattern of CO_2 fluxes closely resembled patterns observed in other urban areas, but of particular interest at the Sunset site was an apparent relationship between wind direction and flux strength. Throughout the year, when the wind was coming from the direction of a nearby busy intersection, fluxes were higher than when the wind was coming from all other directions. This indicates that fluxes may not be well mixed at the sensor height. This directional bias was not observed in the fluxes of heat or water vapour indicating that there may be significant spatial differences in the sources of CO_2 and/or an inequality in the transfer efficiencies of different entities.

Table of Contents

List of Tables

List of Figures

List of Acronyms

BL	– Boundary layer
BOREAS	– Boreal Ecosystem Atmosphere Study
CO_2	– Carbon dioxide
GHG	– Greenhouse gas
GVRD	– Greater Vancouver Regional District
H_2O	– Water
IPCC	– International Panel on Climate Change
ISL	– Inertial sublayer
IU	– Indiana University
LAT	– Local Apparent Time
LI-7500	– Li-cor 7500 infrared gas analyzer
NOAA	– National Oceanic and Atmospheric Administration
PAR	– Photosynthetically active radiation
PBL	– Planetary boundary layer
PST	– Pacific Standard Time
RH	– Relative humidity
RSL	– Roughness sublayer
UBL	– Urban boundary layer
UCL	– Urban canopy layer
UCZ	– Urban climate zone
YD	– Year day

List of Symbols

α	– albedo (dimensionless)
ε	– emissivity of the atmosphere (dimensionless)
ε_o	– emissivity of the surface (dimensionless)
λ_F	– frontal area index (dimensionless)
λ_S	– canyon aspect ratio (dimensionless)
σ	– Stefan Boltzmann proportionality constant (5.67×10^{-8} W m^{-2} K^{-4})
ρ	– density of air (kg m^{-3})
a	– downwind edge of the source area (m)
A_C	– surface area (%)
A_I	– plan area of impervious ground (%)
A_P	– total plan area (%)
A_R	– plan area of roofs (%)
A_V	– plan area vegetated (%)
A_W	– surface area of walls (%)
c	– carbon dioxide mixing ratio (µmol mol^{-1})
c_p	– specific heat of air at constant pressure (J kg^{-1} K^{-1})
d	– lateral half dimension of the source area (m)
d	– zero plane displacement length (m)
E	– height tower is recessed below surrounding terrain (m)
F	– radiometer view factor (%)

K↓	– incoming shortwave radiation flux density (W m^{-2})
K↑	– reflected shortwave radiation flux density (W m^{-2})
L↓	– incoming longwave radiation flux density (W m^{-2})
L↑	– emitted and reflected longwave radiation flux density (W m^{-2})
q	– specific humidity (g kg^{-1})
Q*	– net all-wave radiation flux density (W m^{-2})
Q_E	– latent heat flux density (W m^{-2})
Q_F	– anthropogenic heat flux density (W m^{-2})
Q_H	– sensible heat flux density (W m^{-2})
ΔQ_S	– net heat flux density stored in urban materials (W m^{-2})
ΔQ_A	– net horizontal heat advection (W m^{-2})
r	– radius of the circular radiative source area surface disc (m)
T	– air temperature (K)
T_a	– atmospheric temperature (K)
T_o	– surface temperature (K)
u	– horizontal wind velocity (m s^{-1})
v	– crosswind wind velocity (m s^{-1})
w	– vertical wind velocity (m s^{-1})
x_m	– maximum source location (m)
z	– instrument height above ground level (m)
z'	– effective instrument height (m)
z_o	– aerodynamic roughness length (m)

List of Units

μm	– micrometers
μmol	– micromole
g	– grams
Gt	– gigatons
Hz	– Hertz
J	– Joules
K	– Kelvin
kg	– kilogram
m	– meters
ppm	– parts per million
ppmv	– parts per million (volume)
s	– seconds
yr	– year
W	– Watt

Acknowledgements

I would like to thank my supervisor, Tim Oke, for his support, kind words and encouragement through this process. He provided an exciting environment, and many opportunities, which I feel privileged to have been involved with. I would also like to sincerely thank the members of the Oke lab whose support and entertainment were priceless. Sarah Roberts, Andres Soux, Trevor Newton, and Geoff Doerksen – I learned a lot about both science and life from you. I'll never forget the months and years that we all spent in the Oke Instrumentation Museum debating the finer points of life.

I'd also like to extend special thanks to Sue Grimmond. Without Sue's involvement this project would have been difficult to complete. I would like to thank both Sue and Brian Offerle for assisting with the data acquisition and processing throughout the project. Additional thanks are extended to Jenny Salmond who pushed me and believed in me, and taught me the finer details of how to dangle off a tower without losing the instrument in my hand. I would also like to thank the Marseille crew from whom I was introduced to Urban Climatology and urban fieldwork. Pheobe, Sarah and Jenny it was a memorable experience. Thanks are also extended to the UBC Biomet lab and Elyn Humphries for providing not only lab resources but also a wealth of knowledge. Andy Black was also an inspiration both in teaching and research and I appreciate his support and assistance.

I appreciate the financial support of the Natural Science and Engineering Research Council of Canada (NSERC), the Canadian Foundation for Climate and Atmospheric Sciences (CFCAS), and University of British Columbia research and teaching assistantships.

Additional thanks are extended to Bill Bailey who was originally responsible for setting me on this path. Throughout this process I was lucky to have my family close by and I am very grateful for their unwavering support. I would like to extend special thanks to Kertis Heidt who was there from the beginning and will be there long past the end. I could not have gone through this process without him. Dustin, Angela, Keegan and, I can't forget, Blue and Toader all provided a welcome and sometimes necessary escape. I am especially grateful to David Guamont-Guay for inspiring me to finish and for bringing energy and excitement back into the scientific process. I thank him for being such a wonderful support and positive addition to my life.

1 LITERATURE REVIEW

1.1 Introduction

As the proportion of the population living in urban areas grows, and as urbanized areas expand, natural surfaces are transformed into housing developments, commercial districts and roadways. The replacement of natural surfaces with impermeable surfaces such as asphalt and concrete often has a measurable effect on the surrounding atmosphere, which can lead to the creation of a distinct urban climate. Unique urban climate effects arise from differences in the exchanges of heat, mass and momentum between the urbanized and the pre-existing landscape. A few well-documented features of these climate effects include the urban heat island, urban induced wind effects, increased precipitation downwind of urban areas, and air pollution. This study focuses on the radiation budget, energy balance and carbon dioxide exchange over a suburban region of a mid-latitude city in North America. Examination of the fluxes of radiation, energy and carbon dioxide reveals important information on the exchanges of heat, mass, and momentum over urbanized landscapes.

Chapter 1 of this thesis reviews the theory of the radiation balance and the energy budget, as well as the role of carbon dioxide in global and urban atmospheres. Chapter 2 explores issues surrounding the measurement of climatic variables in complex urban environments and documents the instrumentation used in the collection of the radiation, energy and carbon dioxide data for this study. Chapter 3 focuses on the presentation and discussion of diurnal and annual trends in the observed data.

1.2 Surface radiation budget

1.2.1 Theory

The surface radiation budget reveals the partitioning of radiant energy into its short- and longwave components and helps to characterize the climatology of the measurement site. The budget is given by the combined net all-wave radiation term, Q* which is equal to the algebraic sum of the shortwave and longwave components:

$$Q^* = (K\downarrow - K\uparrow) + (L\downarrow - L\uparrow) \qquad (\mathrm{W\,m^{-2}}) \qquad [1.1]$$

where K↓ is the incoming shortwave radiation flux density, K↑ is the reflected incoming shortwave radiation flux density, L↓ is the incoming longwave radiation flux density, and L↑ is the emitted and reflected longwave radiation flux density. Shortwave radiation has wavelengths ranging from 0.15 to 3.0 μm, whereas longwave radiation consists of wavelengths between 3.0 to 100 μm (Oke, 1987).

Shortwave radiation is essentially energy from sunlight. K↓ is affected by the angle of incidence of solar radiation, which depends on the time of year, latitude, and time of day. It is also affected by the presence of clouds, pollution or other particulates in the atmosphere, which effectively reflect, scatter or absorb solar radiation, reducing the amount of direct solar radiation that reaches Earth's surface.

$K\uparrow$ depends on the amount of incident energy ($K\downarrow$), and upon the surface reflectivity, which integrated across the solar spectrum is called the albedo (α), given by:

$$\alpha = K\uparrow / K\downarrow \qquad (\mathrm{W\ m^{-2}}) \qquad [1.2]$$

where $K\uparrow$ is the reflected shortwave radition and $K\downarrow$ is the incoming solar radiation. α is largely related to the color of the surface, with lighter colored surfaces having a higher albedo. A typical value for the integrated α of a suburban area is about 15% (Oke, 1988). In urban areas, the most reflective surfaces are those painted white, light colored tiles and bricks, and light colored concrete. These surfaces may reflect up to 40% of the incoming solar radiation, whereas, dark colored surfaces such as asphalt, and dark painted surfaces may only reflect <20% of incoming solar radiation (Oke, 1987).

$L\downarrow$ is the infrared energy emitted by the atmosphere and clouds and received at the Earth's surface. The amount of $L\downarrow$ emitted is determined by:

$$L\downarrow = \varepsilon\sigma T_a^{\ 4} \qquad (\mathrm{W\ m^{-2}}) \qquad [1.3]$$

where σ is the Stefan-Boltzmann proportionality constant (5.67×10^{-8} W m^{-2} K^{-4}), and T_a is the temperature of the sky (in Kelvin). The warmer the atmosphere and the larger the emissivity of the atmosphere (ε), the more longwave radiation emitted. ε increases with the concentration of radiatively active gases such as water vapour, carbon dioxide, ozone, methane, and chloro-fluoro-carbons and aerosols.

$L\uparrow$ is the outgoing infrared energy from the Earth's surface, and its magnitude is determined by:

$$L\uparrow = \varepsilon_0 \sigma T_0^4 + (1 - \varepsilon_0) L\downarrow \qquad (\mathrm{W\ m^{-2}}) \qquad [1.4]$$

where ε_0 is the surface emissivity, and T_0 is the surface temperature (in Kelvin). The $\varepsilon_0 \sigma T_0^4$ portion accounts for the longwave emission from the surface and the $(1 - \varepsilon_0)$ term accounts for the small amount of reflected $L\downarrow$.

1.2.2 Changes in the radiation balance as a result of anthropogenic modifications

All components of the surface radiation balance are somewhat altered or influenced by properties of urban surfaces or the surrounding atmosphere (Oke, 1987). $K\downarrow$ is reduced due to pollution in the atmosphere. Particulate matter acts to reflect, absorb and scatter shortwave radiation, reducing the amount received by the surface. $K\uparrow$ is also reduced because the urban surface albedo is generally lower than that of natural surfaces. This is due to trapping of radiation by multiple reflection in the urban canopy layer and the generally darker surfaces absorbing more shortwave radiation than rural surfaces. In contrast $L\downarrow$ is increased because of the air pollution and the warmer urban boundary layer (the heat island). $L\uparrow$ is also greater due to the warmer urban surfaces of the heat island.

1.3 Surface energy balance

1.3.1 Theory

The surface energy balance provides the driving force behind the vertical transfer of heat, momentum and mass and is fundamental to understanding the climatology of any meteorological site (Oke, 1987). In particular the partitioning of available energy into the turbulent fluxes of sensible and latent heat is critical to the determination of the thermal structure and hence the atmospheric stability and depth of the urban mixing layer. In addition, energy balance observations are used to evaluate numerical models which are designed to include a range of meteorological conditions to correctly represent 'real world' conditions.

The surface energy balance of an urban area, expressed as spatially-averaged fluxes at the top of an urban 'box' at the base of the urban boundary layer (Figure 1 - 1) is given by:

$$Q^* + Q_F = Q_H + Q_E + \Delta Q_S + \Delta Q_A \qquad (\mathrm{W\ m^{-2}}) \qquad [1.5]$$

where Q^* is the net all-wave radiation; Q_F, the anthropogenic heat flux density due to combustion; Q_H, the turbulent sensible heat flux density; Q_E, the turbulent latent heat flux density; ΔQ_S, the net heat flux density stored in urban materials; and ΔQ_A, the net horizontal heat advection.

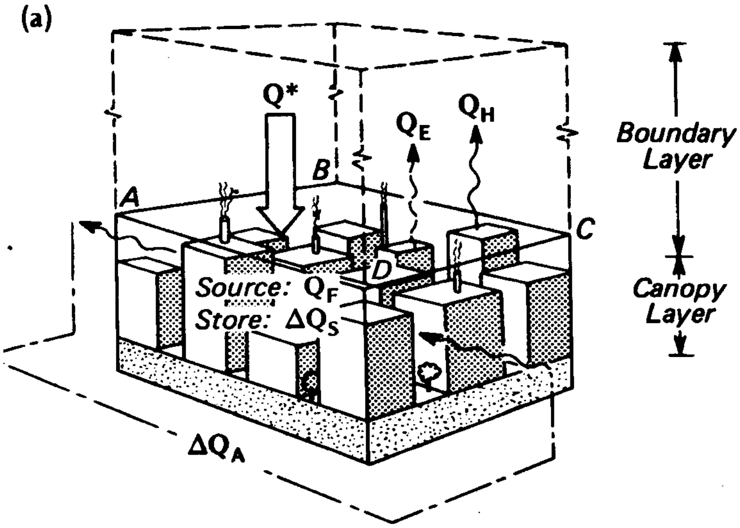

Figure 1 - 1 Box model of energy balance components (Oke, 1987).

1.3.1.1 Net radiation

Q*, first presented in Equation 1.1, is not only the end result of the surface radiation budget, but is also an important component of the surface energy balance. When Q* is positive, a net gain in radiative energy at the surface has been achieved, and when it is negative there has been a net loss. Q* is either measured as the sum of the individual fluxes, where K↓, K↑, L↓, and L↑ are measured using upward and downward facing pyranometers and pyrgeometers, respectively, or collectively using a net pyrradiometer.

1.3.1.2 Anthropogenic heat

Q_F is mainly a result of fossil fuel combustion. In a suburban area, it comes from all individual residences but most is expected to come from heat released by vehicles on main roads and large energy users, such as strip malls (Grimmond, 1992). Q_F is considered a function of population density and per capita energy use. The magnitude of Q_F is controlled by the human activity cycle and is not directly influenced by atmospheric or solar influences (Oke, 1987). At the diurnal time scale, vehicular, building, and metabolic inputs to the Q_F flux follow courses like those in Figure 1 - 2. Seasonal differences in Q_F are expected due to increased energy demands (heating) in the winter.

Until recently, analysis of the urban energy balance assumed that energy entering the urban 'box' as Q_F was sensed by instrumentation as either Q^*, Q_H or Q_E. Q_F has typically been incorporated as a portion of ΔQ_S. Recent discussions (e.g. Grimmond *et al.*, 2004) indicate a separate estimation of Q_F should be included, and that when it is, a more accurate ΔQ_S term results. In order to attain a detailed estimation of the annual and daily variations of Q_F inventory data and/or models would be needed, but for the most part, since fine resolution is not the focus, a constant estimation of Q_F is often adopted based on the residual term of the energy balance (Christen and Vogt, 2004).

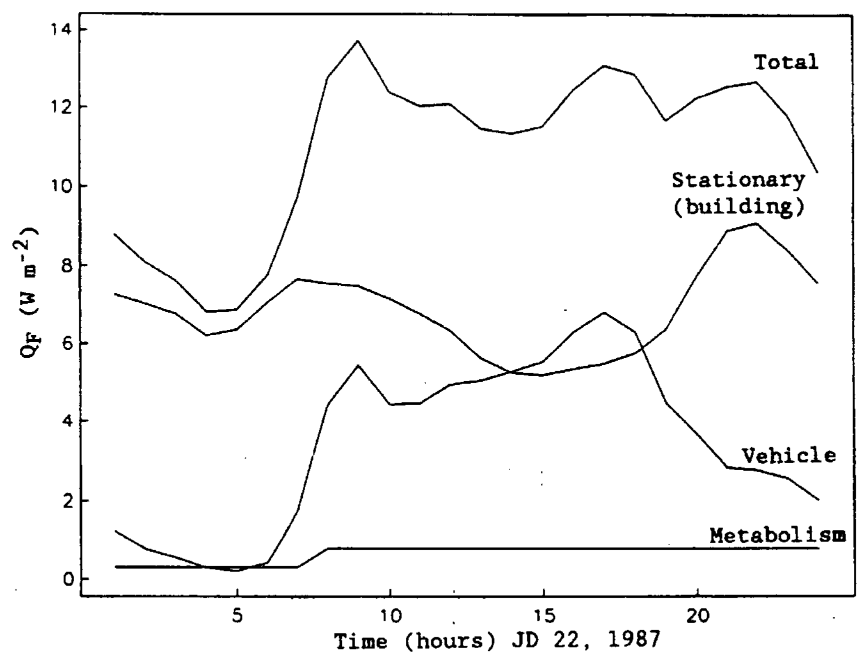

Figure 1 - 2 Anthropogenic heat flux (Q_F) for 1987, year day (YD) 22, with the three components (building, vehicle, and metabolism) and the total hourly flux (Grimmond, 1988).

1.3.1.3 Sensible and latent heat

Q_H is the energy that can be sensed, whereas Q_E is the energy released or absorbed by a system due to changes of phase (e.g. as water evaporates, or condenses). Q_H is transferred by turbulent eddies and the direction of the transfer (upward, positive; downward, negative) is determined by the vertical temperature gradient; where a positive temperature gradient (or inversion) means a transfer of heat towards the surface and visa versa (Oke, 1987). Over open country, in rural areas, Q_H is usually away from the surface during the day and towards it during the night.

The flux of Q_E determines the exchange of water between the surface and the atmosphere. This flux of water is primarily upward, as water is continually evaporated and transpired from the surface. Highest positive Q_E fluxes occur during the day. Sometimes, usually at night, negative fluxes return water to the surface in the form of dew.

Modern field projects measure Q_H and Q_E using eddy covariance techniques. Details of the eddy covariance technique are presented in Chapter 2. Errors in the eddy covariance methodology have been outlined and widely documented by Twine *et al.* (2000), Baldocchi *et al.* (2001), Meyers (2001), and include a possible underestimation of Q_H and Q_E, and insufficient energy balance closure for vegetated land surfaces.

1.3.1.4 Heat storage

ΔQ_S in the materials of the urban 'box' are difficult to measure directly due to the great variety of building and surface materials, and due to the three-dimensionality of the urban surface. Energy is readily accepted by urban surfaces during the day, stored, and released later at night. Heat flux plates can be installed to measure to conductive heat exchange for a given surface, but it is not possible to determine the heat exchanged by all surface fabrics and all surface aspects within the urban system. Therefore, ΔQ_S is usually determined by:

$$\Delta Q_S = Q^* + Q_F - (Q_H + Q_E) \qquad (\mathrm{W\ m^{-2}}) \qquad [1.6]$$

where ΔQ_S is the residual resulting from the from direct measurements of net radiation (Q^*), sensible heat (Q_H) and latent heat (Q_E), and calculated or modelled values of anthropogenic heat (Q_F).

A weakness of this method is that the error terms from other energy balance components are compounded into the residual term. Such errors include normal instrument and measurement errors plus those introduced by the spatial heterogeneity of the surface and the corresponding turbulent source areas (which are sensitive to wind direction, stability, and surface roughness) (Schmid *et al.,* 1991). Additional errors are introduced into ΔQ_S because errors in the estimation of the Q_F flux are included.

1.3.1.5 Heat advection

ΔQ_A depends on the direction of the regional flow, the heterogeneity of the surface and the distance of the measurement from contrasting surfaces (Grimmond and Oke, 1999a). Advection becomes a concern when surfaces of anomalous composition are closely proximate. It is difficult to determine the exact magnitude of ΔQ_A. A study from Marseille, France, indicates that horizontal moisture and heat flux advection are of similar magnitude but of opposite sign, so that they cancel out (Grimmond *et al.,* 2004). Another study in Vancouver, at the Sunset site, stated that ΔQ_A may play a small role at different times of the day, or year, but that overall this term averages to zero (Steyn, 1985).

1.3.2 Changes in the energy balance as a result of anthropogenic modifications

A particularly important difference in the surface energy balance of natural surfaces and anthropogenically-modified systems occurs following rainfall events. In a natural system moisture percolates into the ground and the surface is able to remain moist after rainfall until evaporation, natural ground drainage, or transpiration by vegetation removes the precipitation. In contrast, urban surfaces are designed to quickly channel water off surfaces such as roofs, sidewalks, and roadways and into sewers and storm drains. Even the natural drainage of backyards and parks is altered and they are designed to eliminate pooling and to facilitate drainage. As a result, water is effectively removed from the urban surface and does not remain available for evaporation. Following rainfall water on impervious surfaces is quickly evaporated causing much faster drying of urban systems compared to their rural counterparts. The urban system is limited by water availability and hence Q_E is often reduced in urban compared to rural areas (Oke, 1987).

In contrast to Q_E, Q_H is expected to be higher in a city than its countryside because of the dryness and the roughness of the urban system. ΔQ_S is a dominant term in the surface energy balance of urban areas whereas it is the smallest term in rural areas (Oke, 1987). It is expected that ΔQ_S in urban areas is greater than its rural counterpart due to the thermal conductivity and heat capacity of urban surface fabrics, and the increased surface area presented by a crenellated surface. Additionally, the materials and geometric configuration of the urban canopy layer give it large thermal inertia. Heat is readily accepted and stored in urban fabrics during the daytime and then after sunset the heat is released back into the urban atmosphere. Overall, we expect higher Q_H and lower Q_E fluxes, and a more dominant ΔQ_S term in the urban environment.

When considering seasonal variations, an urban environment changes little throughout the year because structures are permanent and the surface itself is often covered with impervious surface fabrics. This often results in less seasonal variations in energy balance components when compared to natural surfaces at the same latitude (Oke, 1987). Natural surfaces often experience greater changes in surface characteristics throughout the year, leading to greater variations in the surface energy balance. Take a deciduous forest, for example, significant changes in the appearance and the structure of this system resulting from the presence or absence of leaves creates variations in the surface energy balance throughout the year.

1.4 Carbon dioxide

Carbon dioxide (CO_2) is a 'greenhouse gas' (GHG) absorbing wavelengths of radiation in the ranges of 2.5-3.0 μm, 4-5 μm and greater than 15 μm. This absorption of radiation in the atmosphere leads to increases in air temperature. On a molecular basis CO_2 is not as effective an absorber of radiation as other GHG's such as methane, but deforestation and the large anthropogenic contribution of CO_2 to the atmosphere make it the leading contributor to climate change (Rodhe, 1990). Currently, CO_2 is thought to contribute up to half of the total greenhouse effect of Earth's atmosphere (Rodhe, 1990).

Over the next 50 to 100 years the global concentration of atmospheric CO_2 is expected to double, leading to a 1.5-4.5 degree Celsius warming of the planet (Houghton *et al.,* 1992). As the global population grows the potential for climate change resulting from GHG accumulation in the atmosphere is becoming increasingly important. As less developed countries become more industrialized, the number of people residing in urban areas is expected to double over the next twenty-five years, raising the percentage of the global population living in urban areas from 48% in 2000, to 58% of the total population by 2025. Currently, in Canada, 77% of the population already resides in urban environments and by 2025 this percentage is expected to rise to approximately 82% (World Resources, 1996). These population trends indicate that natural resources will be increasingly and disproportionately consumed in urban regions, resulting in concentrated fossil fuel combustion and therefore high carbon dioxide emissions. Due to the large potential for cities to produce CO_2, urban areas present an increasingly valuable research laboratory.

1.4.1 Global context of carbon dioxide

Exchanges that occur between active surface pools of carbon in the terrestrial biosphere, ocean and atmosphere are illustrated in Figure 1 - 3. The large fluxes of CO_2 between these systems are key to understanding the relationship between emissions of CO_2 and its atmospheric levels (Schimel, 1998). As the relatively large store of fossil fuels is consumed, CO_2 will be released into the atmosphere, increasing the atmospheric content. Weil *et al.,* (1998) note that anthropogenic emissions are responsible for a large proportion of the increase in atmospheric CO_2. Urban areas have a large potential to produce this anthropogenic source of carbon, and are therefore of great interest when considering the global carbon budget.

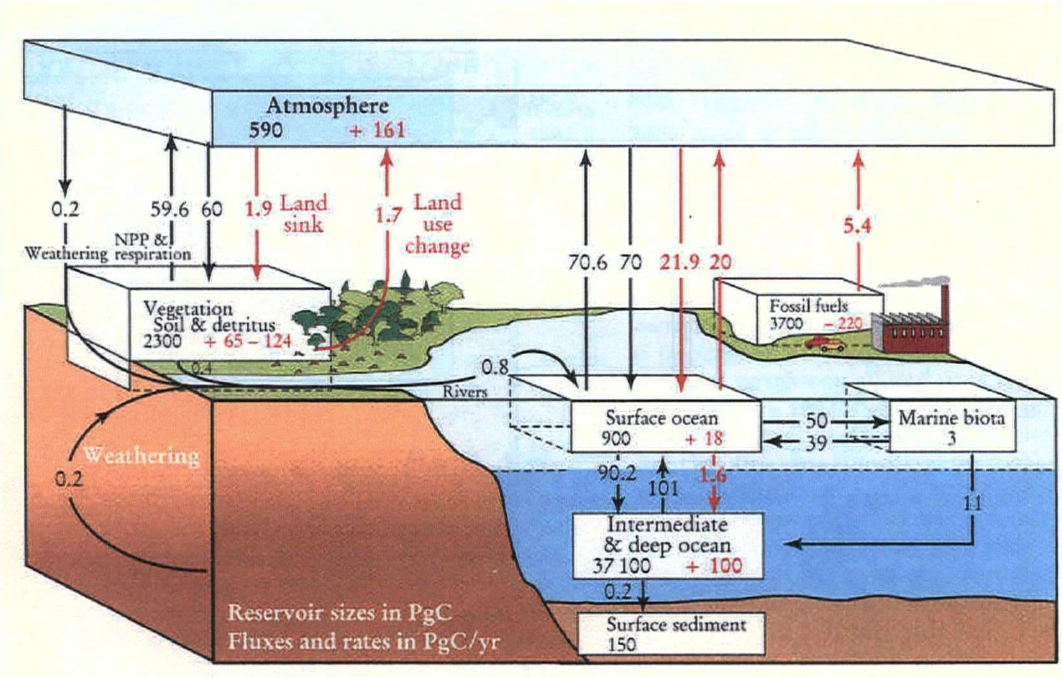

Figure 1 - 3 The global carbon cycle. Anthropogenic fluxes are red, natural are black. Arrows indicate the flux between the atmosphere and the two major sinks, land and ocean. Net fluxes are balanced for natural, but not anthropogenic sources. Black numbers indicate pre-industrial levels, whereas the red numbers represent the change due to anthropogenic influences since that time. The first red number in the land sink box represents an inferred sink value, whereas the second red number represents decreases in the land sink due to deforestation. NPP is the net primary production. (Sarmiento and Gruber, 2002).

Before the Industrial Revolution (approximately 1850) the global carbon budget was considered "in balance" or in a "steady state" indicating that sources were in balance with sinks resulting in no excess accumulation of CO_2 in any of the systems: terrestrial, ocean or atmosphere. Since the Industrial Revolution fossil fuels have been the primary source of power to run industry, and, as a result atmospheric CO_2 concentrations (a waste product resulting from the burning of fossil fuels) have been increasing rapidly (Figure 1 - 4). This dramatic rise indicates that carbon sinks, such as the terrestrial biosphere or the ocean, for example, are not strong enough to offset the excess CO_2 produced by fossil fuel combustion. To this day fossil fuels remain the primary source of fuel to power our vehicles, industries and businesses, and hence, atmospheric CO_2 concentrations continue to rise.

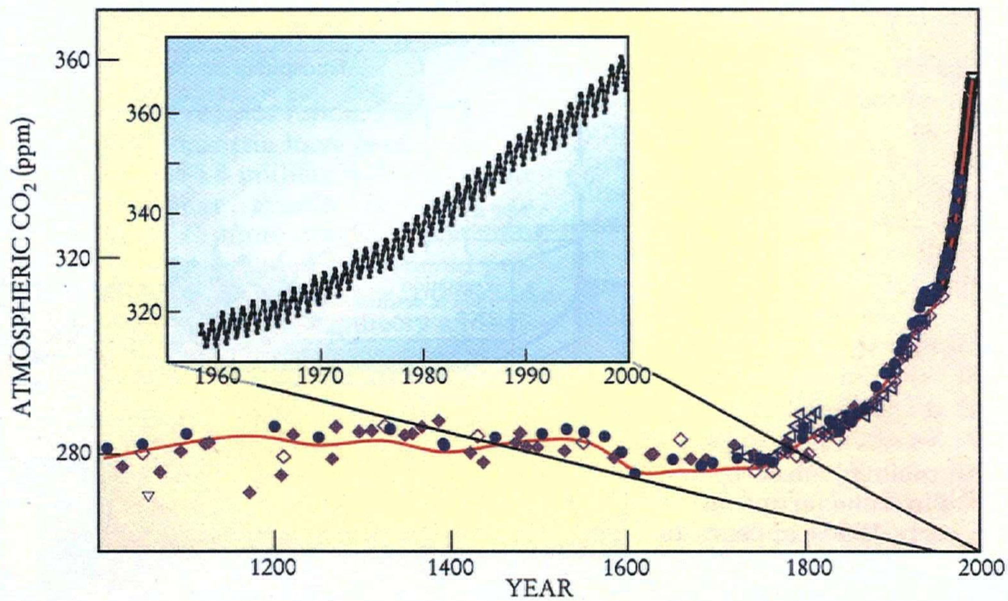

Figure 1 - 4 Increase in atmospheric CO_2 since the Industrial Revolution. Seasonal variations reflect the strong influence of the terrestrial biosphere in the Northern Hemisphere, which sequesters CO_2 during the spring and summer creating an annual oscillation in global CO_2 concentrations (Sarmiento and Gruber, 2002), (see also Figure 1 – 5).

1.4.1.1 The role of terrestrial systems

Terrestrial systems are inherently linked to atmospheric CO_2 levels. As terrestrial systems take up CO_2, atmospheric levels decline, in contrast, if terrestrial ecosystems emit CO_2, atmospheric levels rise. During the growing season, atmospheric CO_2 levels decline as terrestrial ecosystems sequester, or take in, CO_2 through the process of photosynthesis. During the winter months photosynthesis is reduced or absent in many parts of the mid- and northern latitudes resulting in reduced terrestrial CO_2 sequestration, and hence increased atmospheric CO_2. The seasonal and latitudinal patterns of CO_2 are seen in Figure 1 - 5. Seasonal differences in CO_2 concentrations are more pronounced in the northern latitudes.

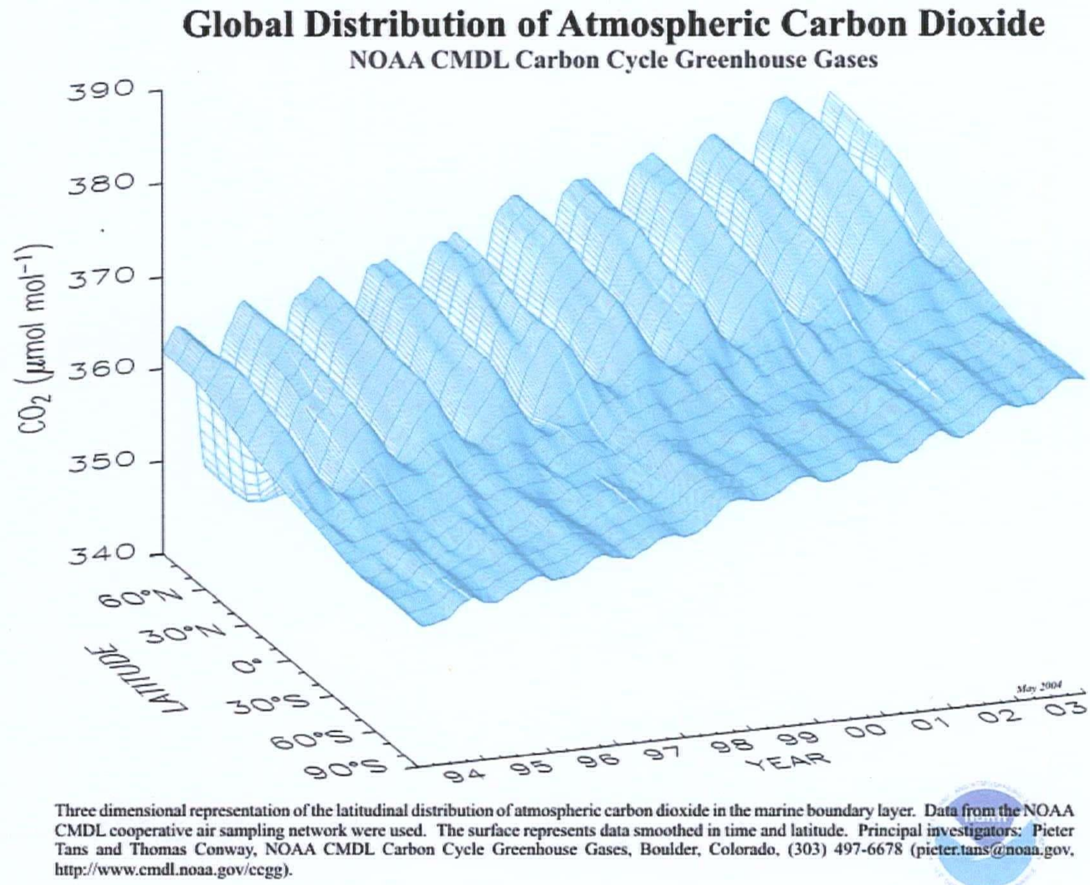

Figure 1 - 5 Spatial and temporal variability of global atmospheric CO_2 concentrations. Peaks and troughs are due to seasonal variations in global atmospheric CO_2 levels (NOAA, 2005).

1.4.1.1 Atmospheric carbon dioxide

CO_2 has an estimated half-life of 50-200 years (Houghton *et al.,* 1998). This extended decay allows CO_2 to become well mixed in the troposphere. Although the lifetime is great, it has been estimated that the turnover time of CO_2 in the atmosphere is 3 to 4 years (Crane, 1985). This is how long a molecule remains in the atmosphere before it is sequestered by biota or the ocean surface, and has no direct relation to decay time. Sequestration is a very important method of removing CO_2 from the atmosphere. In the absence of land and ocean sequestration (sinks), if all CO_2 produced annually by fossil fuel combustion were to remain in the atmosphere, the atmospheric concentration would increase by 0.8% per year. Fortunately sinks sequester 50-60% of anthropogenic CO_2, so that only the remaining 40-50% stays in the atmosphere (Houghton, 1997). This equates to a current atmospheric increase of approximately 4% per decade. In order to determine the carbon budget, we must be able to quantify the uptake of CO_2 by terrestrial and oceanic sinks. Estimates suggest that the ocean sequesters approximately 30%, but this number is difficult to quantify and predictions may over or underestimate the true oceanic uptake (Houghton *et al.,* 1998). The question of where the remaining 20-30% of the carbon is sequestered is of great interest and debate. The terrestrial biosphere no doubt plays a large part in sequestration of the remaining carbon but the controversy and debate surrounding the "missing sink" has extended for decades (Figure 1 - 6).

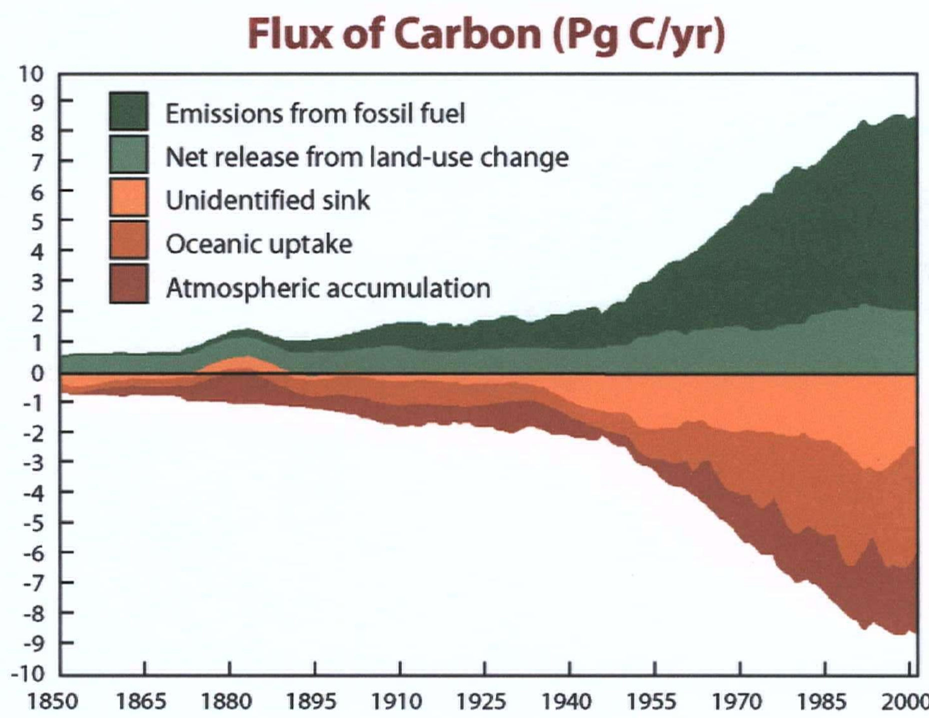

Figure 1 - 6 Global accumulations and releases of carbon. The missing sink is shown in light orange (Woods Hole Research Center, 2005)

1.4.2 The missing sink

There are many theories proposed regarding the location of the missing sink and it is easy to understand why it is surrounded by controversy. In the past, boreal forests were thought to sequester large amounts of carbon and were considered one of the major terrestrial sinks. Recent literature from the BOREAS project, however, indicates that boreal forests are actually only a weak sink for carbon. This is because the system is saturated with nitrogen, and therefore increased carbon uptake resulting from nitrogen-deposition does not occur (Nadelhoffer *et al.*, 1999). In nitrogen-limited systems increased nitrogen-deposition can simulate biological activity and the increased productivity in turn sequesters CO_2 from the atmosphere through the process of photosynthesis (Nadelhoffer *et al.*, 1999). An increase in nitrogen-deposition is due to elevated amounts of nitrogen in the atmosphere resulting from agricultural practices and releases of nitrous oxides from fossil fuel combustion.

There are many studies indicating the location of the missing carbon sink. Phillips *et al.*, (1998) suggest that 40% of the terrestrial carbon is sequestered by tropical rainforest ecosystems. Schindler (1999), on the other hand, proposes that oceans take up excess carbon and that uptake values are currently severely underestimated. Evidence from the BOREAS project indicates that wetlands and peatlands, which currently represent a large pool for CO_2, may act as sources or sinks depending on the time of year, the vegetation present, and the current climatic and soil conditions (temperature and water content) (Joiner *et al.*, 1999; Lafleur *et al.*, 1997). It is difficult to predict which systems will be definite sinks for carbon in the future.

1.4.2.1 Ocean

Due to the lack of homogeneity over the ocean surface including differing temperatures, cycling, currents, and deep water formation it is difficult to determine a reliable estimate of dissolved carbon in the ocean (Poisson, 1998). The capacity for the oceans to sequester CO_2 is assumed to be a function of chemical buffering of sea water and the solubility of CO_2 itself. Chemical buffering refers to the reaction of CO_2 molecules with carbonate ions to produce bicarbonate ions (Sarmiento and Gruber, 2002). There is a lag in the ocean's ability to take up carbon due to the sluggishness of oceanic circulation patterns. Surface water containing dissolved CO_2 is forced into deep water circulation primarily in the Northern Atlantic through the process of the thermohaline circulation. Thermohaline circulation occurs due to differences in temperature and salinity levels that occur near melting sea ice in the North Atlantic. Gradients in these properties cause denser surface water to sink and then enter circulation patterns deep beneath the surface. Upwelling occurs hundreds of years later returning nutrients and cold water to the surface. In the Northern Pacific, research indicates that upwelling sea water was last at the surface over a 1000 years ago. The primary area of upwelling is the Northern Pacific, but other areas of upwelling include the tropics and Southern oceans near Antarctica. Upwelling water has a large capacity to take up CO_2 because hundreds of years ago when it first entered thermohaline circulation it contained little dissolved carbon. It is therefore not surprising that the greatest rates of sequestration are present in areas of upwelling (Sarmiento and Gruber, 2002).

1.4.2.2 Terrestrial

In general, it is widely accepted that terrestrial systems act as the missing sink for carbon, but the mechanisms driving uptake are not well understood (Houghton *et al.,* 1998). The role of terrestrial ecosystems in the carbon budget can essentially be thought of as a black box. It is often very difficult to quantify terrestrial systems due to spatial variability, which leads to enormous uncertainty in measurement processes. Possible explanations for the terrestrial sink are CO_2 fertilization (increased CO_2 allows for increased photosynthesis and therefore CO_2 uptake), nitrogen deposition (which adds a limiting nutrient and stimulates growth and photosynthesis), and forest or vegetation growth following disturbance (Houghton *et al.,* 1998). It is easy to attribute the missing sink to a terrestrial ecosystem with a large spatial extent such as the boreal or rainforests, but smaller systems (peatlands, wetlands, arctic, agricultural, urban) can no longer be overlooked if knowledge of the true partitioning of the carbon balance is desired.

Warmer temperatures and wetter conditions resulting from climate change could lead to an increased release of carbon into the atmosphere from most terrestrial ecosystems (Houghton *et al.,* 1998) due to elevated metabolic rates of plants and microorganisms, which through respiration processes, emit CO_2 as a bi-product. This could act to increase atmospheric CO_2 levels and therefore be a positive feedback on global warming. On the other hand, there is the suggestion that the terrestrial biosphere may act as an increasing sink as atmospheric CO_2 levels rise, due to increased photosynthetic rates, acting as negative feedback to global warming as indicated by Takagi *et al.* (1998) and Nowak (1993).

With regards to urban environments, a better understanding of exchanges between the atmosphere and the Earth may aid in determining the magnitude and location of part of the missing sink. Cities are assumed to be emitting considerably more CO_2 than they are taking in. However, if this assumption is wrong and cities are actually sequestering more CO_2 than currently assumed, then the vegetation in the urban environment may be a small part of the missing sink. In contrast, if cities are large sources, a part of the missing sink may lie in the terrestrial ecosystems of their surrounding countryside, (e.g. downwind) which may take up additional CO_2. Human perturbations to the global carbon budget are listed in Table 1 - 1. This table includes only human-induced sources (and does not include natural sources). We can see that these sources are almost equal to the natural CO_2 sinks, leading to a large need for additional uptake of carbon by the terrestrial or oceanic biospheres in order to have all natural and anthropogenic sources balance with available sinks.

Table 1 - 1 Human perturbations to the global carbon budget (IPCC, 1995).

CO_2 sources	*Flux (Gt C yr^{-1})*
Tropical deforestation	1.6 ± 1.0
Fossil fuel combustion and cement production	5.5 ± 0.5
Total anthropogenic emissions	***7.1 ±1.5***
CO_2 sinks	
Storage in the atmosphere	3.3 ± 0.2
Uptake by the ocean	2.0 ± 0.8
Northern hemisphere regrowth	0.5 ± 0.5
Missing sink	1.3 ± 1.5
Total sinks	***7.1 ±3.0***

With a predicted doubling of CO_2 in the atmosphere over the next few decades the race to understand and quantify uptake and release of carbon from as many ecosystems as possible is critical. Urban areas have been largely ignored but may provide valuable insight into the human role in sequestration and release of CO_2. The following sections explore sources and sinks of CO_2 in the urban environment.

1.4.3 Urban CO_2 sources

There are a number of processes that act to increase the concentration of CO_2 in the urban atmosphere. Sources in urban areas are mainly a result of CO_2 emissions from fossil fuel combustion that arise from our industrial, space heating/cooling, and transportation demands, but also include natural processes which emit CO_2 as a byproduct of respiration.

1.4.3.1 Anthropogenic CO_2 sources

Fossil fuel combustion is a large contributor to CO_2 emissions because hydrocarbons present in fossil fuels are almost completely oxidized to CO_2 when combusted. The combustion of fossil fuels alone produces about 5.5×10^{15} g C yr^{-1} (Houghton *et al.*, 1998). Anthropogenic sources of CO_2 in urban areas are primarily from the combustion of liquid, solid and gaseous fossil fuels (Harvey, 1993) mainly for transportation and space heating.

Buildings are another main source of CO_2, accounting for 25-30% of total energy-related CO_2 emissions (Weil *et al.*, 1998). Between 1980 and 1990 CO_2 emissions from buildings have grown by a global average of 1.7% per year, with rates up to four times greater than this in developed nations (Weil *et al.*, 1998). The high energy demand of buildings is due to insufficient insulation and heating, appliances and lighting (Urgasal and Fung, 1998). Moriwaki and Kanda (2004) note that there is an unequal distribution of CO_2 emitted from houses in the winter compared to the summer, due to 50% more energy being consumed in the winter (in Tokyo, Japan).

Minor urban anthropogenic sources include cement production, which can contribute up to 7% of anthropogenic emissions, chemical processing, waste disposal and animal respiration (Reid, 1995). A study by Clarke and Faoro (1966) in Cincinnati suggests that respiration by humans can contribute 3% of anthropogenic CO_2 emissions.

1.4.3.2 Natural CO_2 sources

The natural processes of plant dark respiration and soil respiration (Equation 1.7) also emit carbon dioxide into the urban atmosphere.

Respiration:

Carbohydrate + Oxygen → Carbon Dioxide + Water Vapour + Combustion Energy [1.7]

Dark respiration converts organic carbon in plants back into CO_2; this CO_2 is then emitted through leaves, stems and branches (into the air) and roots (into the soil). This process is independent of light and therefore occurs constantly; a night-time build up of CO_2 is seen in the near-surface atmosphere due to the nocturnal dominance of this process. Stable atmospheric conditions at night prevent the mixing of CO_2 into the upper atmosphere. Dark respiration is temperature dependent; increased rates occur at elevated temperatures. In temperate cities, summer values often reach twice that of spring values. In contrast, during the winter, dark respiration is almost absent. In Calgary, Alberta for example, dark respiration was absent in the fall and winter, while farther south in New York, minimal dark respiration was apparent throughout most of the winter (Leahey and Hansen, 1992). The other natural process that emits CO_2 into the atmosphere is soil respiration, which occurs through decomposition of organic material in the soil. Soil organisms consume (break down) dead organic material, which causes CO_2 emissions through oxidation of the available carbon. Emissions depend on the rate of decomposition, temperature, soil moisture, wind speed and the CO_2 concentration gradient between the soil and the air.

1.4.3.3 Contributions by Canada and Vancouver

Canada is one of the highest per capita energy consumers in the world (Ugursal and Fung, 1998). Energy demands in Canada are elevated due to the geographic (northerly) location and climate of the country. Also, a large percentage of Canada's population is living in urban areas, and therefore energy demands are high in cities, and fossil fuel combustion is great. The expanse of the land requires reliance on individual vehicular use and overland supply transport, and Canada's long winters create large heating requirements. Currently, in British Columbia, approximately 49% of CO_2 emissions are from transportation sources (Province of British Columbia, 1995). A break down of Greater Vancouver Regional District CO_2 sources are shown in Figure 1 - 7 and summarized in Table 1 - 2.

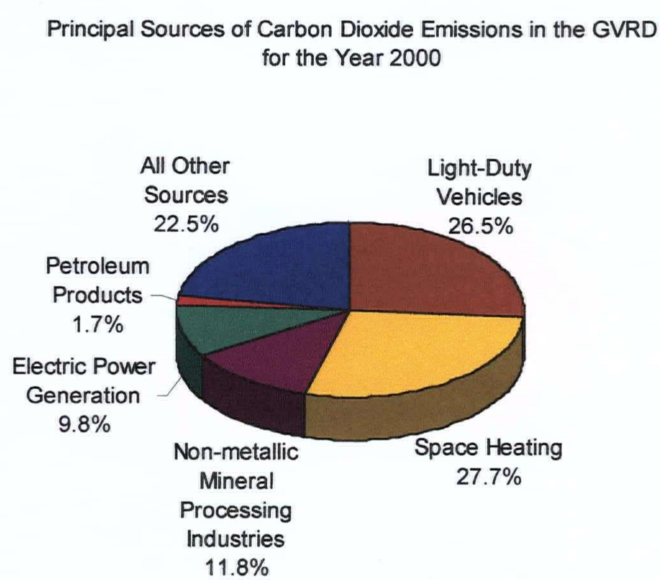

Figure 1 - 7 Sources of carbon dioxide in the Greater Vancouver Regional District for the year 2000 (GVRD, 2002).

Table 1 - 2 Summary of Carbon Dioxide Emissions (metric tonnes) (GVRD, 2002).

Category	CO_2 (metric tonnes)
Light-Duty Vehicles	4,223,497
Space Heating	4,417,175
Electric Power Generation	1,561,483
Non-metallic Mineral	1,874,339
Petroleum Products	270,597
All Other Sources	3,575,994
Total	15,923,087

1.4.4 Urban CO_2 sinks

Urban vegetation has an important role in uptake and storage of CO_2 (Nowak, 1993), through the process of photosynthesis. In the urban environment, vegetation including trees, shrubbery and lawns, are the main sinks for CO_2.

Photosynthesis:

Carbon Dioxide + Water Vapour + Light Energy → Carbohydrates + Oxygen [1.8]

Photosynthesis (Equation 1.8) causes a draw-down of CO_2 by vegetation during the day, but at night, when photosynthesis ceases, the vegetative sink is no longer available. This creates a diurnal trend of high (night) and low (day) CO_2 concentrations in both urban and rural environments.

1.4.4.1 Urban forests

It is currently estimated that urban trees in the United States store 350 to 725 million tons of carbon, but there is a gap in the literature when quantifying the amount stored in shrubs, bushes, soils and grass (Nowak, 1993). The amount stored is dependent on tree trunk diameter, and since most urban vegetation is small (approximately 67% of urban vegetation has a trunk diameter of less than 15 cm) there is a large potential for increased uptake as urban trees mature (Nowak, 1993). This requires present urban vegetation to persist in order to ensure vegetation remains a net CO_2 sink and not a source. Unfortunately, tree death and decay cause the release of stored carbon, making trees only a relatively short-term (hundreds of years) storage reservoir (Nowak, 1993).

Nocturnally, vegetation acts as a source through the process of nocturnal dark respiration, but the overwhelming uptake of CO_2 during the day via photosynthesis usually results in urban vegetation being a net sink. Knowledge of carbon cycling in urban forests is limited and more research is needed to determine the optimum species and vegetative density for maximal carbon sequestration.

1.4.5 The challenge of research in urban environments – complex terrain

Cities are known for their microscale complexity and to complicate matters further their geographic setting is often in complex terrain. This makes measurement of CO_2 fluxes and concentrations challenging. An aircraft study at 30 m over heterogeneous terrain indicated that as much as half of the variance in CO_2 and H_2O fluxes at that height can be explained by surface heterogeneity in the spatial distribution of sources and sinks of CO_2 and H_2O (Mahrt *et al.*, 1994).

Urban areas are classified as complex due to the lack of contiguously similar terrain. Buildings are of different heights and sizes, roads are of varying width and density and vegetation cover is interspersed with built surfaces. The main effects of this inhomogeneity of relevance here are the spatial and temporal variability in CO_2 concentrations and fluxes. Additionally, large surface roughness values in suburban and urban areas also make low-level measurements difficult. There is also the ubiquitous presence of human influences in urban environments, which must be accounted for, but is often difficult to predict.

1.4.6 Current research

In the past, attempts to quantify the role of CO_2 exchange in urban environments have focused on emission inventories, and vegetative carbon sequestration (Grimmond *et al.,* 2002a). At this time, studies of atmospheric CO_2 in urban and suburban regions are relatively few, and the knowledge of urban CO_2 is only basic. Unfortunately detailed emission inventories are not present in many large cities and are often inaccurate or simply rough estimates. Other studies have attempted to quantify the spatial variability of near-surface CO_2 concentrations across urban regions through transects, and other studies to measure concentrations from a point (or tower) site. These studies present valuable information, but knowledge of CO_2 flux measurements in urban areas is scant. Dabberdt *et al.* (1993) state that it is knowledge of the fluxes of CO_2 and their diffusive characteristics in urban environments that are key to quantifying climatic and biospheric impacts of increasing CO_2. The following sections are designed to review present knowledge specifically in the field of urban CO_2, including both flux and concentration research.

Most urban studies explain diurnal variation of CO_2 concentrations as the difference between mean daytime and night-time concentrations and the deviations from the background concentration. A background concentration is the CO_2 concentration of relatively undisturbed "clean" air. A common source of background concentration is the South Pole, where in 2002, the annually averaged background concentration was 370.65 ppmv (Keeling *et al.,* 2004). Often, in the summer, when photosynthesis is at its peak, afternoon rural concentrations can reach 15 ppmv below the background concentration whereas similar conditions in the city will only produce 2-3 ppmv below background value (Reid and Steyn, 1997). Urban-rural differences are attributed to a decrease in vegetation in urban areas and an increase in fossil fuel combustion compared to rural areas.

1.4.6.1 Concentrations – exploring the diurnal trend

The diurnal trend of CO_2 concentration generally follows a double peak in urban environments (Figure 1 - 8). These peaks correspond to human activity, specifically the morning and afternoon rush hours. An emissions inventory in Phoenix, Arizona determined that 80% of the CO_2 source was attributable to vehicular emissions (Koerner and Klopatek, 2002). Examining the daily trend of CO_2 concentrations at the Sunset site in Vancouver, BC (Figure 1 - 8) reveals maximum pre-dawn values, due to the build up of CO_2 throughout the night. Build up during the night is a result of respiration in the absence of photosynthesis combined with the morning rush-hour combustion of fossil fuels and stable atmospheric conditions that prevent mixing and dispersion (Reid, 1995, Grimmond *et al.,* 2002a). A pre-dawn maximum is also apparent in rural areas, however, in the city, rural values are supplemented by CO_2 contributions resulting from fossil fuel combustion.

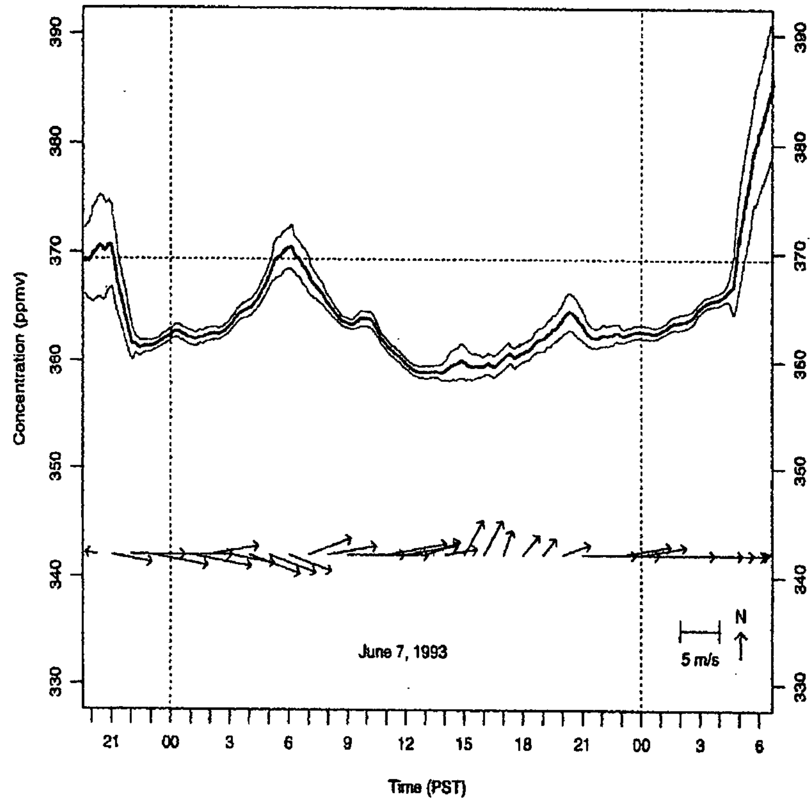

Figure 1 - 8. Atmospheric CO_2 concentration trace for June 7, 1993 at the Sunset site, Vancouver, BC. The thick line represents observations smoothed by a 60 minute running mean. Thin lines represent one standard deviation on either side of the mean. Hourly wind observations are shown as vectors. The background concentration (369.4 ppmv) is shown as a dotted line. A morning peak is apparent at approximately 7:00 with a smaller peak apparent at approximately 21:00. These peaks correspond to rush hours. High concentrations are seen at the end of the trace due to stable night conditions (Reid, 1995).

With the rise of the Sun, carbon uptake increases due to an increase in photosynthetically active radiation (PAR) (Wofsy *et al.*, 1993). This supports photosynthesis and creates a downward flux of CO_2 towards the surface. Daytime convective mixing drives convective plumes and turbulence, which aid the dispersion and mixing of CO_2 in the troposphere (Reid and Steyn, 1997). In the late afternoon, when heating and PAR are reduced, a second smaller peak is often apparent. This peak corresponds to CO_2 emitted from traffic during the evening rush hour. The traffic peak is offset by the photosynthetic sink that is acting to sequester CO_2.

Berry and Colls, (1990a, 1990b) measured urban/rural differences at fixed points as well as morning and afternoon transects in Nottingham, England. Morning transects show an increase in CO_2 concentration as the city is approached in the winter, but the opposite in the summer (Berry and Colls, 1990b). This is due to the strength of soil respiration in the summer in rural, highly vegetated areas. Afternoon transects revealed an average increase as the city was approached at all times of the year. Measurements at the transect ends are presented in Figure 1 - 9 (a) and (b). A double peak related to human activity is apparent in winter urban traces but not in the summer due to strong vegetative influences (Berry and Colls, 1990a). Rural values are highly dependent on vegetation, which explains the large decrease in afternoon summer values resulting from photosynthesis.

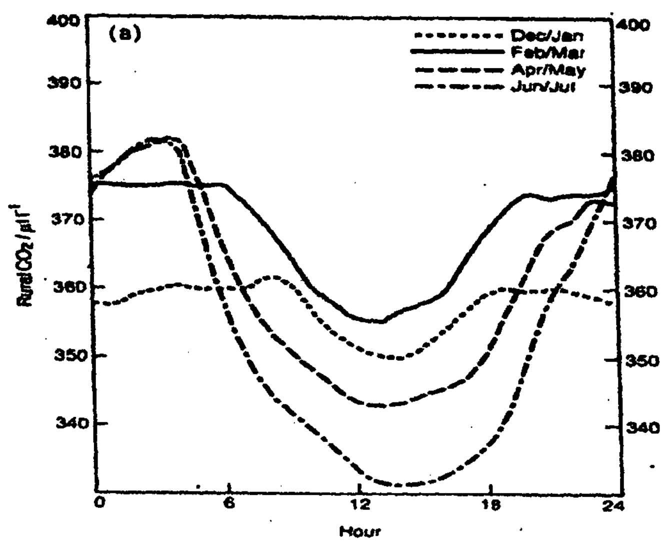

Figure 1 - 9 (a): Bi-monthly-averaged diurnal variations in the CO_2 concentration at the rural site (December 1984-July 1985) (Berry and Colls, 1990a).

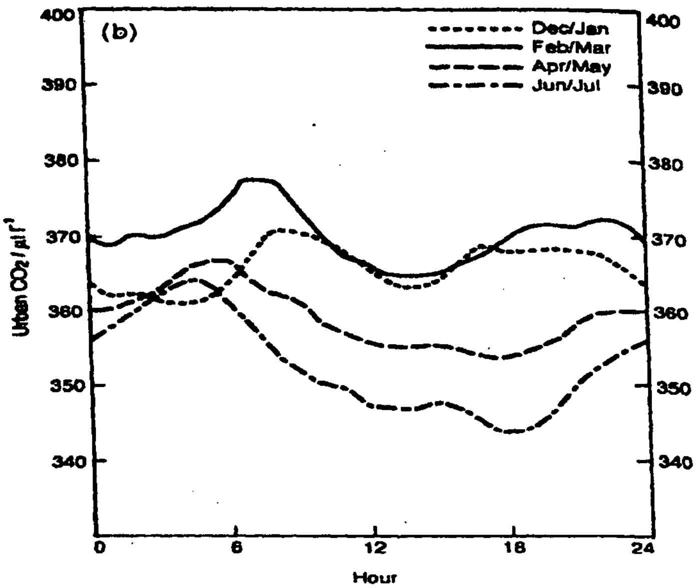

Figure 1 - 9 (b): Bi-monthly-averaged diurnal variations in the CO_2 concentration at the urban site (December 1984-July 1985) (Berry and Colls, 1990a).

1.4.6.2 The "Urban CO_2 Dome"

Studies by Idso and Balling (1998, 2001) indicate the presence of an "Urban CO_2 dome" over urbanized areas resulting from the build up of CO_2 from fossil fuel combustion in the city core. Concentrations are elevated as the city center is approached. Results indicate a 50% increase above background concentrations in the hours before dawn, and a 30% increase in the mid-afternoon. These studies also noted apparent differences between weekend and weekday concentrations, which again illustrates the dependence of urban CO_2 concentrations on human activity. Studies such as these clearly indicate high spatial and temporal variability of CO_2 concentrations in the urban environment.

Idso and Balling (2001) suggest that cities make ideal "natural laboratories" for research on elevated CO_2 effects and climate change. Information from the effects of elevated CO_2

concentrations in urban areas might be used to determine how increasing global CO_2 may influence climate change in other areas.

1.4.6.3 CO_2 fluxes

Although some information on CO_2 concentrations in urban areas is available, fluxes of carbon dioxide (F_C) are not well documented in the urban environment. At this time there are very few refereed papers focusing on urban F_C. A few studies by Grimmond *et al.* (2004), Marseille; Grimmond *et al.* (2002a), Chicago; Soegaard and Moller-Jensen, (2003), Copenhagen; Nemitz *et al.* (2002), Edinburgh; and Moriwaki and Kanda (2004), Tokyo, have been published. The field is beginning to develop, and reports by Grimmond *et al.* (2002b), Baltimore; Vogt *et al.* (2004), Basel; Anderson and Taggart (2002), Denver; Salmond *et al.* (2005), Marseille; and McFadden *et al.* (2004), Roseville, Minneapolis, are beginning to emerge in conference proceedings and journal pre-prints (see http://www.indiana.edu/~iauc/). Overall results from these studies indicate that vegetation:built fraction and human activities appear to impact F_C (Grimmond *et al.*, 2004).

The sign convention for F_C is such that a flux away from the surface (emission) is positive and a flux towards the surface (sequestration) is negative.

F_C follows a number of patterns and trends that are both spatially and temporally variable. For example, at a suburban site, midday F_C in the summer months is likely to be negative (towards the surface) when vegetation sequesters CO_2 from the atmosphere via photosynthesis at rates greater than contributions from emissions. In contrast, in winter positive F_C will likely dominate due to the prevalence of vehicular emissions in the absence of the photosynthetic sink. Winter F_C should also be greater due to space heating emissions from residential buildings. Moriwaki and

Kanda (2004) note that although traffic is a main source of CO_2, this source does not vary significantly over the year, and therefore seasonal differences in F_C can not be attributed to traffic (Moriwaki and Kanda, 2004).

Agricultural sites record maximum F_C toward the ground in the midday hours due to photosynthesis. In contrast, bare soil shows F_C as positive, or, into the atmosphere due to soil respiration during the midday (Soegaard, 1999). F_C in urban environments is on average positive, indicating that established urban zones are net sources of carbon dioxide (Grimmond *et al.,* 2002, Moriwaki and Kanda, 2004). F_C at a site in Baltimore, in a newly created suburb on the edge of greenspace, however, is still mainly negative, especially in the summer, indicating that the vegetative sink continues to dominates (Grimmond *et al.,* 2002b) (Figure 1 - 10a). In contrast, fluxes from Marseille, France, a sparsely vegetated area, show positive fluxes due to the absence of a strong vegetative sink (Grimmond *et al.,* 2004) (Figure 1 - 10b).

(a)

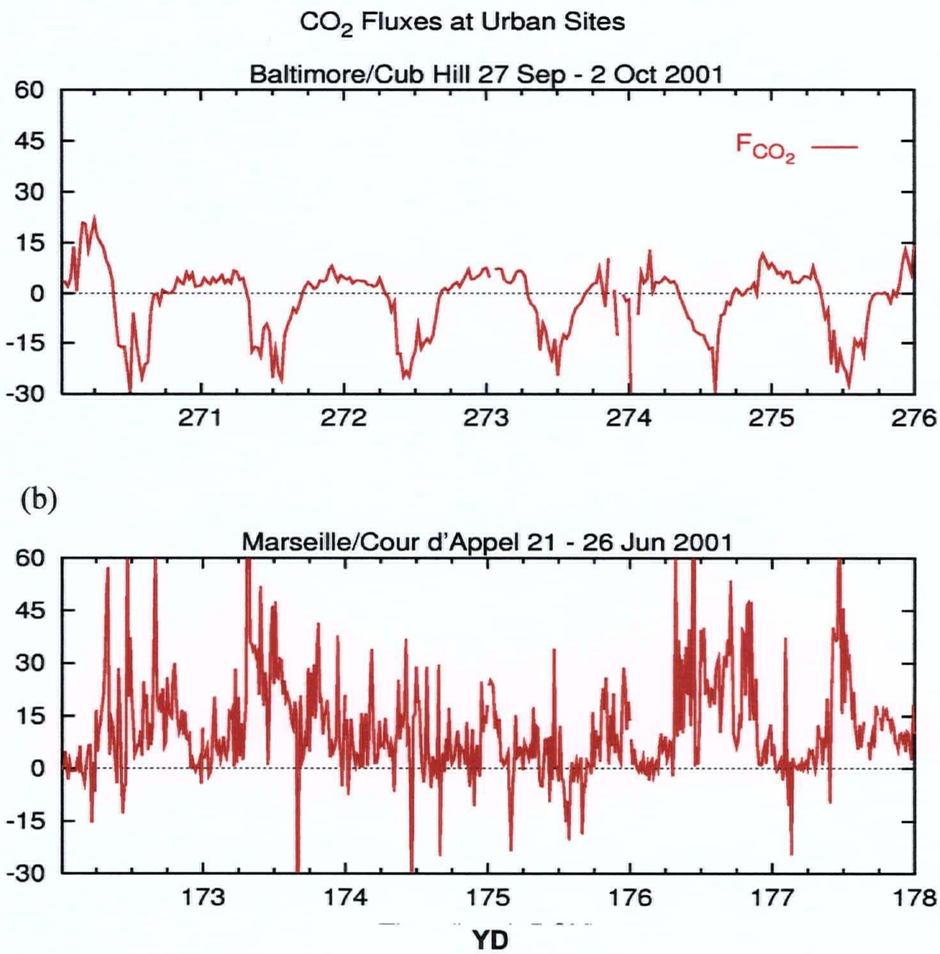

Figure 1 - 10 Baltimore and Marseille hourly CO_2 fluxes for 6 days. (a) The Baltimore F_C is, on average, below zero indicating sequestration rates are high. (b) The Marseille F_C is, on average, above zero indicating a net emission of CO_2 into the atmosphere (Grimmond *et al.*, 2002b).

A typical diurnal cycle of F_C has low positive values throughout the night due to the stable nocturnal boundary layer. Fluxes begin to rise in the morning as convective mixing increases. In highly urbanized areas a mid-morning peak is seen corresponding to human activity and traffic patterns. In the afternoon a draw down of carbon dioxide may be present if the vegetative sink is able to offset anthropogenic emissions. If the vegetative cover is high and consumption of fossil fuels low, negative F_C may be seen during the day. Moriwaki and Kanda (2004) compared the pattern of suburban F_C to that of house emissions and found that the patterns were similar indicating that fossil fuel consumption trends are related to F_C.

1.4.7 Importance of CO_2 measurements

With increasing global deforestation, changes in land use, and expanding urbanization, long-term stores of carbon are being released into the atmosphere throwing the carbon budget further off balance. Urbanization usually results in a diminished terrestrial sink as forests and natural ecosystems are removed to make way for parking lots, buildings and roads. Without knowledge of the magnitude or location of urban sources and sinks it is difficult to predict how climate change and a doubling of atmospheric CO_2 will affect the earth. Studying CO_2 in urban areas, where the sources of CO_2 emissions are highly concentrated may provide insight as to how ecosystems will react to elevated CO_2 levels and how they might be controlled.

There is strong need for increased knowledge of F_C in the urban environment. Only then can the role of cities as a contributor to the greenhouse effect be understood, and intelligent mitigation strategies developed to reduce the impact of climate change. This study focuses on the atmospheric CO_2 in a suburban region of Vancouver; an environment where sources and sinks struggle to offset one another.

1.5 Objectives

A year-long project to measure surface-atmosphere exchanges of carbon dioxide, radiation and energy balance components was conducted over a suburban region of Vancouver, British Columbia. The objectives of this thesis are:

- To observe the surface-atmosphere exchanges of carbon dioxide, and the associated fluxes of radiation, latent, and sensible between a residential suburb and its atmospheric boundary layer in Vancouver for a period of at least one year.

- To document the nature of the diurnal and seasonal variability of the fluxes of carbon dioxide, radiation and energy in such an environment.

- To determine whether the fluxes of carbon dioxide, radiation and energy have surface source areas that are co-located.

2 METHODOLOGY

2.1 General observational approach

There are a number of possible measurement techniques to quantify CO_2 and energy fluxes from an urban environment. Traditional micrometeorological techniques include aerodynamic profiles, Bowen ratio systems, and other flux-gradient methods to assess surface-air exchanges, or fluxes. Flaws in flux-gradient eddy exchange coefficients can arise when measurements are taken over tall surface elements, or during the night (Baldocchi *et al.,* 2001). Advances in technology including sonic anemometry and spectrometry, as well as in computer processing speeds, and data storage, favour the 'eddy covariance' technique. This approach is widely used in the global FLUXNET program over forest, wetland and grassland ecosystems to quantify spatial and temporal aspects of CO_2 exchange.

2.1.1 Eddy covariance theory

The eddy covariance technique relies on direct measurement of water vapour, CO_2, speed of sound, and orthogonal wind components from fast response sensors mounted on towers. Instruments are designed to capture small turbulent eddies and the scalars carried by these eddies. By mounting instruments that measure eddies and scalars in close proximity it is possible to capture separate signals and calculate their instantaneous product, and further, it is possible to average these products over time to investigate temporal trends. This technique was first applied over bare soil and agricultural fields in the 1960s and 70s but soon expanded to measurements over tall roughness elements such as forest canopies.

In this technique, exchanges of heat, moisture and CO_2 between the surface and the atmosphere are related to the correlation between entities (scalars) of interest and the vertical wind velocity. When the product of the instantaneous deviation of the entity of interest and the vertical velocity is positive, there is an upward flux of the entity, and when it is negative there is a net downward flux. The vertical turbulent flux densities of Q_H, Q_E, and CO_2 can be calculated from the mean covariance of the vertical wind speed, with the fluctuation of the respective entity of interest, (temperature for Q_H (Equation 2.1), specific humidity for Q_E (Equation 2.2), and CO_2 concentration for CO_2 (Equation 2.3)).

Sensible heat flux:

$$Q_H = \rho c_p \overline{w'T'} \qquad [2.1]$$

Latent heat flux:

$$Q_E = \rho L_v \overline{w'q'} \qquad [2.2]$$

CO_2 flux:

$$F_C = \rho \overline{w'c'} \qquad [2.3]$$

where ρ is the density of dry air (kg m^{-3}), c_p is the specific heat of air at constant pressure (J kg^{-1} K^{-1}), L_v is the latent heat of vapourization (J kg^{-1}), T is the air temperature (K), q is the specific humidity (g kg^{-1}), c is the carbon dioxide concentration (μmol mol^{-1} dry air), and w is the vertical wind velocity (m s^{-1}). In these equations the prime indicates an instantaneous deviation from the time mean and the overbar indicates the temporal average of the instantaneous products.

Although these measurements are taken from one point in space (from a tower), they are designed to represent an integrated response from the surface characteristics of the corresponding source area (as discussed in Source areas, Section 2.2.2). Instruments mounted on towers allow for measurements of energy and CO_2 fluxes over long time scales, thereby capturing seasonal and inter-annual patterns.

There are a number of weaknesses associated with the eddy covariance technique. Ideally measurements are restricted to areas of smooth topography and homogeneous fetch to ensure an internal boundary layer where fluxes are constant with height (Kaimal and Finnigan, 1994). With uneven or patchy surface characteristics, horizontal advection can become significant (Lee, 1998; Finnigan, 1999). In the case of urban areas it is important to choose an area of relatively homogenous urban terrain (i.e. similar type and intensity of development extending in all directions from the tower). It is also relevant to mention that measurements from an eddy covariance system represent only the surrounding neighborhood, the results cannot be scaled up to represent an entire city or scaled down to represent specific surfaces.

The overall advantages of the eddy covariance method far outweigh its limitations. Long-term studies can provide valuable information on the seasonal and inter-annual variations in energy and CO_2 fluxes. Implementation of eddy covariance systems over tall roughness elements such as forests has provided valuable insight into how to measure similar entities over urban areas.

2.1.1.1 Eddy covariance instrumentation

Equipment to implement the eddy covariance approach includes fast response instruments mounted on a tower. A 3-dimensional sonic anemometer is used to capture small and large fluctuations in turbulent wind eddies reaching the tower. Wind vectors are measured as wind passes through pairs of ultrasonic transducers located on the anemometer sensor head. The transducers alternately transmit and receive pulses of high frequency ultrasound. By re-arranging ultrasound signals into different orientations transmitted between the 3 pairs of sonic transducers the wind direction and horizontal, crosswind and vertical velocities (u, v and w, respectively) can be derived. The speed of sound is similarly measured and the virtual temperature derived. Fluctuations in the vertical velocity of wind are especially important as this indicates whether the flow of an entity is towards or away from the surface.

Scalar entities such as CO_2 and water vapour are measured using either open or closed path, fast response infrared gas analysers. Both types of sensors have advantages and disadvantages. Closed path sensors have an intake tube located in close proximity to the sonic anemometer transducers whereas open path sensors are mounted adjacent to the sonic anemometer, preferably within 0.5 m of the center of the anemometer (Baldocchi *et al.*, 2000, Meyers, 2001). When using closed path sensors, air is drawn down a tube into a gas transducer, which is often located at the base of the tower. This creates a possible source of error as diffusive smearing of eddies and a delay in airflow can occur in the tube. Closed path sensors require calibration more often than open path sensors and are therefore more labour intensive to operate. For this reason it is often more cost and time efficient to install open path sensors which have a more stable calibration and can remain on the tower for long periods of time. A major disadvantage of open path sensors is that the optical path is easily disrupted by precipitation leading to data loss. For this reason reliable output from open path sensors is generally limited to periods free of precipitation.

The sampling duration of fast response instruments must be considered in order to capture the appropriate response of the atmosphere. Sampling duration must be long enough to capture the low frequency contributions to the flux covariance, but short enough that fluctuations in temperature, CO_2 and water vapour are not lost from the analysis (Baldocchi *et al.*, 2001). Sampling rates between 10-20 Hz are ideal, as these rates ensure adequate sampling of the high-frequency flux co-spectrum (Anderson *et al.*, 1984).

2.2 General site requirements

2.2.1 Measurement height

The urban boundary layer consists of several distinct layers (Figure 2 - 1), and hence, measurement height is important to consider when observing meteorological variables over urban areas (Oke, 2004). The roughness sublayer (RSL) extends from the ground to about 2.5 to 4 times the building height and measurements taken within this sublayer are influenced by the micro-scale. Within this layer entities are not well mixed and therefore CO_2 concentrations, for example, are likely to be highly variable, and dependent on exactly where they are measured. Above the RSL it is possible to capture an integrated (well-blended) response of all surface features located in the upwind source region that is representative of the local scale (10^2 to 10^4 m). This is the constant flux, or inertial sublayer (ISL), and fluxes or heat, mass and momentum are expected to be spatially homogenous throughout the layer (Rotach, 2000). In the ISL we can assume that wake effects of individual buildings or other effects of individual surfaces do not disrupt airflow or other properties reaching the instruments on the tower (Pasquill, 1972). At urban sites, to ensure measurements are within the ISL, an emerging rule-of-thumb is that instruments be mounted at greater than 2.5 times the height of the mean roughness elements as depicted in Figure 2 - 2. The height appears to depend on the density of the elements and the factor may range from 1.5 at very dense sites to 4 with open element spacing (Oke, 2004).

When considering CO_2, the greatest fluxes in a city are likely to be measured above the downtown core or over an industrial area, where emissions are most concentrated, however it is difficult to take meaningful measurements in a city center in North America. A tower is necessary for long-term measurements, but tower erection in highly urbanized zones is not practical due to the height of the buildings and the relatively limited horizontal extent of the core. For example, a building that is 150 meters tall would require measurements to be taken above 375 meters (2.5 times building height), and even if a tower were mounted on this building's roof it would still have to be over 200 meters tall and there would need to be about 20 km of fetch over similar surfaces. Although cities are widely acknowledged as major sources of CO_2, few studies have quantified the fluxes in urban environments because of such challenges. It is, however, practical to study suburban areas or downtown cores that do not have high buildings as long as they are relatively homogeneous and horizontally extensive.

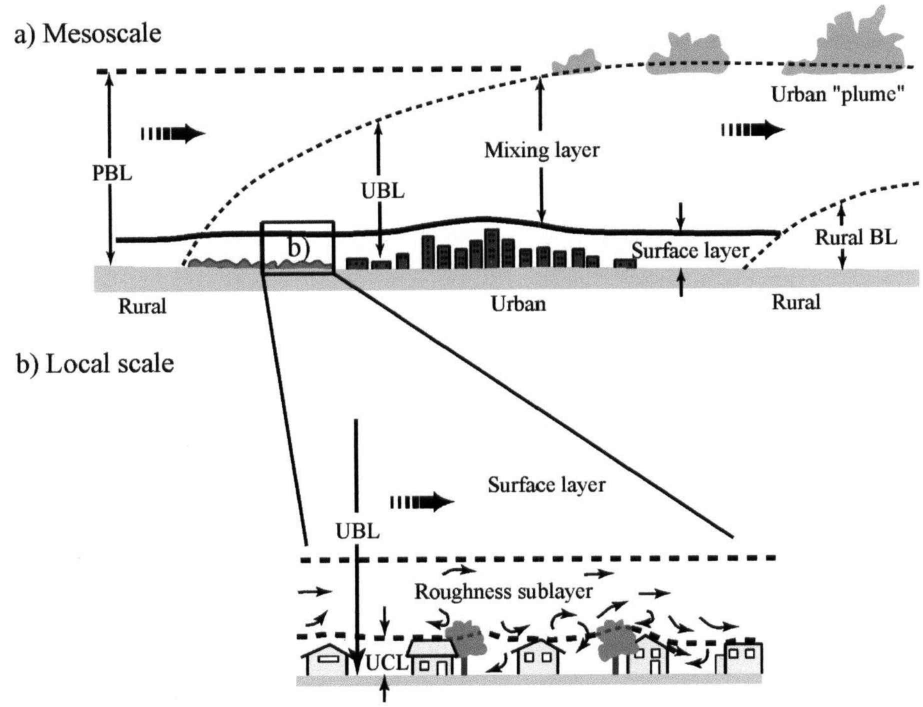

Figure 2 - 1 Idealized arrangement of boundary layer structures over an urban surface a) mesoscale and b) local scale representing a single urban terrain zone. PBL - planetary boundary layer; UBL - urban boundary layer; and UCL - urban canopy layer. (Oke, 2004).

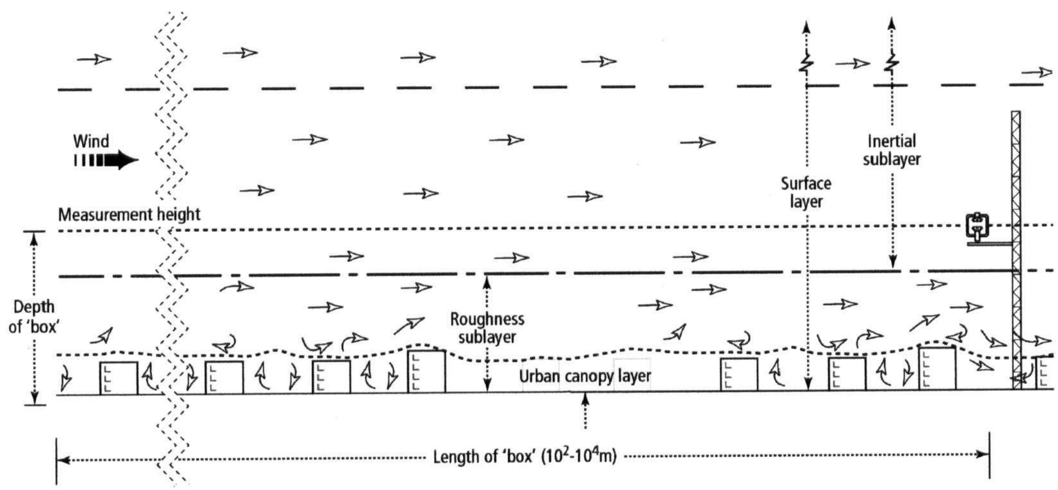

Figure 2 - 2 Relation of measurement height to the RSL and other layers in a city (Grimmond and Oke, 2002).

It is possible that a homogenous, well mixed surface layer may not always exist over complex urban surfaces (Rotach, 1993, Roth, 2000). Even with careful siting of the instruments at a measurement height above the RSL, it is possible that measurements taken are not always truly in the ISL. In consequence, not all fluxes may be well blended at the measurement height and a directional dependence may be seen in some fluxes depending on the characteristics of the underlying source area.

2.2.2 Source areas

In addition to mounting instruments at a height that correctly represents an integrated, well-blended, response to the surface elements, the source area of each instrument must be considered. A source area is the portion of the surface that influences the sensor, and depends on the mounting height and the component being monitored. Energy balance components are measured by different instruments, some of which have different source areas. Radiation source areas are fixed, whereas turbulent source areas vary with wind direction and stability. In an urban environment this may pose a mismatch in source areas 'seen', because areas surrounding the tower are not identical in urban structure. There is little that can be done to prevent a mismatch of source area besides choosing an area of similar surfaces and using measurement heights that optimize the agreement between the source areas.

2.2.2.1 Radiative source areas

When considering a radiometer, a circular patch on the ground surface represents its source area, with the tower at its center. On the tower, the downward sensor element of the radiometer projects a field-of-view onto the surface with the radius of this radiative source area given by Equation 2.4:

$$r = \left(\frac{1}{F} - 1 \right)^{-1/2} \qquad [2.4]$$

where F is the view factor and r is the radius of the circular surface disc (Reifsnyder, 1967). The source area therefore remains fixed unless the radiometer is physically moved to another mounting height.

2.2.2.2 Turbulent source areas

Source areas or 'footprints' of entities carried by turbulent transfer of heat mass and momentum, (for example, Q_H and Q_E and CO_2) are more complex and dynamic. In this case the sensor is influenced by a spatially averaged contribution of an elliptical surface patch located upwind from the tower. However, the size and position of turbulent source areas change as the wind direction and stability vary through the day. In the urban environment the measured signal is then the integrated response of an array of buildings, roads, and vegetation. The typical dimensions of a source area isopleth are illustrated in Figure 2 - 3. The source area extends upwind from the tower to a distance that depends on the wind speed and direction, atmospheric stability and surface roughness (Schmid, 1991). This upwind edge may be anywhere from a few hundred to several kilometers upstream.

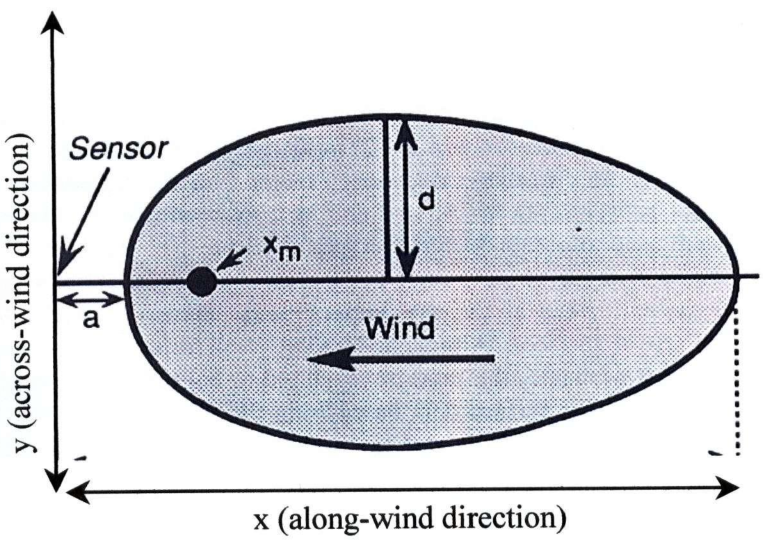

Figure 2 - 3 Plan view of the dimensions of a turbulent source area isopleth. x_m: maximum source location, a: downwind edge; and d: lateral half-dimension of the source area. (Schmid, 1991)

For unstable conditions, the size of the source area that contributes to half of (50%) the total surface effect experienced by the sensor can be approximated using the following equations (Schmid *et al.*, 1990):

$$\psi(z_s/L, p) = (1 - p \cdot z_s/L)^{1/4} - 1 \qquad [2.5\ a]$$

$$x_m \cong 1.7 \cdot z_s^{1.03} \cdot [\ln(z_s/z_o) - \psi(z_s/L, 76)] \cdot (1 - z_s/L)^{-1/2} \qquad [2.5\ b]$$

$$e_{0.5} \cong 7.7 \cdot z_s^{0.96} \cdot [\ln(0.23 \cdot z_s/z_o) - \psi(z_s/L, 30)] \cdot [\ln(-L)]^{-1/2} \qquad [2.5\ c]$$

$$d_{0.5} \cong 0.24 \cdot z_s \cdot [6 + \ln(z_s/z_o)]^{-1/2} \cdot [\ln(-L)]^{4/5} \cdot \sigma_v/u_* \qquad [2.5\ d]$$

$$a_{0.5} \cong 0.335 \cdot x_m \qquad [2.5\ e]$$

$$Ar_{0.5} \cong 0.47 \cdot \pi \cdot (e - a) \cdot d \qquad [2.5\ f]$$

where Equation 2.5 a is an auxillary expression which needs to be evaluated with the appropriate p for each equation and z_s is the sensor height (units m), L is the Obukhov length (units m), z_o is the roughness length (units m), x_m is the distance from sensor to the maximum source location (units m) and $e_{0.5}$, $d_{0.5}$, $a_{0.5}$ are the upwind, downwind and lateral dimensions of the P=0.5 source area respectively (units m). $Ar_{0.5}$ is the respective surface area (units m^2), σ_v is the standard deviation of the lateral wind fluctuations (units m s^{-1}), and u_* is the friction velocity (units m s^{-1}).

The size of the source area varies from small, when the atmosphere is very unstable (convective activity is able to convey entities readily upward), to large when it is stable (convection suppressed). Therefore, due to the diurnal variation of atmospheric stability large nocturnal source areas are expected as a result of stable atmospheric conditions and low wind speeds. Throughout daylight hours the source areas are smaller and more variable due to greater convective mixing and increased wind speeds.

It is desirable to have a homogeneous region surrounding the tower so that the character of the surface inside the source area is similar regardless of the wind direction. In the case of an urban environment it is often a challenge to find such a site. We are looking for a region that is fairly spatially homogeneous, for example, most buildings are of the same height, backyards and roads are of similar dimensions. It is also desirable to select a site with fairly homogeneous surroundings to avoid advective influences from adjacent areas that are not of similar composition. In order to avoid horizontal advection effects the upwind fetch from the tower location must be on the order of a few kilometers (Roth, 1988).

2.3 Considerations for measurement of carbon dioxide

Due to controls exerted by anthropogenic emission patterns, solar radiation and temperature, soil biology, plant phenology and airflow, urban CO_2 concentrations vary with time of day, time of year, and location. Further urban factors provide additional challenges for the measurement and interpretation of F_C compared to Q_H and Q_E. The spatial heterogeneity of the sources and sinks of CO_2 in urban areas are not well known, but are assumed to be considerable given the patchy nature of the distribution of buildings, roads, and vegetation. Although F_C is measured in the inertial sublayer, where entities are expected to be well-mixed, changes in the character of turbulent source areas and corresponding source and sink strengths may have a large effect on the fluxes as the wind direction changes. If winds are from a direction that contains busy roadways and commercial districts the F_C from that source area may be higher than if the winds pick up the response of a quiet suburban residential area. It is also important to appreciate that source strengths continually change in response to human activity cycles, and therefore the source strength from even the same source area varies temporally over the courses of diurnal and annual cycles. For example, transport patterns cause roadways to contribute more to F_C during rush hours and heating demands in residential areas increase fluxes during the winter. The inherent spatial and temporal heterogeneity of CO_2 fluxes may necessitate the use of an even greater height of measurement than normal. In this way it might be possible to obtain an integrated response from a larger surface source area, or it may require filtering the flux data by wind direction to facilitate analysis and interpretation.

2.4 Climatology of the study region

The measurement site is located in a suburb of Vancouver, British Columbia. The city of Vancouver is situated at the mouth of the Lower Fraser River Valley, which is V-shaped (Figure 2 - 4). The city of Vancouver is topographically bounded by the Coast mountain chain 13 km to the north, and the Cascade mountain range over 40 km to the south. To the west, Vancouver is separated from the open Pacific Ocean by the Straight of Georgia and Vancouver Island.

Figure 2 - 4 Lower Fraser River Valley. Urbanized areas are bounded by mountains to the north and the south and by water to the west.

The climate of Vancouver is characterized by airflow from the east throughout the year due to topographic channeling and the sea breeze system. Upper level flows are the strongest in the winter when the equator-pole temperature gradient is the largest, and weakest in the summer when the gradient is reduced. High-pressure systems are seen throughout the year, but dominate in the summer months when the subtropical high strengthens and moves northward towards Vancouver. These anti-cyclonic systems bring periods of warm, sunny weather. Usually in September or October there is a shift in weather patterns, and cyclonic activity begins to dominate as cold arctic air expands southward, and the subtropical high weakens and contracts. Low-pressure storm tracks dominate throughout the winter and into spring, frequently dousing the region with high amounts of precipitation and stronger winds. The moderating effect of the ocean ensures the city and surrounding region rarely get snow despite close proximity to surrounding mountain terrain. Temperatures are the lowest in January and reach a maximum in July and August (Oke and Hay, 1998).

Airflow reaching Vancouver is predominantly from the Pacific Ocean, and it has therefore been only weakly influenced by anthropogenic emissions from Vancouver Island, situated 35 km to the west, across the Straight of Georgia. Land-sea breeze circulations occur throughout the year, but are most common during the summer months when high-pressure systems dominate and the land/sea temperature gradient is the largest. A sea breeze usually builds within 4 hours of sunrise and breaks down within 1-2 hours after sunset. After sunset there is a shift in wind direction and a nocturnal land breeze returns air back towards the ocean. Mountain valley circulations also facilitate air transfer back into the urbanized valley area.

In Vancouver, the climatology in the lower layers is influenced by topography, urban development, and proximity to water bodies (Oke and Hay, 1998) producing differing weather conditions and changing microclimates. Due to the microscale complexity of urban areas a field program to measure climatological variables must be carefully designed. Details of the field program used for this study are presented in the following sections.

2.5 Site description

The measurement site (Sunset) is located near the corner of Knight Street and 49th Avenue (49° 16' N, 123° 06' W) within the confines of a BC Hydro substation (Figure 2 - 5). A 30-meter open construction lattice tower stands in the southeast corner of the substation, with its base recessed 5 m below the level of the surrounding ground.

Topography surrounding the tower is relatively even with only slight undulations and a gentle slope southward towards the Fraser River. Within a 2 km radius, the urban structure is approximately 80% suburban, low density, 1-2 story housing with an average building height of 8.5 m. Most lots have a front lawn, a few trees, and shrubbery. Vegetation is only partially irrigated during the drier summer months due to water restrictions. In addition to residential uses, the surrounding region includes a school building with gravel play yards 100 meters to the east, commercial and industrial districts 1-2 km to the south, a park and cemetery 0.75-2 km to the northwest, and the busy 49th Avenue and Knight Street intersection 75 meters to the southeast (Figure 2 - 6 and Figure 2 - 7). Knight Street is now designated as the main north-south truck route into downtown Vancouver. Knight Street carries between 38,000 and 55,000 vehicles per day (City of Vancouver, 2003).

More specifically, the measurement site can be characterized in terms of (a) the plan-area vegetated (trees, grass, etc.), (b) the plan-area impervious (concrete, asphalt, roads, parking lots, sidewalks, etc.), and (c) the three-dimensional surface area of the buildings, subdivided into the area of roofs and walls (Grimmond and Oke, 1999a). The surface area (A_C) can then be calculated using the following equation:

$$A_C = A_V + A_I + A_R + A_W \qquad [2.5]$$

where A_V is the plan-area vegetated, A_I is the plan area of the impervious ground, A_R is the area of the roofs and A_W is the surface area of the walls. Values for the Sunset site are presented in Table 2 - 1. The ratio of A_C to A_P (total plan area) is a measure of the three dimensional morphology of the site (Grimmond and Oke, 1999a).

Table 2 - 1 Fractions of surface cover for the Sunset site (A_C, A_V, A_I, A_R, A_W defined in text) for a circle with a 5 km radius centered on the tower (Grimmond and Oke 1999a).

Wind Directions Analysed	Urban Climate Zone	A_V	A_R	A_I	A_W	A_C/A_P
0-360	3	0.33	0.22	0.17	0.29	1.42

Additionally, in order to characterize the surface geometry, the active surface exposed to oncoming flow, called the frontal area index (λ_F) can be used. This variable combines mean height, breadth and density of the roughness elements. Further details on the calculation of the frontal area index are discussed in Grimmond and Oke (1999b). For the Sunset site, λ_F is 0.19, based on the assumption that surface elements have not changed significantly since 1992 when a detailed surface inventory of the area encompassing the Sunset site was conducted by Grimmond (1992). The canyon aspect ratio (λ_S), which is defined as the ratio of the canyon height to the street width, is also a fundamental property of surface morphology. The Sunset site has a λ_S of 0.90 (based again on 1992 data). Additional details on surface cover fractions and surface morphology ratios, including comparison of these values with values from other sites, are available in Grimmond and Oke (1999a and 1999b). The aerodynamic roughness length (z_o) ranges between 0.4 and 0.7 m with an average of 0.5 m (Steyn, 1985); the zero-plane displacement length (d) is approximately 4.5 m based on morphometric analysis of the urban geometry (Grimmond and Oke, 2002). The suburban area extends at least 1.5 km in all directions from the tower giving relatively homogenous fetch. A study at the Sunset site by Steyn (1985) indicated that horizontal advection is not a concern.

Oke (2004) has defined a simple classification of urban forms based on roughness length, aspect ratio and percentage built (or impermeable surfaces). This classification system, termed the

Urban Climate Zone classification (UCZ) is discussed in detail in Oke (2004)). The Sunset site falls into UCZ 5, as defined by the following parameters:

- Description: medium development, low density suburban with 1 or 2 storey houses.
- Roughness class: 6 "Very Rough" (Davenport classification (Davenport *et al.*, 2000)) (z_o is ~0.5 m at the Sunset site).
- Aspect ratio: 0.2 - 0.6, up to >1 with trees (aspect ratio of 0.9 at Sunset site).
- % Built: 35-65 (34% built (buildings and impervious surfaces) at Sunset site (Cleugh, 1990)).

Figure 2 - 5 Location of Sunset tower site in Vancouver (head of arrow). Downtown Vancouver is located in the top left corner of the map. North is approximately vertical (MapQuest, 2002)

The Sunset site was chosen, in part, due to the presence of the measurement tower. In addition, studies have been conducted at this site since 1980. Previous climatological studies by Kalanda (1979), Steyn (1980), Grimmond (1988), Cleugh (1990), Roth (1991), and Reid (1995) provide a historical database of measurements and information from this site. Also, this particular suburban district has terrain and urban development that are characteristic of much of suburban Vancouver and suburbs of other North American west-coast cities.

Figure 2 - 6 Airphoto of the area surrounding the site. Tower location is marked with an X (City of Vancouver, 2002).

Figure 2 - 7 Photographic view looking to the south from the top of the tower.

2.6 Instrumentation

2.6.1 Fast response instrumentation

For implementation at the Sunset Site, a Solent Gill 3-dimensional asymmetric sonic anemometer was used to measure the u, v and w wind components. A Li-cor Model 7500 (LI-7500) infrared gas analyser was used to measure concentrations of CO_2 and water vapour. The LI-7500 gas analyzer is a high speed, high precision, open path CO_2/H_2O gas analyser that accurately measures absolute densities of CO_2 and water vapour of air as it passes through the optical path of the sensor. Features of the LI-7500 include high precision, low noise, stable calibration, and low power consumption, making it an ideal candidate for long term monitoring. The LI-7500 is an absolute analyser, meaning that as air passes through the open path of the sensor head the absolute densities of CO_2 and H_2O are calculated from the difference in absorption of infrared radiation between the source and the detector. A control box houses the analyser electronics and connectors in a weatherproof enclosure. Sealed external connectors on the box allow access for power, the RS-232 and DAC outputs, analogue inputs, and the Synchronous Device for Measurement (SDM) port. All turbulent entities were sampled at 10 Hz throughout the measurement period.

2.6.2 Slow response instrumentation

The temperature and relative humidity (RH) of the air were measured by an HMP35A capacitance sensor. The radiation balance components of interest included K↓, K↑, L↓, and L↑. These variables and were measured by a CNR1 Kipp and Zonen Net Radiometer. An RM Young wind vane and cup anemometer (wind sentry) was installed to monitor wind speed and direction as a backup to the sonic anemometer. Surface wetness and atmospheric pressure were also measured at ground level but proved unreliable and the data was not used. Precipitation observations were collected at the University of British Columbia climate station near Totem Park, by the Soil Biometeorology group, using a tipping bucket rain gauge.

2.7 Mounting arrangement

Instruments were mounted on the Sunset tower and run continuously from August 2001 to December 2002 in order to capture an array of conditions and seasonal variations. Instruments were mounted at two levels. The LI-7500 and sonic anemometer were mounted adjacent to each other 27.0 m above ground level. Instruments were mounted on a boom so that they sat 1.8 meters upwind from the tower thereby avoiding wake interference from the tower itself. Spacing between the eddy covariance instruments was 0.5 m from August 2001 – July 30, 2002 and 0.2 m from July 30, 2002 – December 31, 2002. The instruments were moved closer together to confirm that lag effects were not an issue. The set-up with the 0.2 m spacing arrangement is shown in Figure 2 - 8. According to Baldocchi *et al.* (2000) and Meyers (2001), the distance between the middle of the sonic anemometer and the carbon dioxide sensors should be less than 0.5 m to minimize flow distortion and lag effects. Both set-ups were within this range. The wind sentry was mounted slightly higher than the sonic and the gas analyser, at a height of 27.8 meters above ground level. The radiometer was originally mounted at 20.1 meters, but was moved to a higher location (27.8 meters) on August 22, 2002 to eliminate shadowing on the instrument from the tower. The temperature and humidity instruments were mounted at 20.1 meters.

The effective instrument height (z') was calculated using the following equation:

$$z' = z - (E + d) \qquad [2.6]$$

where z is the actual height above ground level (m), E is the height the tower is recessed below the surrounding terrain (5 m) (Figure 2 - 9) and d is the zero plane displacement (m). The value of d for the site is approximately 4.5 m, based on estimates of land-use reported in Grimmond and Oke (1999b). The effective heights and the arrangement of the instruments on the tower are presented schematically in Figure 2 - 10.

Figure 2 - 8 The mounting arrangement of the LI-7500 (right) and the Gill sonic anemometer (left).

Figure 2 - 9 Photograph of the Sunset tower. At the base, on the right, is the camper that housed the computer.

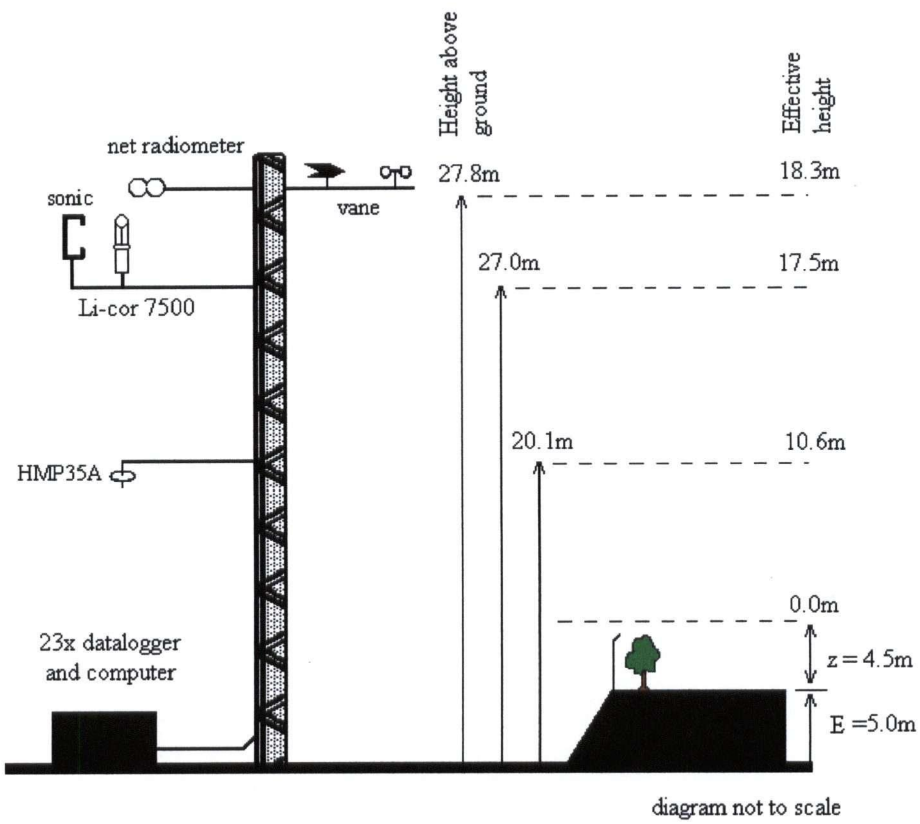

Figure 2 - 10 Schematic diagram of the tower set-up and the effective instrument height.

2.8 Operational routine

The Sunset site was maintained regularly from August 2001 through until December 2002. A more intense routine was carried out in the summer and fall of 2002, to ensure accurate data during periods of cloudless skies and the dry conditions that prevailed during this period. When scheduling allowed, the site was visited three times a week to ensure that the computer, datalogger and instruments performed well.

2.9 Data acquisition and processing

2.9.1 Logging

A permanent on-site computer was located within a camper at the base of the tower. All data (except that from the sonic anemometer) were recorded on a Campbell Scientific Inc. 23X datalogger housed in the same camper. Fast response data were automatically downloaded from the datalogger to the computer every 30 minutes. The slow response instruments were sampled at 5-second intervals and data were automatically downloaded every 24 hours to the computer. Sonic data was fed directly into the computer and stored adjacent to the LI-7500 infrared gas analyzer data in two separate hourly files. Software to run this system was designed by C.S.B. Grimmond and B. Offerle (Atmospheric Science Research Group at Indiana University (IU)) and adapted to run at the Sunset site.

2.9.2 Processing

Raw sonic and LI-7500 data was sent to IU for flux calculations. Eddy covariance fluxes were calculated based on methods described in Schmid *et al.* (2000, 2003), Offerle *et al.* (2003) and Schmid *et al.* (2004). 10 Hz data were block-averaged for one hour periods. All data presented are based on one-hour averages with the time stamp indicating the end of the hourly period. Times are local time, labeled as Pacific Standard Time (PST).

Processing of data using IU resources provided assurance of data quality control and accurate flux calculations. F_C data can be calculated in a number of ways depending on software and procedures. The processing at IU ensured standardized procedures used by many national and international F_C sites were followed. After completion of flux calculations, the data were examined for daily, weekly and seasonal trends.

Limitations and difficulties

2.9.3 Data loss

There are a number of ways in which data can be lost when attempting to gather a full year of data. The largest loss is often a result of precipitation, which in Vancouver, resulted in large data losses, especially during the winter months. Precipitation disrupts the optical path of the open-path infrared gas analyser and the path between the sonic transducers. Also, pooling of precipitation on the LI-7500 lower sensor window prevents continuous measurements thereby leaving gaps in the data. To minimize this the LI-7500 was mounted at a slight angle (< 5 degrees from the vertical) and RAINEX was sprayed on the sensor windows to prevent water from pooling. Regardless of these preventative measures gaps in the data are present when rain fell.

Gaps in the data also occur when the LI-7500 instrument was removed for calibration in the laboratory. Although the LI-7500 calibration is fairly stable, calibration was performed before the observation period began as well as on November 26, 2001, March 14, 2002 and November 21, 2002. In all instances the calibration was considered good, meaning there was little drift or variation from the previous calibration. Calibration was conducted in the Biometeorology Laboratory at UBC and the period between removal from the tower to re-installation took anywhere from two days to a week depending on laboratory availability and appropriate weather conditions for mounting. Calibration of the LI-7500 involved the use of gas samples of known concentration to span and zero the CO_2 readings. A dew-point generator was also used to produce a predetermined relative humidity against which the instrument was compared.

Other difficulties that produce gaps in the data include power outages, and computer problems. Computer software and hardware have the potential to fail at any point and hence, there is always a potential for data loss. During the measurement period two hard drives 'crashed' resulting in loss of data. There are also random acts that can disable parts of the system. Possibilities include vandalism or theft of instruments, or interference by birds or other wildlife that can damage sensors or cable lines. Wind, ice, snow storms or lightning during inclement weather can also create problems resulting in lost data. During the measurement period there were a number of events that caused a loss of data including power outages, wind storms, and intense rain. Data collection for one year often results in only 65% to 75% of data recovery due to system failures or data rejection (Falge *et al.*, 2001). In this study, for the year 2002, 70% of the data is considered usable, but further cleaning of the data reduced this percentage to 48%.

3 Results and Discussion

3.1 Meteorological conditions during the project

Environment Canada Climate Normals (1971-2000) compare well with temperatures recorded in 2002 at the Sunset site (Table 3 - 1), indicating that overall thermal conditions were not significantly abnormal in 2002. Examination of the 10-day running mean temperature over the year shows the coldest temperatures during late January (~YD 25) and during a period in March (~YD 60-80) (Figure 3 - 1 (a)). Temperatures steadily rise to a peak around mid-July (YD 200). Note that daily average temperatures do not fall below zero at any time during 2002.

The seasonal trend in precipitation is given in Figure 3 - 1 (b). Since precipitation was not measured at the Sunset site data from the UBC Totem Park climate station (15 km to the west) was used as the most representative data set. 2002 was drier than average for Vancouver with a total of 857.6 mm compared to the Environment Canada Climate Normals (1971-2000) annual total of 1199.0 mm indicating that, in 2002, Vancouver received only about 72% of the normal precipitation input. All months, except January, had lower than average precipitation (Table 3 - 1). August and October had extremely low precipitation with monthly totals of only 5.8 and 18.3 mm, respectively, compared to precipitation normals of 39.1 and 112.6 mm (Table 3 - 1). In attempts to conserve the municipal water supply, watering restrictions were put in place early in the summer of 2002 causing vegetation, particularly grass, to turn brown early in the growing season. In a normal year about 300 mm of water is added to the external environment via garden irrigation and swimming pools (Grimmond and Oke, 1986) but it is possible that this value may have been lower in 2002 due to the watering restrictions.

(a)

(b)

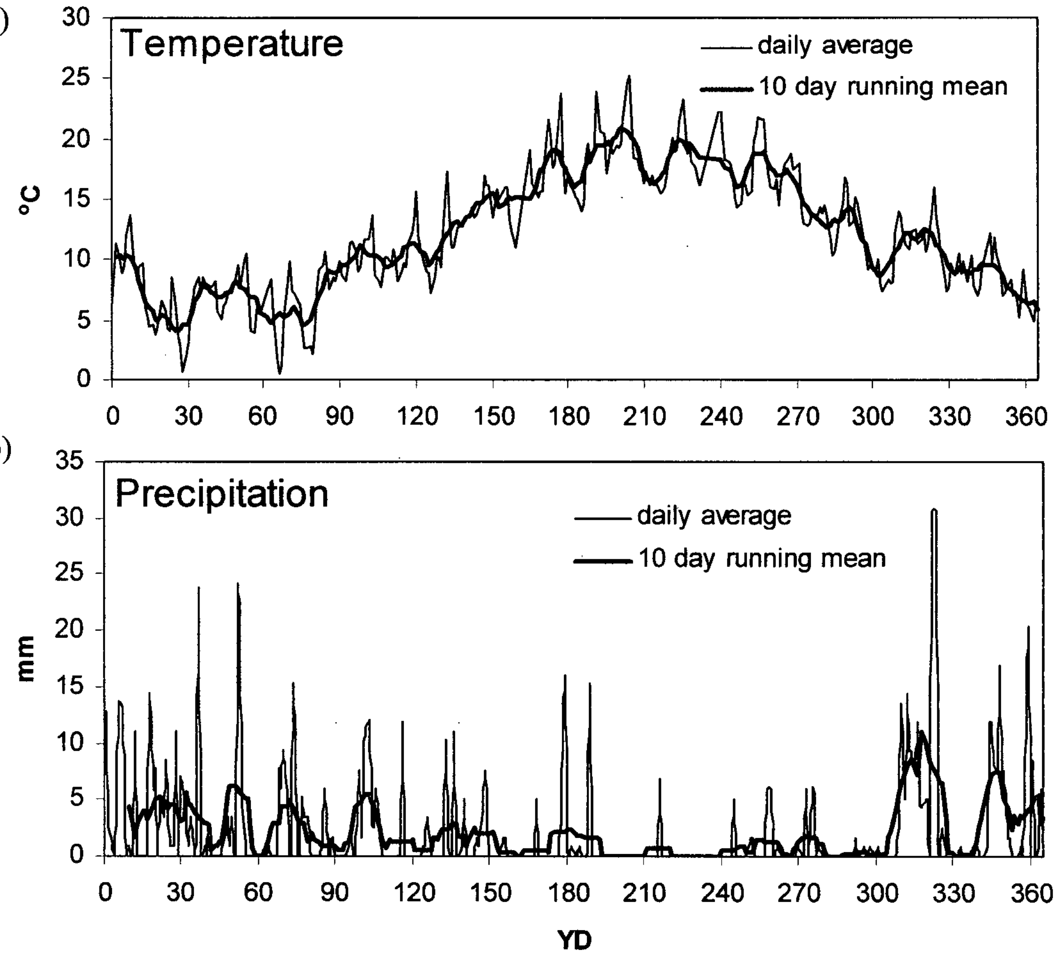

Figure 3 - 1 (a) Seasonal temperature trend for 2002 (data from Sunset site). (b) Seasonal precipitation trend for 2002 (data from Totem Park meteorological station, UBC). The thin and thick lines represent the daily average and the 10-day running mean, respectively.

Table 3 - 1 Average temperature and total precipitation for 2002. To allow for direct comparison, all data are taken from the Environment Canada Vancouver International Airport climate station (less than 15 km from the Sunset site). Monthly precipitation and temperature data for 2002 are compared with Environment Canada Climate Normals (1971-2000). (Environment Canada, 2004).

Month	**Average Temperature (°C) (2002)**	**Average Temperature (°C) (normal)**	**Total Precipitation (mm) (2002)**	**Total Precipitation (mm) (normal)**
January	4.2	3.3	161.5	153.6
February	4.8	4.8	103.3	123.1
March	4.3	6.6	67.1	114.3
April	8.7	9.2	82.3	84.0
May	11.7	12.5	51.5	67.9
June	16.4	15.2	30.8	54.8
July	17.9	17.5	15.2	39.6
August	17.9	17.6	5.8	39.1
September	15.0	14.6	34.6	53.5
October	9.7	10.1	18.3	112.6
November	7.7	6.0	147.7	181.0
December	5.3	3.5	139.5	175.7
Sum of Precipitation			**857.6**	**1199.0**
Mean Temperature	**10.3**	**10.1**		

3.2 Analysis of data quality

Removal of data from the CO_2 and energy flux databases was necessary during times of precipitation. Removal of data was unavoidable due to interruption of the infrared gas analyzer signal by raindrops that caused data spikes and unrealistic values in the CO_2 and H_2O signals. In order to determine when the gas analyzer signal may have been interrupted, precipitation data from the Totem Park UBC climate station was utilized. However, due to the high spatial variability of precipitation it was difficult to determine precisely when rainfall occurred at the Sunset site. To maximize the accuracy of the data set, days with greater than 1.0 mm of recorded precipitation were removed. Removal of data during times of precipitation is a standard procedure for open path infrared gas analysers (Baldocchi *et al.*, 2001).

The overall radiation flux coverage was very good (90.5% of the whole year). Removal of data from CO_2 and energy flux datasets resulted in low data coverage for many months, especially in the winter. In January, November and December only 23.7, 15.8 and 31.7% of the total data coverage was realized. In July and October, when precipitation totals were low, higher data coverage (86.0 and 65.7%, respectively) was achieved. Overall, for the CO_2 and energy components respectively, 48.3 and 47.9% of the data was useable for the year 2002.

Table 3 - 2 Data coverage for radiation, energy and CO_2 flux datasets for each month in 2002 at the Sunset site. N = number of hours of data per month, % = percentage of total data coverage.

Month	Radiation Fluxes		Energy Fluxes		CO_2	
	N	%	N	%	N	%
January	696	93.5	176	23.7	176	23.7
February	659	98.1	304	45.2	304	45.2
March	719	96.6	268	36.0	268	36.0
April	677	94.0	293	40.7	293	40.7
May	725	97.4	403	54.2	403	54.2
June	551	76.5	403	56.0	403	56.0
July	718	96.5	640	86.0	640	86.0
August	426	57.3	398	53.5	436	58.6
September	633	92.1	469	65.1	469	65.1
October	699	94.0	489	65.7	489	65.7
November	695	96.5	114	15.8	114	15.8
December	696	93.5	236	31.7	235	31.7
Year	**7924**	**90.5**	**4193**	**47.9**	**4230**	**48.3**

3.3 Radiation balance

3.3.1 Radiative source areas

As discussed in Chapter 2, the field of view of a radiometer is fixed and therefore always contains the same surface features regardless of wind direction or changes in atmospheric stability. Radiant source areas for the Sunset site net radiometer (z = 27.8 m, z' = 18.3 m) are 4.60×10^4 m^2 for a view factor of 0.95, and 1.62×10^5 m^2 for a view factor of 0.99 (Table 3 - 3), and are displayed graphically in Figure 3 - 2.

Table 3 - 3 Upwelling radiative source areas for the Sunset tower.

View Factor	Source area radius (m)	Source area (m^2)
0.95	121 m	4.60×10^4 m^2
0.99	227 m	1.62×10^5 m^2

Figure 3 - 2 Upwelling radiative source areas overlaid on an air photo of the Sunset site. The tower location is marked with a yellow X.

The surface features within the 0.99 view factor consist of a mix of surface covers consisting mainly of impervious ground cover, grass, and gravel substrate. Gravel surfaces occupy approximately one quarter of the 95% source area. These are located within the BC hydro substation compound directly below the tower, and in the nearby schoolyards (Figure 3 - 2). Impervious surfaces include the surrounding roadways, driveways, sidewalks, and roofs. The other dominant groundcover is grass, which through most of the year was not irrigated. Based on surveys conducted in the 1980s the surrounding area consists of 64% greenspace including lawns, gardens and parks; 24% buildings and houses; and 11% pavement (Cleugh and Oke, 1986).

3.3.2 Surface albedo

The mean surface albedo for 2002 at the Sunset site is 12.4% when all values of K↑ and K↓ are included in the calculation, or 12.0% when only values of K↑ and K↓ greater than 5 W m^{-2} are considered. The latter value is probably more reliable since horizon effects may become significant at low Sun angles. A typical suburban albedo is 15% (Oke, 1988). The slightly lower than typical albedo for the Sunset site may be a result of the gravel substrate located directly beneath the tower at the BC Hydro substation. This surface type is over-represented in the 95% radiation source area. Summer measurements from past studies at the Sunset site gave values of 13 to 15% (Steyn and Oke, 1980).

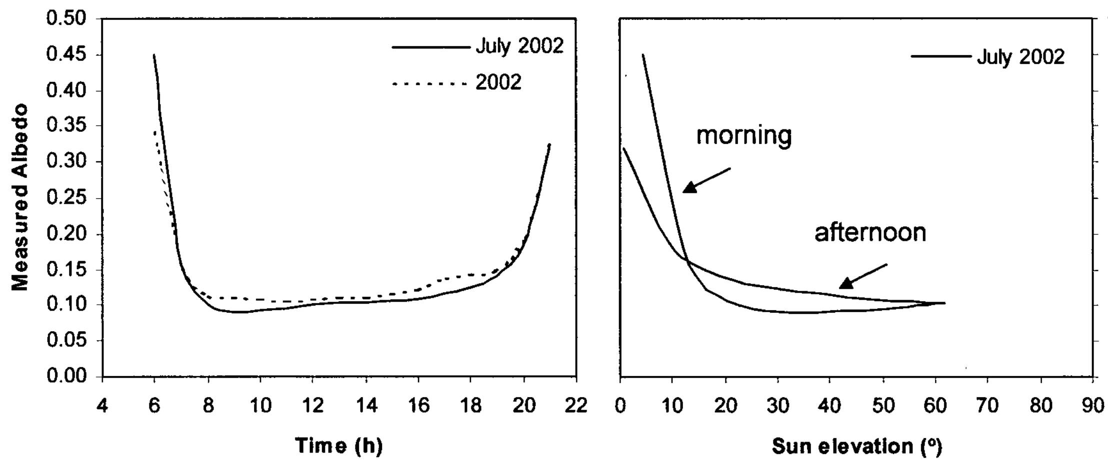

Figure 3 - 3 (a) Mean diurnal surface albedo for 2002 (dashed) and July 2002 (solid). (b) Angular variation in the average albedo in July 2002, assuming similar elevation of the Sun for the month.

The mean diurnal pattern of surface albedo for 2002 at the Sunset site (Figure 3 - 3(a)) is 'U'-shaped. This is characteristic of a number of urban, rural, complex, and simple surface types (Oke, 1987). There is a slight diurnal asymmetry to the curve with afternoon values being greater than morning values at the same zenith angle. Explanations for the asymmetry in the 'U'-shape include differences in the spectral composition of the incoming radiation, or the possibility that the net radiometer was not perfectly level. It is also possible that surfaces with very different albedo are encountered during the day as the Sun moves across the sky, and that orientation of surface structures may cast different shadows in the morning compared to the afternoon. Other studies have reported diurnal asymmetry, and have attributed this feature to persistent afternoon cloudiness (Newton, 1999; Grimmond *et al.*, 2004). This seems an unlikely explanation for the Vancouver results. The angular variation in the albedo is demonstrated for the month of July in Figure 3 - 3 (b). July was selected because it represents a period of low precipitation and therefore high data coverage. Additionally, day length is long in July and therefore, a greater range of solar elevations are captured. Sun elevation was calculated for July 15 and similar solar elevation was assumed for the month. There appears to be a dependence of albedo on solar elevation, especially when it is below 20°. Christen and Vogt (2004) measured suburban and urban albedos in Basel, Switzerland and attributed the strong angular dependence below 20° to the highly directional reflectance of the horizontal surfaces in an urban environment.

3.3.3 Surface temperature

The surface temperature was calculated from $L\uparrow$ using Equation 1.4 (see Chapter 1) and an assumed emissivity of 0.95 (Newton, 1999). Comparison of measured air temperatures with calculated surface temperatures for the year 2002 are presented in Figure 3 - 4. Before dawn the surface is slightly cooler than the overlying air due to radiative cooling during the nocturnal period. After sunrise the suburban surface heats quickly, peaking a few hours past noon. Air temperature lags behind surface temperature peaking in the late afternoon. As the Sun drops towards the horizon the surface temperature also drops and, as radiative heating decreases, heat stored during the day is slowly released back into the atmosphere. This release of heat contributes to the peak in air temperature in the late afternoon. Surface temperature and air temperature reach a similar magnitude near midnight.

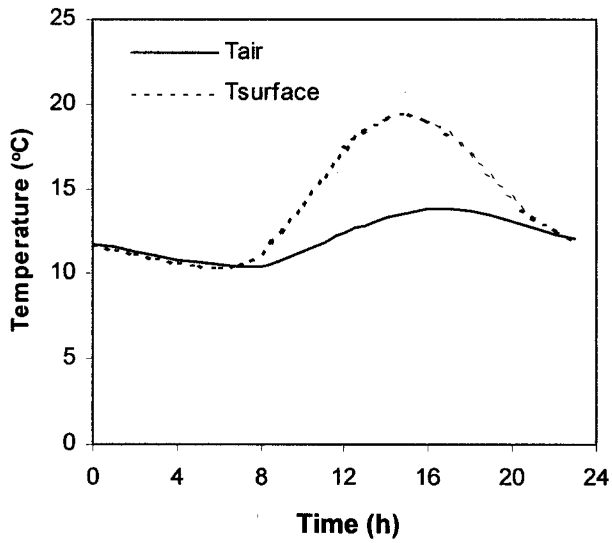

Figure 3 - 4 The diurnal cycles of surface temperature (Tsurface) and air temperature (Tair) for 2002. Surface temperature was calculated from L↑ using Equation 1.4 and an emissivity of 0.95.

3.3.4 Seasonal and diurnal trends in radiation budget component fluxes

Ensemble hourly averages of the radiation balance components are presented for each month in 2002 (Figure 3 - 5). Upwelling longwave and shortwave fluxes are plotted as absolute values. This is opposite to the micrometeorology convention where these fluxes are plotted as negative. As seen in Figure 3-5, the radiation balance is dominated by K↓ at both the diurnal and annual time scales. The ensemble average summer (May-Sep) maximum K↓ was 950 W m^{-2}, whereas in the winter (Jan-Apr and Oct-Dec) the maximum K↓ dropped to an average of 570 W m^{-2}. Low K↓ in the winter is a function of latitude and cloud cover. Winter months show signatures typical of mid-latitude conditions. During the winter, the region was doused with storms and rain and cloud cover greatly reduced the amount of K↓ reaching the surface. K↓ is also limited by day length in the winter. In the summer, days are longer and cloud cover is less prevalent resulting in higher levels of K↓. Summer months have signatures typical of mid-latitude, anti-cyclonic conditions.

L↓ was fairly constant through the year with a mean of 315 W m^{-2}. L↑ was slightly higher (mean of 368 W m^{-2}) than L↓ throughout the year. This result is expected, as the temperature of the surface is on average warmer than the atmospheric temperature. During the summer months, L↑ is slightly out of phase with Q*, peaking slightly after solar noon as a result of surface heating. In the winter when surface heating is low and as a result, the L↑ plot is essentially flat throughout the day.

The ensemble average diurnal course for 2002 and the annual course of the monthly radiation fluxes are given in Figure 3 - 6 (a) and (b). Results are similar to those presented by Christen and Vogt (2004) from an urban site in Basel, Switzerland.

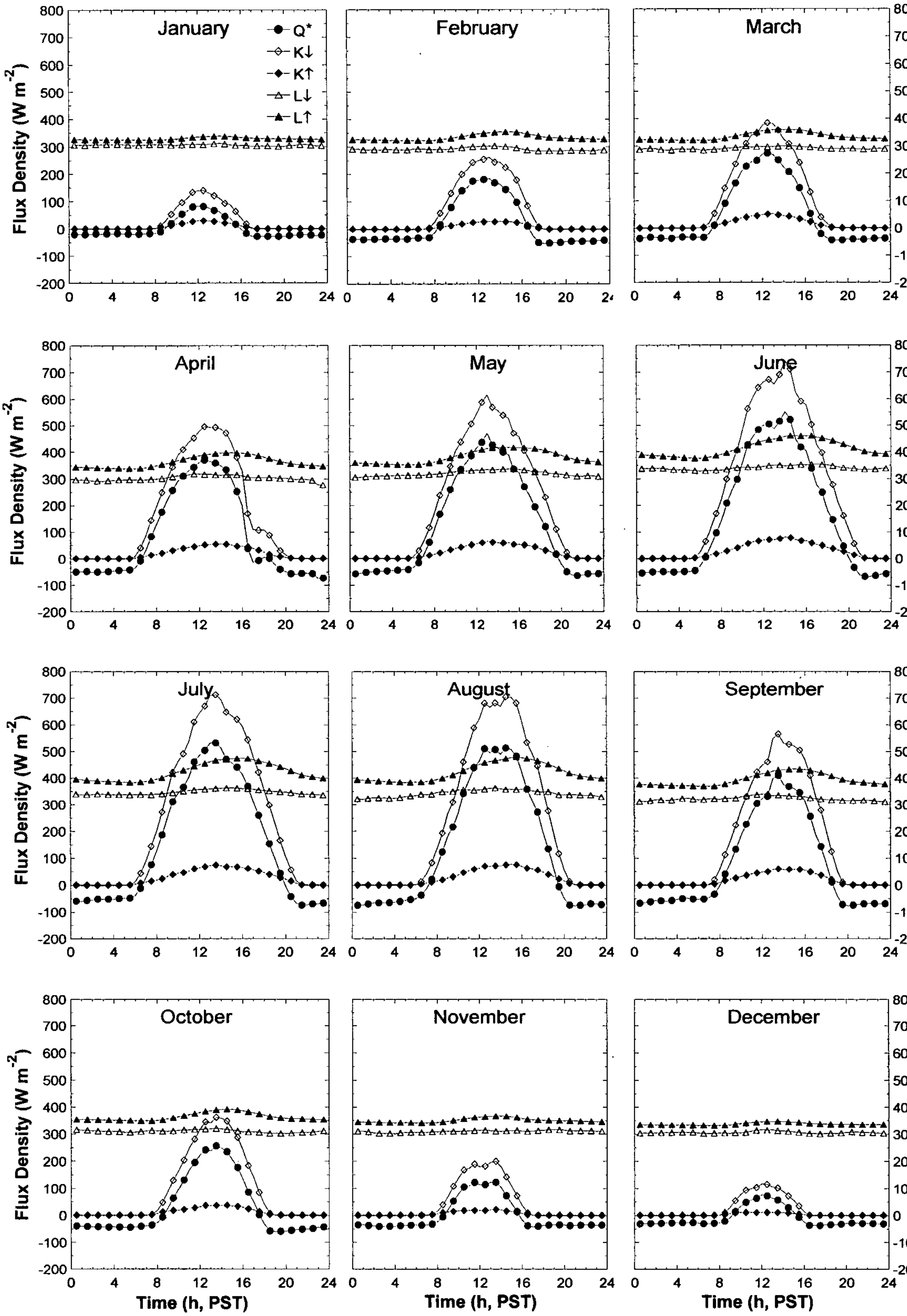

Figure 3 - 5 Ensemble diurnal (mean hourly) radiation balance components for each month in 2002. Absolute values are plotted.

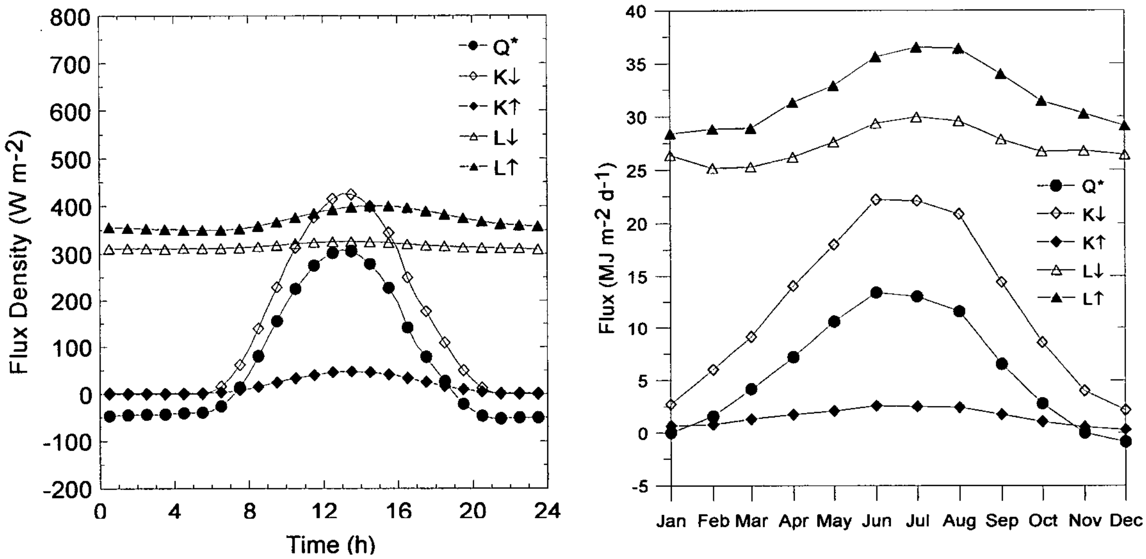

Figure 3 - 6 (a) Ensemble diurnal (mean hourly) course of radiation balance components for the year 2002, all sky conditions. (b) Annual variation in the monthly radiation balance components. Absolute values are plotted.

3.4 Energy balance

Energy fluxes have been measured at the Sunset site as part of several studies (e.g. Grimmond, 1992; Roth, 1991; Cleugh, 1990). Most studies have focused on a few weeks to a few months of data, primarily in the summer (with the exception of Grimmond, 1992, which spanned a winter and spring period). The year-long dataset here permits documentation of temporal changes in the energy balance components and their partitioning over the full annual range of synoptic and surface conditions.

3.4.1 Turbulent source areas

As discussed in Chapter 2, turbulent source areas change depending on atmospheric stability and wind direction. Although turbulent source areas were not calculated for this study, previous estimations for the Sunset site are included here for reference. Five sample source isopleths calculated over the course of a day are illustrated in Figure 3 - 7. Source areas were calculated using equations presented in the Section 2.2.2.2, and in Schmid *et al.* (1991). The isopleths presented in Figure 3 - 7 demonstrate typical temporal and spatial variability of source areas over complex terrain.

Since surface conditions have not changed considerably since the time of the Schmid *et al.* (1990) study, a description of the diurnal pattern of the source areas has been included here. The evolution of the source area isopleths over the day was consistent with the sea-breeze regime common to Vancouver. The source area at 8:00 Local Apparent Time (LAT) was calculated approximately 2 hours after sunrise. At this time the source area was relatively small indicating that convective activity was already well developed. The surfaces encountered in the 8:00 LAT source area include a neighbourhood commercial area and the Knight Street / 49th Avenue intersection. The 10:00 LAT source area was the smallest of the five indicating that at this time convective activity was at a maximum for the day. The 10:00 LAT source area consists mainly of residential housing. By 13:00 LAT the source area shifted west and the surfaces encountered included residential homes and a small park. As the day progressed the source areas shifted to the northwest and became larger as convection became weaker. The relationship between convection and the source area size is especially evident when the 14:30 and 17:30 isopleths are compared. The larger isopleth at 17:30 was a result of weakened convection.

It is important to note that the turbulent source areas illustrated in Figure 3 - 7 represent the 0.5-level source areas meaning that there is only a 50% chance that the elements inside these areas are affecting the sensors. Due to this limitation it is often difficult to correlate source areas with flux measurements. Additional details are available in Schmid *et al.* (1991).

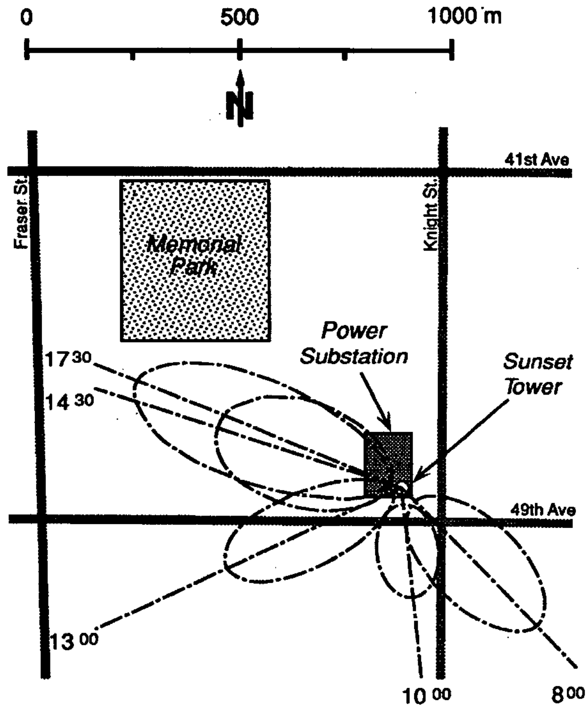

Figure 3 - 7 Evolution of the 0.5-level turbulent source area (5-hr average) calculated for the Sunset site during YD 86/231 (Schmid, 1991).

3.4.2 Estimation of anthropogenic heat

As mentioned in Chapter 1, recent discussions indicate that including an estimate for Q_F in the observed surface energy balance provides a more reliable calculation of ΔQ_S. In this study, approximation of Q_F was based on calculations presented by Grimmond (1992) for the Sunset site. Grimmond determined vehicular, metabolic and residential energy inputs to Q_F and created both temporal and spatial estimates. Here Grimmond's estimates of the diurnal Q_F cycle (Figure 1-2) have been simplified and its mean magnitude increased slightly to account for an increase in energy use and traffic over the last decade. This increase in the approximated Q_F is only a rough estimate. Values of 9 W m^{-2} and 15 W m^{-2} were used for the mean night and day values, respectively, and based on this, hourly values of Q_F were interpolated and are presented in Table 3 - 4 and plotted in Figure 3 - 8. Although slight seasonal differences may occur, they are expected to be only about 1-2 W m^{-2} and are neglected here.

Table 3 - 4 Estimates of anthropogenic heat (Q_F) for 2002 at the Sunset site.

Hours	Q_F (W m^{-2})
22-06	9.0
07, 21	10.5
08, 20	12.0
09, 19	13.5
10-18	15.0

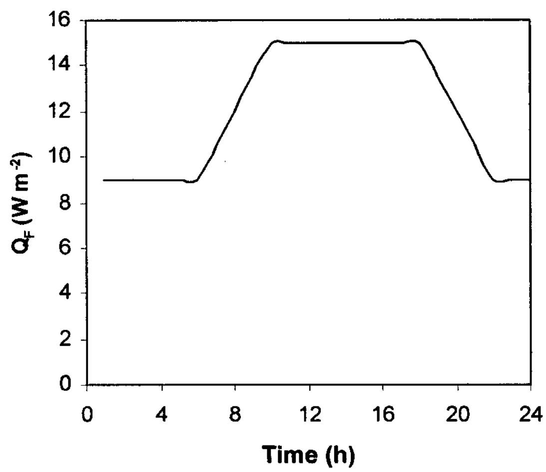

Figure 3 - 8 Estimates of anthropogenic heat (Q_F) for 2002 at the Sunset site.

3.4.3 Seasonal trends in the energy balance

The seasonal trends of Q_E, Q_H, and Q* are given in Figure 3 - 9. The 10-day running mean of the daily net radiation shows Q* to be slightly negative at the beginning of the year at approximately -25 W m^{-2}, and peaking near the end of May (YD 150) at 200 W m^{-2} when greater energy is available. Q* is variable throughout the summer, with large day-to-day variations in the daily averages. A gradual decline in the 10-day running mean begins in mid-August (YD 220), becoming slightly negative again by the beginning of November (YD 310).

Q_E exhibits very small or even negative values from the end of January (YD 30) to the beginning of April (YD 100). The reasons for these low evaporation values are unknown, although available energy is low at this time of the year, the surface is readily supplied with moisture. It is possible that the sensors on the tower were not operating correctly but many tests fail to reveal the reasons. It is also possible that low data coverage due to removal of rain data resulted in a further reduction in Q_E. This speculation casts doubt on the reliability of the data during this time period and it is not possible to draw useful conclusions from this data block. Examination of the results for the rest of the year reveals a peak in Q_E at the end of May (YD 150) of ~50 W m^{-2}. At this time radiation was relatively strong, water was available for evaporation, and vegetation was actively transpiring. Later in the summer, following a very dry July, when drought and an irrigation ban prevailed, Q_E values drop to ~20 W m^{-2} (YD 210). There is a slight rise from YD 240-260 (September) as water again becomes available, but there is a general decline in Q_E throughout the fall and into the winter as the available energy decreases.

The annual pattern of Q_H starts near zero in January, and approximately follows the course of Q*, peaking at the end of July (YD 210) at ~130 W m^{-2}. This peak in Q_H corresponds to a dip in Q_E, due to the extremely dry conditions. Q_H then gradually declines until the end of the year where is reaches a low of nearly 0 W m^{-2} in late December. There are no obvious anomalies in the sensible heat data from YD 30 to YD 100, as are evident in the Q_E record. This suggests the questionable data (mentioned earlier) may arise from the infrared gas analyzer, which uses measurements of water vapour to calculate Q_E.

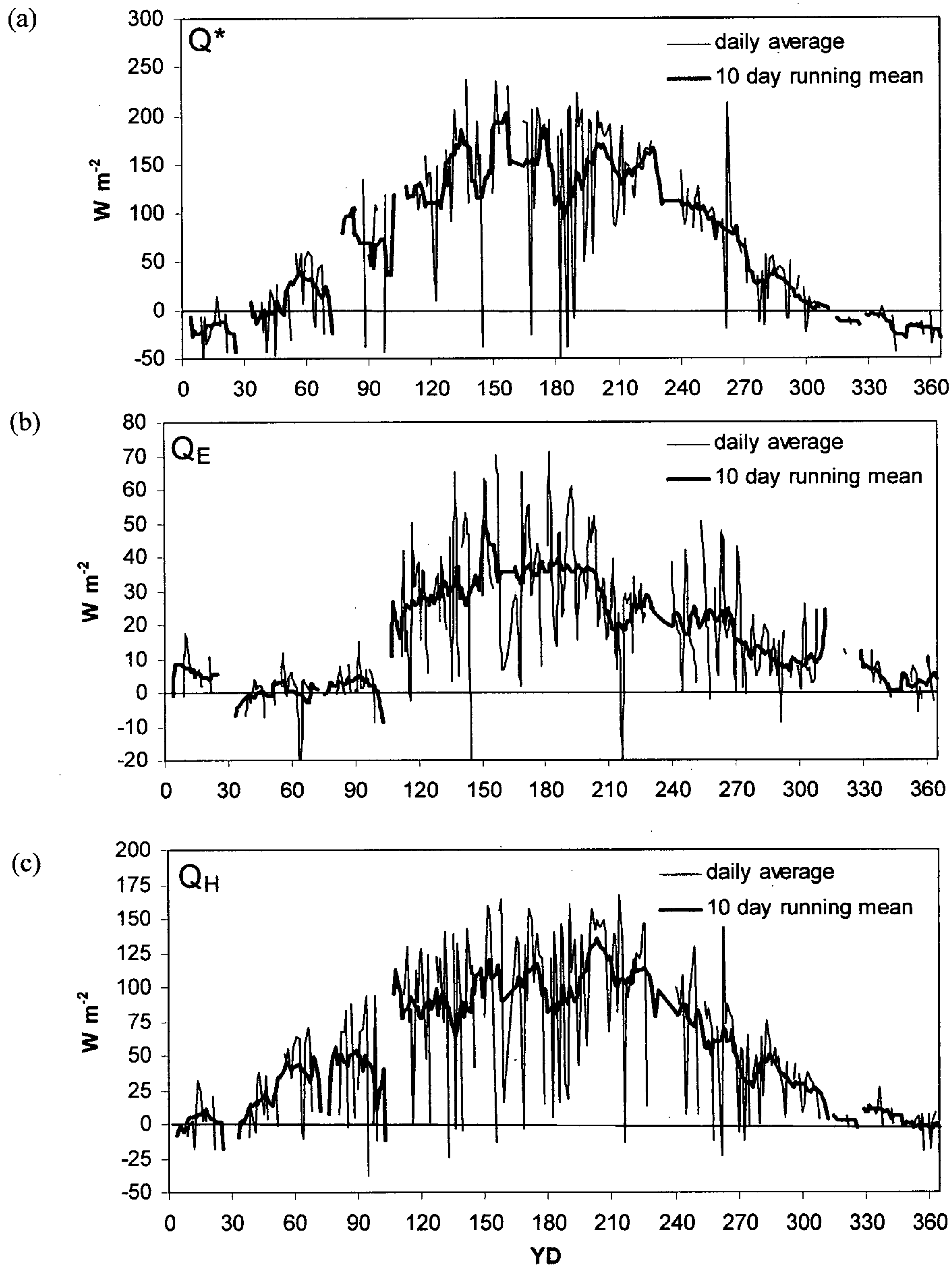

Figure 3 - 9 Seasonal trends in (a) net radiation (Q*), (b) sensible (Q_H) and (c) latent heat (Q_E) flux density (W m^{-2}). The thin and thick lines represent the daily average and the 10-day running mean, respectively. Note: variables have been plotted on different y-axes in order to best display the variability in the fluxes.

3.4.4 Diurnal trends in the energy balance

Diurnal ensemble averages of the energy balance terms were calculated from hourly data for each month (Figure 3 - 10). General trends at the diurnal time scale indicate that Q_H is the dominant term for most months, except in the winter and early spring when the ΔQ_S is equal or greater. Q_H tends to peak slightly after Q*. In the later afternoon and evening when Q* drops rapidly and becomes negative, Q_H becomes increasingly important. This is true at all times of year but is especially prevalent in the summer when positive heat convection (an upward flux) may continue until midnight. This is an almost singularly urban phenomenon that was first observed in Vancouver (Yap and Oke, 1974) and at this site (Kalanda *et al.*, 1980; Cleugh and Oke, 1986). It has since been observed at almost all urban sites around the world and tends to be most pronounced where urban development is greatest (Oke, 1988). This is due to the large release of heat stored in the urban fabric through the daytime. Q_H remains positive or close to zero during the night indicating a near-neutral surface layer probably exists up to the height of the instruments (Offerle, 2003). The variance of Q_H is largely explained by changes in the forcing by Q*. Linear regression of Q_H on Q* yields a good relationship, giving an R^2 value of 0.86 for the year ($Q_H = 0.51 \bullet Q^* + 31.90$) (data not shown).

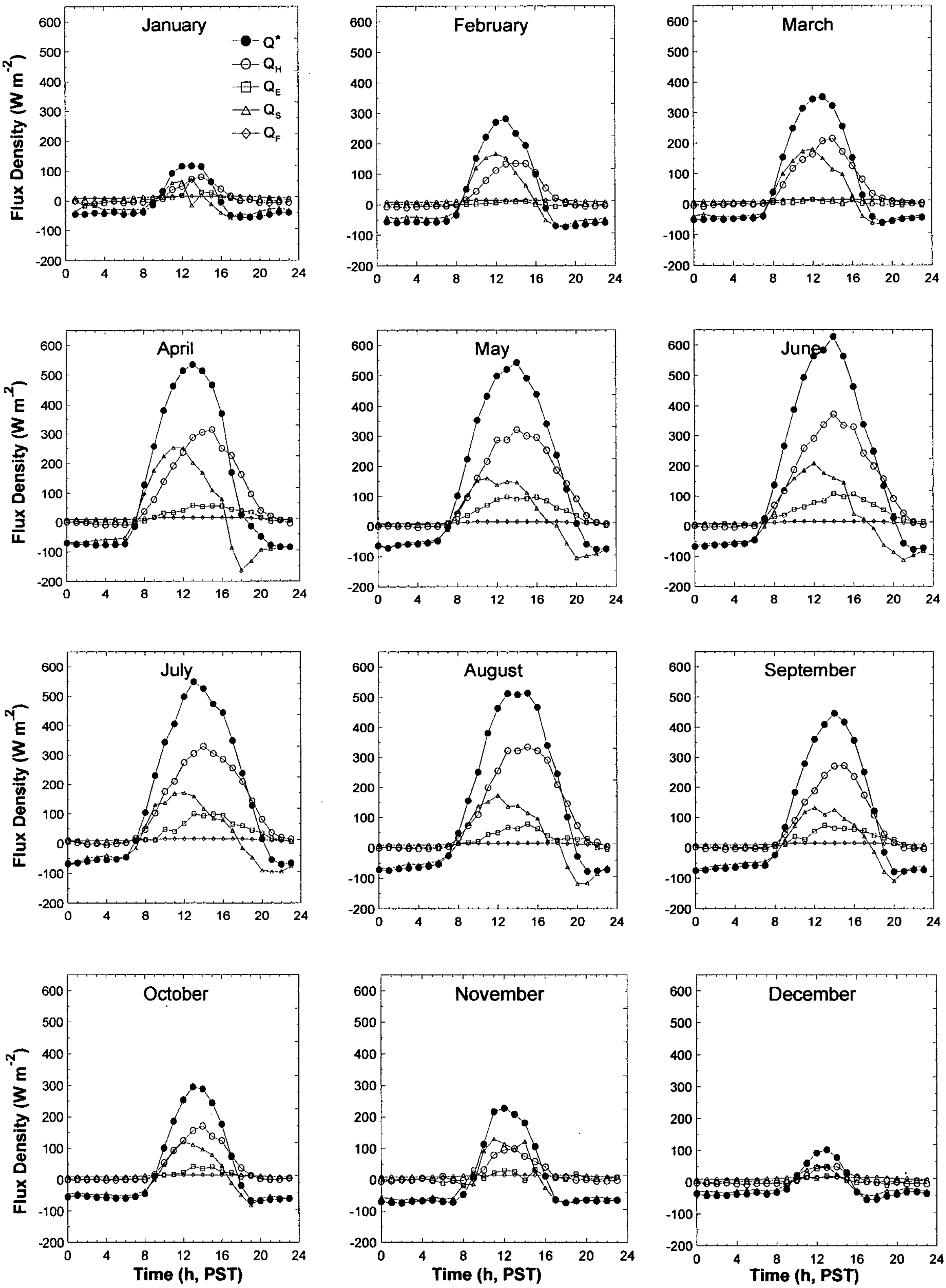

Figure 3 - 10 Ensemble mean diurnal energy balance components for the year 2002 (by month). Absolute values are plotted.

Q_E is generally fairly small, in part a result of the impervious ground cover (which channels water off the surface). But it must also be said that the evaporation is lower than has been seen at this site in most of the earlier studies. This is most likely due to the lower than average precipitation throughout the year of observation, the restriction of garden irrigation, and the inexorable conversion of soil and vegetation cover into impervious and non-transpiring uses. Dry conditions mean that energy is channeled into Q_H rather than Q_E. The low Q_E values (close to 0 W m^{-2}) throughout the winter (February and March) are somewhat surprising, and, as mentioned earlier, instrument error and/or very low data coverage and the removal of rain data in day blocks may be responsible. Whilst it is true that in February and March radiant forcing is low, surface wetness and good ventilation should be favourable. Even during the spring and early summer months when water energy should be available to cause sufficient evaporation, average mid-day values do not exceed 100 W m^{-2}. These values are lower than those reported by Grimmond (1992) at the same site. Throughout the year Q_E was small in the morning suggesting that dewfall and morning irrigation were not large contributors to evaporation.

Values of Q_H are significantly larger than Q_E throughout the year. There is a steady increase in the diurnal peak of Q_H from January (peak ~70 W m^{-2}) to June (peak ~370 W m^{-2}) with this peak decreasing from June back down to December (peak ~45 W m^{-2}). Throughout the year the diurnal peak in Q_H occurs slightly after solar noon, and slightly after the peak in Q^*, as expected. The monthly average diurnal cycles of the energy balance fluxes also indicate that Q_H is preferentially channeled into storage in the morning hours. This is commonly a very significant part of the urban surface energy balance. In the morning the mixed layer is relatively shallow and convective activity is somewhat restricted, thus favouring heat transfer into the urban materials by conduction. In the late morning and afternoon convection exceeds conduction as the favoured process for heat transfer. By mid- to late afternoon ΔQ_S reverses sign about two hours before Q* and contributes to the convective heat flux. This forms a temporal hysteresis (Figure 3 - 11), a phenomenon also reported by Christen and Vogt (2004) in Basel, Switzerland. To take this hysteresis effect into account, Grimmond and Oke (1991, 1999a) developed the objective hysteresis model (OHM) to estimate the diurnal course of ΔQ_S in urban areas.

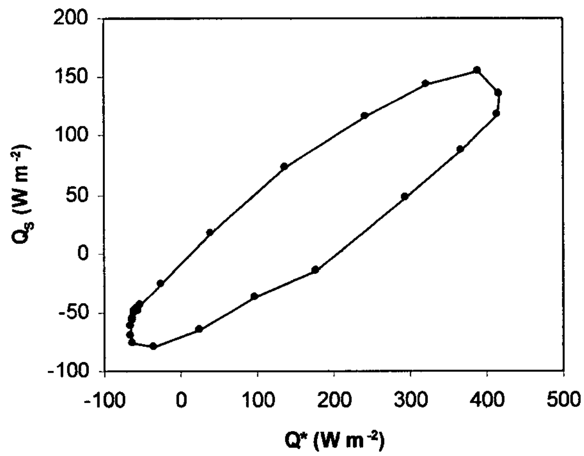

Figure 3 - 11 Diurnal pattern of heat storage (Q_S) plotted against net radiation (Q*) for the Sunset site in 2002. Results indicate a diurnal hysteresis loop; energy is preferentially channeled into storage in the morning and then released back into the urban atmosphere in the evening.

The release of ΔQ_S is the dominant non-radiative term in the nocturnal balance throughout the year. In the winter months ΔQs and Q* follow a very similar course from about one hour after sunset until sunrise (essentially $\Delta Qs \cong Q^*$ and the turbulent terms are small). But starting in April, and extending until September, ΔQs turns negative increasingly earlier than Q* in the afternoon. This late afternoon/early evening heat release is thought to slow the rate of urban surface cooling relative to rural surfaces, support the positive convective heat flux, and is a major reason for the growth of the near surface heat island and the absence of surface-based inversions in urban areas.

Of particular interest are the summer energy balance results because these can be compared with results from previous summer studies at the Sunset site. July results (Figure 3 - 10) look similar to those measured for summer periods in previous studies (Yap and Oke, 1974, Kalanda, 1979, Cleugh, 1986, Grimmond, 1998 and Roth, 1991) except that the role of Q_H appears to have increased and the role of Q_E decreased over the twenty-five year period of work at Sunset. It is difficult to be certain of this, given the inter-annual variability of the forcing conditions, but if true, it would be consistent with the tendency for continued development of building lots, lane paving and increase in vehicle traffic over time. It is also true, however, that over the period there has also been a change in the measurement technology. Commercially available eddy covariance equipment now provides direct measurement of Q_H and Q_E and it is no longer necessary to resort to the flawed flux-gradient methods (Roth and Oke, 1995). However, this reduces the precision with which direct comparison of results from different studies can be made.

3.4.5 Energy partitioning

Bowen's ratio (β) describes the partitioning of available energy (A) (where $A = Q^* - \Delta Q_S$) between the convective terms Q_H and Q_E and is calculated using the following equation:

$$\beta = Q_H/Q_E \qquad [3.1]$$

When the ratio is positive and greater than unity, more energy is used to heat the air rather than to evaporate water and vice versa when it is positive and less than unity. If β is negative one of the fluxes reverses direction. In 2002, for all-day (24h) and daytime ($Q^*>0$) periods, β was 3.63 and 3.90 respectively. Such a strong positive ratio indicates that at the Sunset site, Q_H is the dominant convective flux and evaporation of water is of lesser importance. This is not surprising considering the drier than average conditions for 2002. The data are further skewed towards Q_H due to the efficient removal of rain water from the surface in urban areas, which likely reduced both surface and subsurface water storage at the Sunset site. There is speculation that, like forests, urban areas might evaporate large amounts of water after wetting because of the short-term drop in the surface resistance and the large aerodynamic roughness. When wet, forests can evaporate at rates that are twice the net radiation (Oke, 1987). It is possible that the evaporation events following rainfall were not captured in the 'cleaned-up' data set at the Sunset site for 2002, due to the removal of data in day blocks. With a mean daytime β of 3.67, the 2002 Sunset results are outside the range of daytime β observed in other suburban areas (range 1.37-2.87) compiled by Grimmond and Oke (1999a). Christen and Vogt (2004) report an annual daytime urban β of 2.5.

When considering β for each month of the year, the values are often higher than expected (Table 3 - 5). β calculated here may be erroneously elevated due to the systematic removal of large latent heat flux values after rain events. Also, for some winter months only a few days of rain-free data remained in the analysis. This is especially a concern during the months of February and March 2002, which had β of 15.4 and 18.7 respectively. These values are a result of apparently exceptionally low latent heat fluxes that are possibly explained by the combination of low radiant forcing in combination with large data losses. Interestingly, in a suburban area of Tokyo, Japan, Moriwaki and Kanda (2004) report highest monthly daytime β for February and March (5.81 and 5.00 respectively), indicating that if a more complete data set was available for these months in Vancouver, high values may not be unexpected.

Table 3 - 5 Monthly ensemble daytime Bowen ratio (β) values for 2002

Month	**Bowen Ratio**
January	1.7
February	15.4
March	18.7
April	4.6
May	2.9
June	3.0
July	3.4
August	4.9
September	3.2
October	3.8
November	2.7
December	1.5
Year	***3.6***

Taking into consideration the limitations of the dataset, and ignoring the results for February and March, the Bowen ratios do follow expected seasonal patterns. High β values in April correspond to the change in season when available energy becomes large, but vegetative activity remains low (Christen and Vogt, 2004). Moriwaki and Kanda (2004) report values of 4.51 and 4.78 for April and September respectively, which are comparable to the April and August values from the Sunset site. Relatively high β values are also observed at the Sunset site throughout the summer due to the significant limitations on water availability experienced in 2002.

A fair comparison can be made between the β calculated during a dry summer period in 1992 that spanned from July 25th to September 18th (YD 206-261) at the same site (Grimmond and Oke, 1999a), with the month of July 2002 in this study. This was also a dry period with irrigation restrictions. Although the period in 1992 also included August and September, the data used for comparison are only from July 2002. This is because there was little precipitation during this period, meaning that removal of data was not necessary whereas in August computer failures prevented full data coverage. In 1992, the β was 2.72 (Grimmond and Oke, 1999a) and in 2002 it was 3.37. The values are both high for suburban sites and reasonably similar. The higher value in 2002 may be a result of the area becoming more built with an increase in impervious surfaces.

Additional statistics commonly used to gauge energy partitioning include Q_H/Q^* (χ), Q_E/Q^* (Υ), Q_S/Q^* (Λ) (fluxes normalized by the radiant energy). These ratios are presented in Table 3 - 6 for the year 2002, and for the month of July 2002, along with results from summer measurements made in 1992 at the same site (Grimmond and Oke, 1999a). All day (24h) and daytime only ($Q^*>0$) results are presented. When considering annual statistics, data including and excluding (in brackets) the months of February and March are presented. As seen in the table, statistics change only slightly when February and March are removed from the data set, and therefore, for the remainder of this thesis, statistics and results will include these months.

Table 3 - 6 Energy partitioning for the year of 2002, July 2002 and July-Sept., 1992 (Vs92). Statistics for 2002 with data from February and March removed are presented in parenthesis. N is the number of hours in the data set.

	2002	**July, 2002**	**Vs92**[1]	**2002**	**July, 2002**	**Vs92**[1]
	(24 h)	(24 h)	(24 h)	($Q^* > 0$)	($Q^* > 0$)	($Q^* > 0$)
Q_H/Q_E (β)	3.63 (3.41)	3.37	2.72	3.90 (3.67)	3.53	2.87
Q_H/Q^* (χ)	0.85 (0.83)	0.76	0.82	0.61 (0.62)	0.63	0.62
Q_E/Q^* (Υ)	0.23 (0.24)	0.23	0.3	0.16 (0.17)	0.18	0.22
Q_S/Q^* (Λ)	0.05 (0.04)	0.09	-0.12	0.28 (0.27)	0.23	0.17
N	4193 (3621)	640	572	1860 (1651)	360	14

[1]From Grimmond and Oke, (1999a)

The ratio χ (Q_H/Q^*) describes the fraction of radiant energy partitioned into Q_H. The annual Sunset value of 0.85 is higher in comparison to other suburban and urban sites. Typical suburban values typically fall between 0.39 and 0.62 (Grimmond and Oke, 1999a) while the urban mean is approximately 0.38 (Grimmond and Oke, 1999a). Results from Łodz, Poland were between 0.50 and 0.58 for the summer and between 1.37 and 1.47 for the winter (Offerle, 2003). Although large, the summer values at Sunset are consistent with those for the same site in 1992. Such large values can be explained by the irrigation ban and the drier than normal conditions during July.

The positive value of Q_S/Q^* (Λ) suggests that there is a small net annual gain of energy in 2002. This small net residual could simply be an indication that Q_F has been over-estimated. An example of the impact of this inexactitude is given for central Marseille by Grimmond *et al.* (2004). The size of Q_F is probably not much bigger than the errors in the other terms that accumulate in this residual. For this reason Q_F may not warrant adjustment. The net residual may also be the result of a small systematic advection term.

Q_E/Q^* (Υ) values show that evaporation accounts for about 23% (0.23) of Q^* over full day periods, and 17% (0.17) for the daytime ($Q^*>0$) period. These values are somewhat low when compared with the range of Υ values given by Grimmond and Oke (1999a) for eight suburban sites in North America. Their ranges are 0.28 – 0.46, and 0.22 – 0.37 for daily and daytime values, respectively. Again, appeal is made to the dryness of 2002 and the reduced irrigation regime compared to a normal year. The daytime value compares favourably with values from Christen and Vogt (2004) who calculated daytime Υ ratios of 0.20, 0.30 and 0.60 for urban, suburban and rural sites in Basel, respectively. The Sunset 2002 value is slightly lower than for the summer of 1992, which may be due to development of the district.

The diurnal ensemble non-dimensional ratios for the aforementioned statistics for 2002 at the Sunset site are presented in Figure 3 - 12. The plotted ratios in Figure 3 - 12 (a) follow patterns very similar to those presented by Grimmond and Oke (2002) and Grimmond *et al.* (2004). When Q_H is normalized by Q^* the resulting plot reveals a trace very similar to the data presented for the Sunset site in 1992 (VS92 in Figure 6 (b) of Grimmond and Oke 2002).

The ratio of Q_H/Q_S (κ) indicates the partitioning of sensible heat between the atmosphere (convection) and the surface fabric (conduction) (Figure 3 - 12 (b)). It is related to the ratio of the thermal admittances of the air and the substrate. The pattern at Sunset shows the growing dominance of convection in the afternoon. The sharp shift in late afternoon is related to storage release, which becomes the main focus of the heat balance.

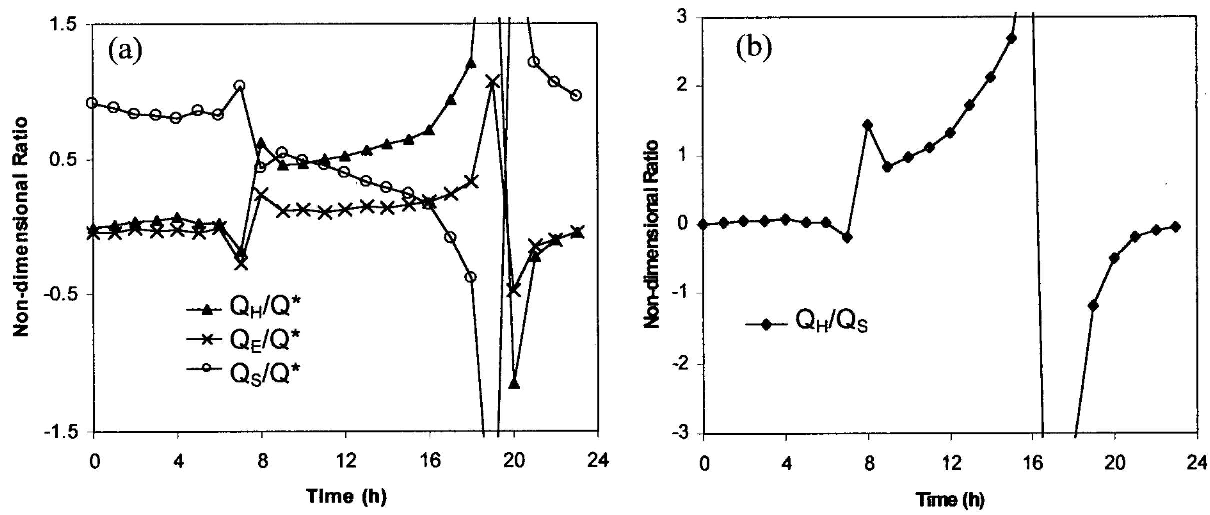

Figure 3 - 12 Diurnal non-dimensional ratios for the year 2002 at the Sunset site. (a) Q_H/Q^* (χ), Q_E/Q^* (Υ) and Q_S/Q^* (Λ) and (b) Q_H/Q_S (κ). Note: the range on the y axis is different for (a) and (b).

Evaporation for the year was 281 mm. This is 33% of the annual precipitation measured at the Vancouver International Airport climate station. Adding the irrigation water to precipitation amounts brings the fraction of evaporated water even lower, to probably less than 25% of the available surface water (the exact amount of irrigation is unknown for 2002). Again, however, it is important to note that the calculated evaporation is probably significantly under-estimated because of the data removal caused by rainfall effects on the instruments. Grimmond and Oke (1986) in a study at the same site calculated that the fraction of the total available water evaporated was approximately 38%.

3.4.6 Annual ensemble energy fluxes for 2002

The annual ensemble energy balance results for the entire year are given in Figure 3 - 13 (a) and (b). Q_H dominates the energy balance throughout the day, but Q_S is a very important term during the morning. During this time its magnitude slightly exceeds Q_H indicating the large acceptance of heat into surface fabrics. This heat is later released back into the system and is illustrated by the role of Q_H in the early evening. At this time the magnitude of Q_H exceeds that of Q^*.

The mean diurnal energy fluxes in MJ m^{-2} d^{-1} for each month were calculated over the year 2002 and are presented in Figure 3 - 13 (b). Again, it is apparent that Q^* and Q_H peak in June, but that Q_E peaks slightly earlier in the year. ΔQ_S and Q_F are also included; their magnitudes are small throughout the year. Q_F, an estimated value, is plotted as a small constant positive flux throughout the year. ΔQ_S is negative for winter months and positive for summer months.

When we examine mean daily (24-h) and mean daytime ($Q^*>0$) energy fluxes (Table 3 - 7) for 2002 we again see that Q_H is much higher than Q_E. It is also apparent that ΔQ_S for the 24-h period is close to zero, as expected, but is a dominant flux during the daytime. Values from Vs92 (Grimmond and Oke, 1999a) have again been included as a comparison with July 2002. An interesting point is the magnitude of Q_H. For the 24-hour mean, Q_H is slightly higher in 2002, but the difference is amplified when we examine the daytime values. This high Q_H flux provides evidence that over the 10 year period, daytime Q_H has indeed risen, likely due to changes in surface cover towards built surfaces and away from natural surfaces.

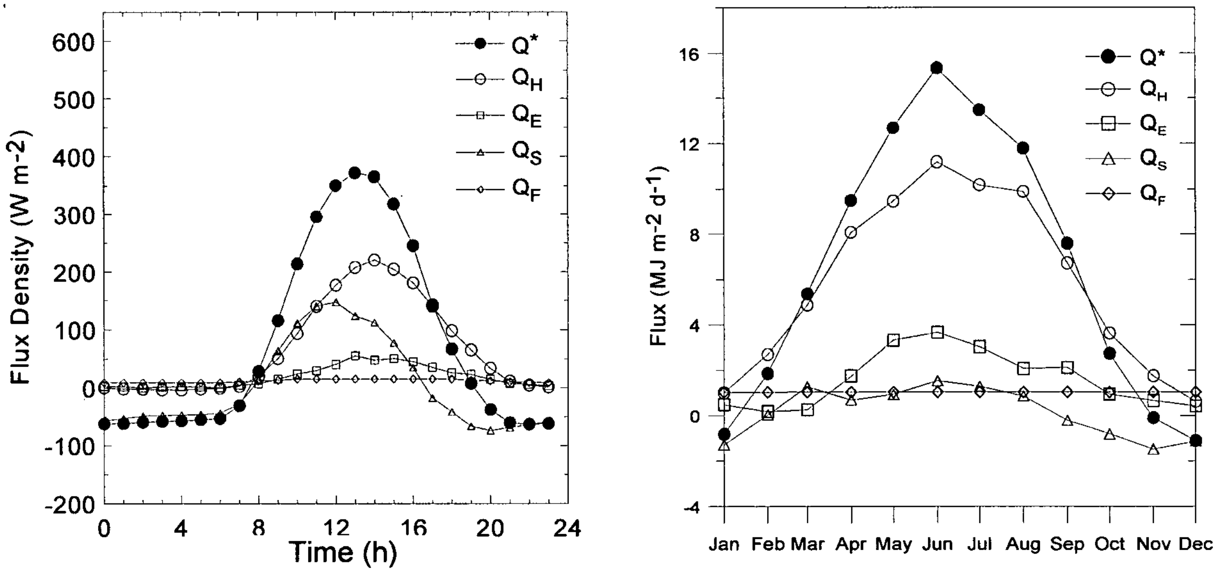

Figure 3 - 13 (a) Ensemble average diurnal course of energy budget components for the year 2002. (b) Annual variation in the energy budget components. Absolute values are plotted.

Table 3 - 7 Daily and daytime ($Q^* > 0$) energy totals (MJ m^{-2} d^{-1}) for 2002, July 2002 and Vs92[1]. *Note*: ΔQ_S calculations include an estimated anthropogenic heat (Q_F).

	Q^*	Q_H	Q_E	ΔQ_S
24h		**MJ m^{-2} d^{-1}**		
2002	8.08	6.85	1.89	0.38
July 2002	13.47	10.19	3.02	1.30
Vs92[1]	8.88	7.26	2.68	-1.09
Q*>0		**MJ m^{-2} d^{-1}**		
2002	25.24	15.52	4.23	6.73
July 2002	27.74	17.51	4.96	6.49
Vs92[1]	12.13	7.50	2.62	2.01

[1]From Grimmond and Oke (1999a).

Mean daily fluxes for the month of July are presented in Figure 3 - 14. July is presented because it represents the largest continuous data range for the year. The traces show the dominance of Q_H. Dips in the Q^* signal are predominantly related to cloud cover (K↓ data not shown). Q^*, Q_H and Q_S follow approximately the same pattern, whereas the pattern of Q_E is more difficult to predict. The magnitude of Q_E is more related to the amount of water available. During the month of July there was little recorded precipitation and Q_E values are low as a result. The small magnitude of Q_E suggests that irrigation also contributed little water to the system. Q_H fuels the convective heating of the atmosphere, with the highest magnitudes recorded on cloudless days.

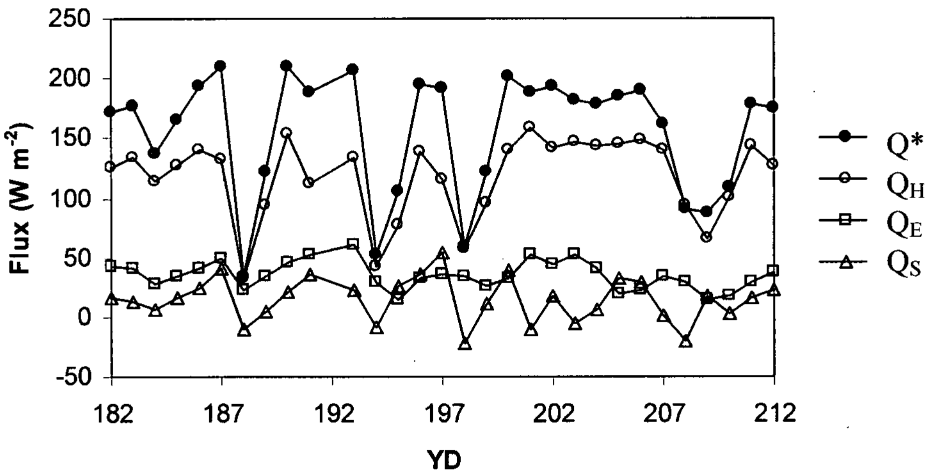

Figure 3 - 14 Mean daily fluxes for the month of July 2002.

3.5 Carbon dioxide

3.5.1 Carbon dioxide concentrations

Monthly average CO_2 concentrations from the Sunset site and Estevan Point on the west coast of Vancouver Island are presented in Table 3 - 8 and graphically in Figure 3 - 15. Data from Estevan Point has been included to represent relatively 'clean air' coming off the Pacific Ocean. The annual average CO_2 concentration for Estevan Point was 372.26 ppm in 2001 (data not available for 2002); the annual average CO_2 concentration for the Sunset site was 373.04. Although annual averages for theses sites are quite similar, of particular interest are the differences that occur throughout the year. During the summer months, concentrations from the Sunset site are lower than Estevan Point, but during the winter the opposite is seen. This indicates that the vegetative sink is acting to reduce CO_2 at the Sunset site in the summer, but that during the winter, in the absence of the photosynthetic sink, concentrations are elevated in comparison with data from Estevan Point. This indicates that the suburban area surrounding the Sunset site is a source of CO_2, probably at all times of the year, but that during the summer vegetative sinks are effectively removing CO_2 from the atmosphere, to levels below those recorded at Estevan Point.

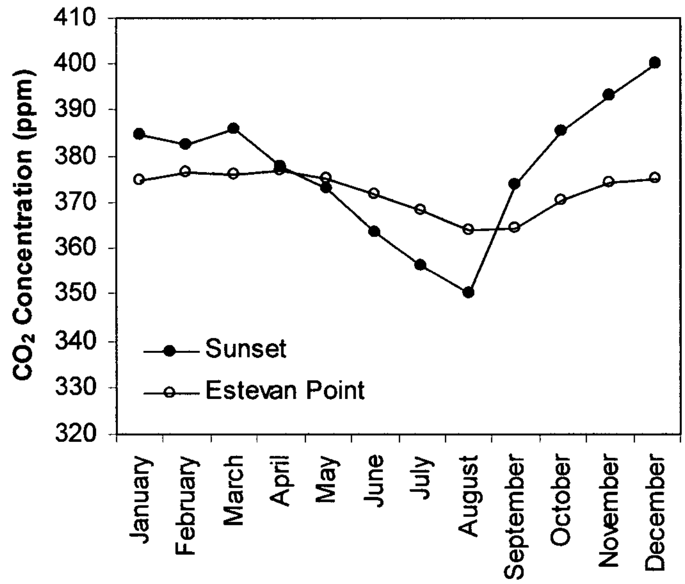

Figure 3 - 15 Annual trend comparison of monthly average CO_2 concentrations. Atmospheric CO_2 concentrations (ppm) derived from flask air at Estevan Point, Canada for 2001 (Steele *et al.*, 2002), and calculated data collected from the Sunset site for 2002.

Table 3 - 8 Atmospheric CO_2 concentrations (ppm) derived from flask air at Estevan Point, Canada for 2001 (Steele *et al.*, 2002), and calculated data collected from the Sunset site for 2002.

Month	**CO_2 Concentration (ppm)**	
	Sunset (2002)	***Estevan Point (2001)***
January	384.75	374.82
February	382.53	376.21
March	385.86	376.02
April	377.53	376.72
May	372.88	375.09
June	363.54	371.76
July	355.98	368.30
August	350.29	363.89
September	373.81	364.20
October	385.36	370.37
November	393.05	374.36
December	400.02	375.33
Annual Average	**373.04**	**372.26**

Seasonal trends of the daily mean and 10-day running mean of CO_2 concentrations at the Sunset site are given in Figure 3 - 16. Examination of the data reveals the highest concentrations in the early spring (~YD 90) and winter (~YD 330) with levels peaking at approximately 425 ppm. The lowest concentrations of 340 ppm are observed in late July (~YD 210). This is expected due to the high photosynthetic uptake by vegetation and is complemented by extended day lengths at this time of the year.

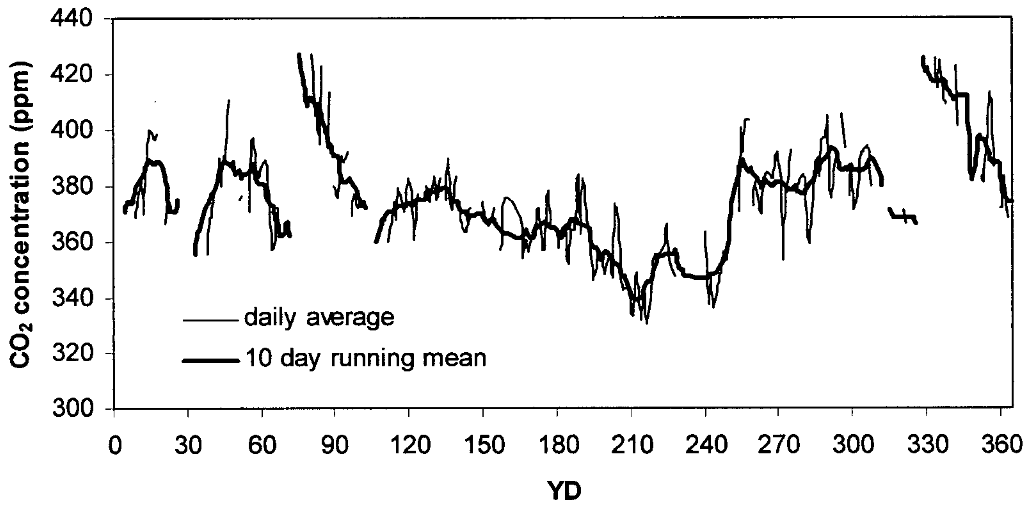

Figure 3 - 16 Seasonal trends in CO_2 concentrations (ppm) plotted against year day (YD). The thin and thick lines represent the daily average and the 10-day running mean respectively.

Diurnal CO_2 concentrations are plotted by month in Figure 3 - 17. The traces reveal the diurnal trend of CO_2 is highest for December, as expected due to house heating and a decrease in the vegetative sink, and lowest in August due to sequestration by vegetation.

Examination of the diurnal trend reveals that throughout all months, a gradual incline is seen throughout the night as CO_2 builds up in the absence of strong turbulence. A peak in this incline is observed mid-morning, as a result of upward mixing of CO_2 trapped near the ground by the stable nocturnal boundary layer. Additionally this peak is timed with the morning rush hour. Mid-afternoon values are lowest due to a draw down of CO_2 by vegetation and enhanced vertical mixing allowing CO_2 near the surface to mix upward. A second, smaller peak corresponding to the afternoon vehicular rush hour is also evident for most of the year, although it is less pronounced in the summer months when photosynthesis is at its peak. In the late afternoon, concentrations increase as people arrive home and residential building emissions rise. Nighttime concentrations are elevated for a number of reasons, including a shallow nocturnal boundary layer, which traps CO_2 originating near the surface from respiration and residential building emissions.

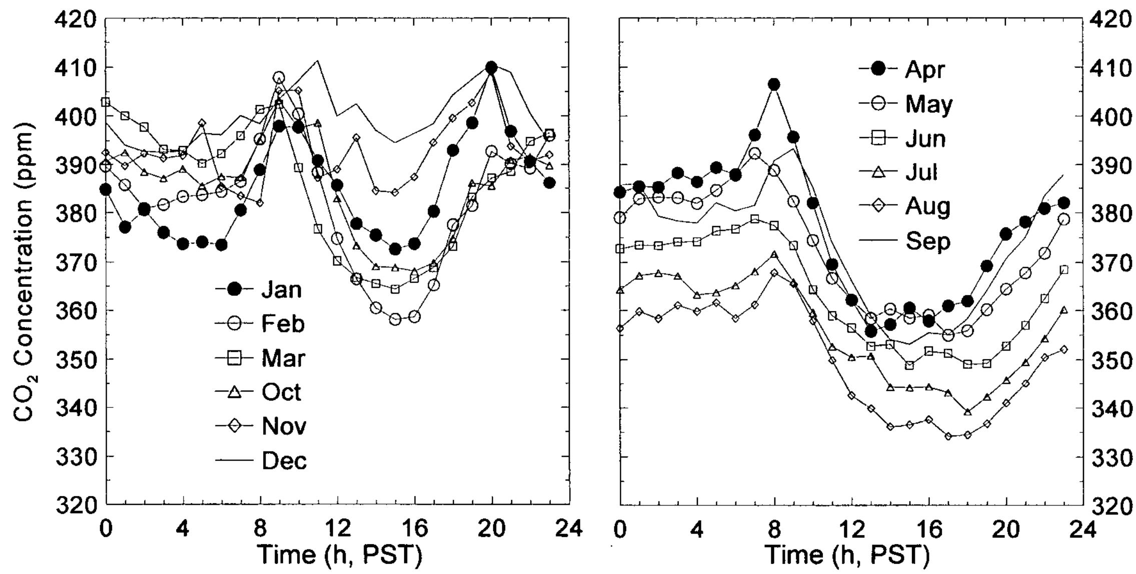

Figure 3 - 17 Diurnal CO_2 concentrations (by month). (a) Winter months: Jan-Mar, Oct-Dec. (b) Summer months: Apr-Sep.

3.5.2 Carbon dioxide fluxes

A plot of all hourly F_C data for 2002 is given in Figure 3 - 18. Here F_C is presented as positive if the flux is away from the surface (source) and negative if the flux is towards the surface (sink). The most obvious feature is the dominant positive hourly fluxes throughout the year, indicating that sources are greater than sinks. However, negative hourly F_C were measured on some occasions indicating temporary sinks.

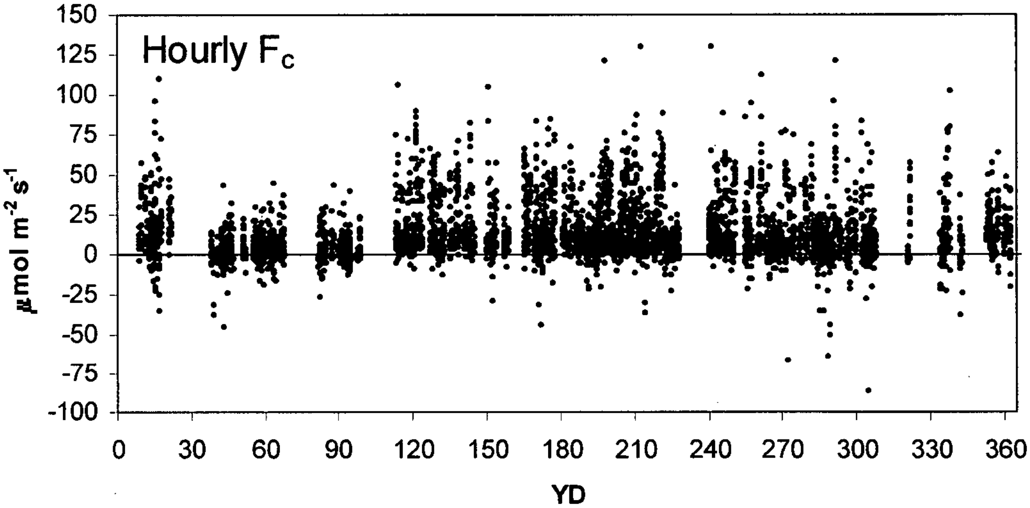

Figure 3 - 18 Hourly turbulent CO_2 flux (F_C) for 2002.

The seasonal trend of daily mean F_C (Figure 3 - 19) reveals large day-to-day variations throughout the year. The mean F_C for the year is 13.28 μmol $s^{-1}m^{-2}$ with a median of 8.11 μmol s^1 m^{-2}. As reported previously for Q_E, we see an anomaly in the data from YD 30 to YD 100, where fluxes become suddenly lower. This anomaly could be related to sensor error and/or low data coverage during this period.

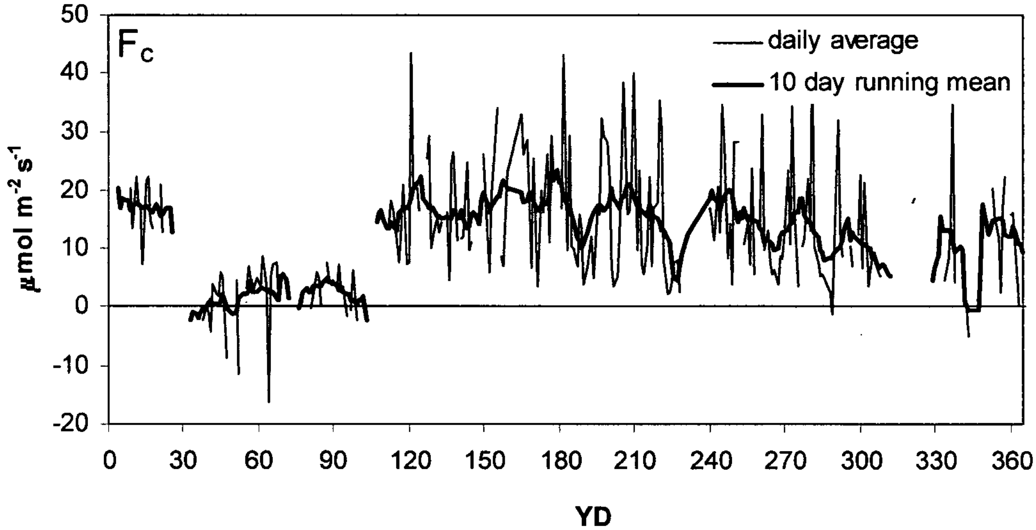

Figure 3 - 19 Seasonal variation in the turbulent CO_2 flux (F_C) for 2002. The thin and thick lines represent the daily average and the 10-day running mean, respectively.

The period of low F_C is also evident in the ensemble average diurnal F_C trace (Figure 3 - 20) for the months of February and March. Overall, the diurnal plots, presented by month, show that negative fluxes are virtually absent throughout the year. This indicates that photosynthetic uptake by vegetation was likely not strong enough to offset CO_2 emitted by respiration and fossil fuel combustion. For all months, low fluxes are seen before dawn due to low turbulence. At this time of day CO_2 is trapped near the surface due to the stable nocturnal boundary layer and are not captured by the eddy covariance sensor. At sunrise a peak in F_C is seen as a result of surface heating and the development of turbulent convective cells. The increase in turbulence facilitates mixing of CO_2 upward. Also, CO_2 sources increase in the morning as the human activity cycle begins, and fossil fuels are burnt as people start their days, and drive to work. Anthropogenic emissions likely contribute to the peak of F_C in the morning, but it is difficult to determine to what extent without detailed emissions inventories, which are extremely difficult to construct. After the morning peak, for most months, a gradual decline in the flux occurs until midnight. July, August and September have persistently high fluxes throughout the day, probably due to convection, and the mixing that ensues in the summer. January's large flux, peaking at mid-day is unusual when compared to the other months. It might be explained by low data coverage, and a few high values of F_C, which act to skew the average higher (Figure 3 - 21). For any given ensemble hourly value, January has, on average, only 7 days that contribute to the average flux. In contrast, the month of July has, on average, 27 days that are used to calculate the mean hourly flux (Figure 3 - 21).

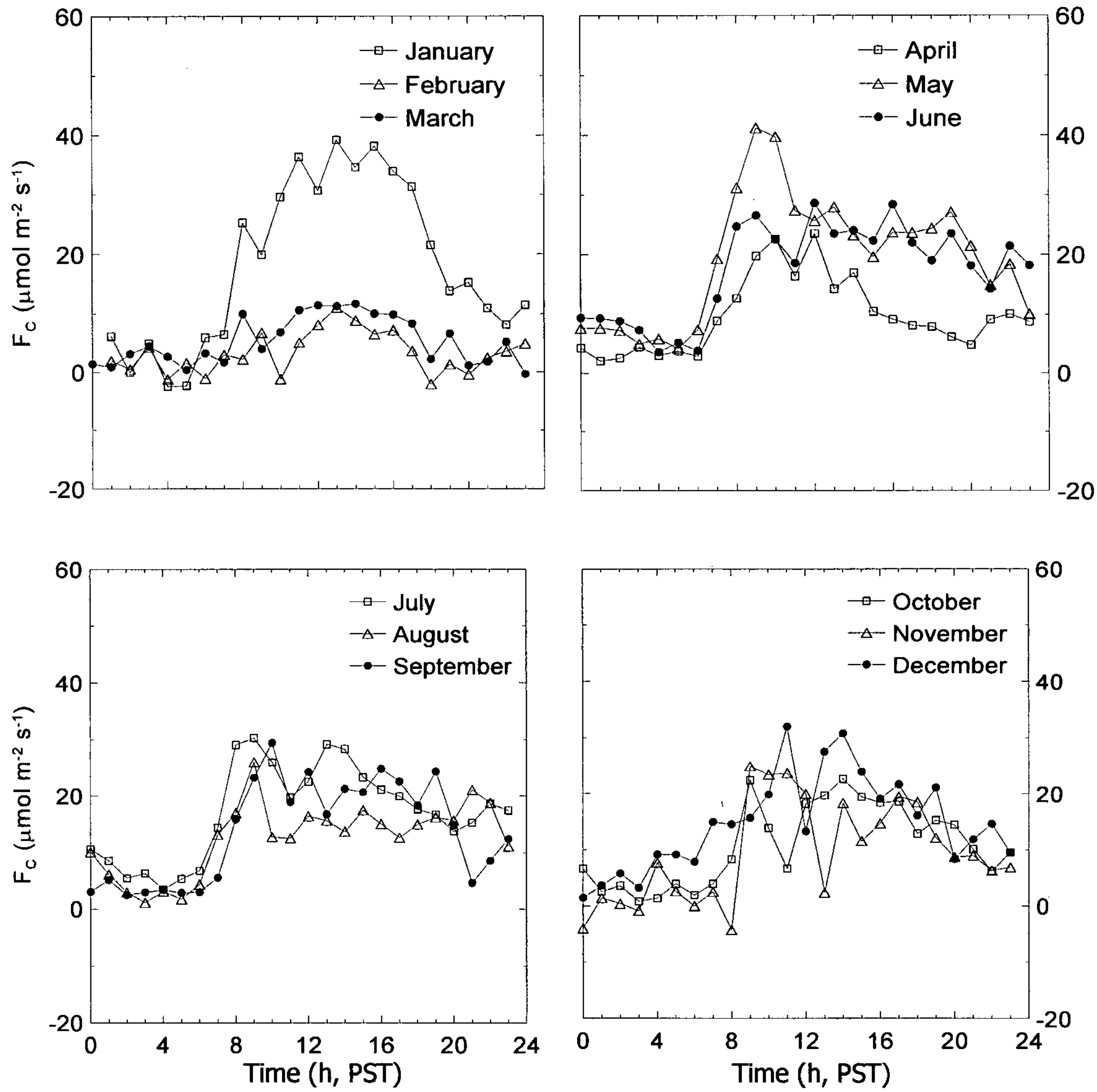

Figure 3 - 20 Variability of average daily CO_2 flux (F_C) for the year 2002; (a) Jan-Mar 2002, (b) Apr-Jun 2002, (c) Jul-Sep 2002, and (d) Oct-Dec 2002.

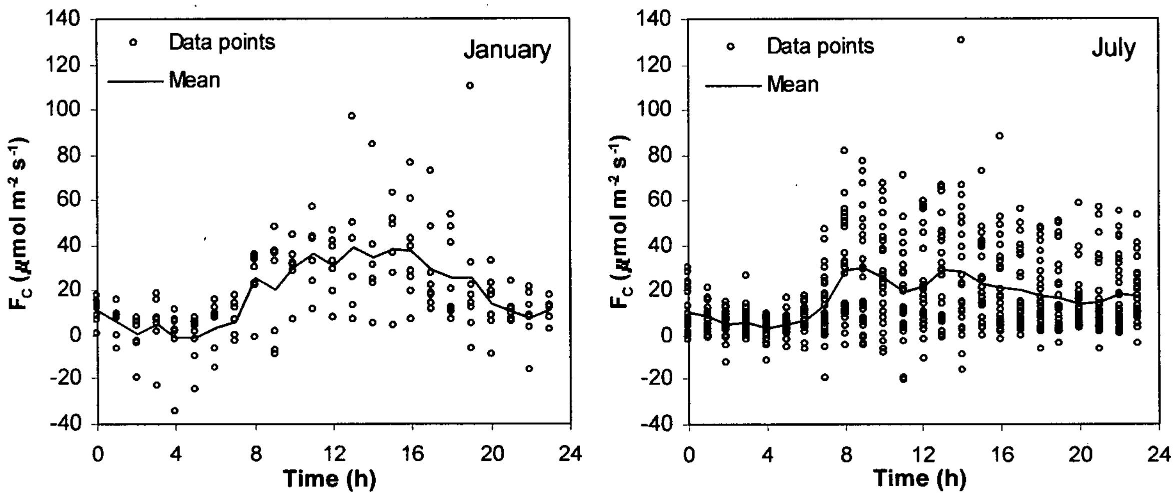

Figure 3 - 21 Data points contributing to the mean hourly turbulent CO_2 flux (F_C) for (a) January (N=7 per hour) and (b) July (N=27 per hour) 2002.

3.5.3 Wind sector analysis

The large fluxes observed during the mid-afternoon throughout the year indicate that emissions of CO_2 in the area must be high regardless of the substantial vegetative cover. Examination of the Sunset site data reveals a correlation between prevailing wind direction and the magnitude of F_C, which is illustrated in Figure 3 - 22 for the week of YD 220-227 (August 8-15). As the wind direction shifts, abrupt changes in F_C are often evident. F_C is specifically high, often reaching >60 μmol m^{-2} s^{-1}, when the wind is coming from 100-180 degrees (south-east). In contrast, F_C values close to 0 μmol m^{-2} s^{-1} are observed when the wind is coming from 200-360 degrees (west to north-west). To examine these observations in more detail, CO_2 data were filtered into eight sectors to determine whether the surface characteristics in the surrounding source areas are significantly affecting F_C. Wind sector divisions and the dominant surface characteristics in each wind sector are given in Table 3 - 9. Figure 3 - 23 displays these sectors overlain onto an airphoto.

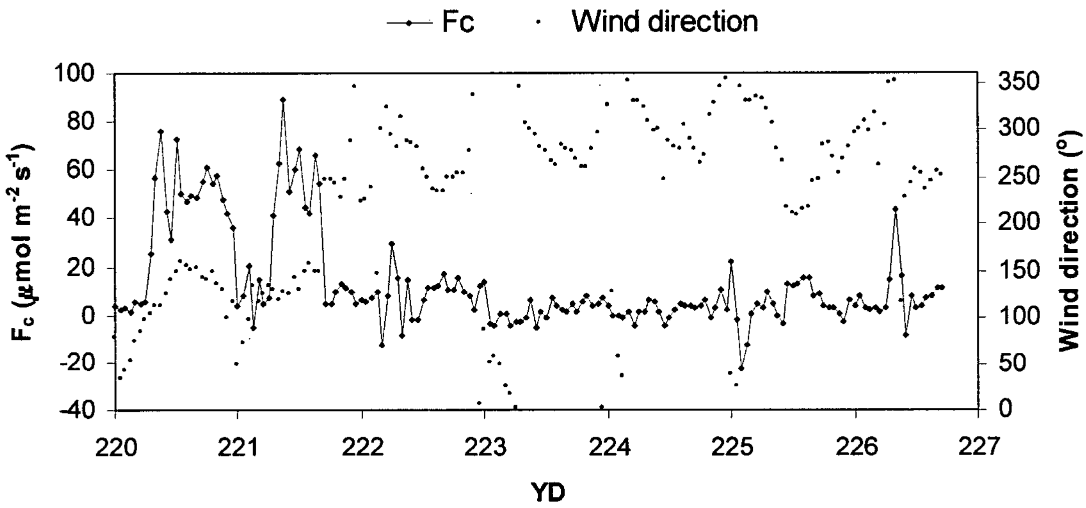

Figure 3 - 22 Hourly course of wind direction and turbulent CO_2 flux (F_C) for August 8-15, 2002.

Table 3 - 9 Wind sector divisions and primary surface features within each sector.

Wind sector	Wind directions included (degrees)	Primary surface features in the source area
Sector 1	0-45°	Road, grass, school-yard
Sector 2	46-90°	School-yard
Sector 3	91-135°	Main road, major intersection
Sector 4	136-180°	Main road, major intersection
Sector 5	181-225°	Residential
Sector 6	226-270°	Road, residential
Sector 7	271-315°	Residential
Sector 8	315-360°	Substation, grass

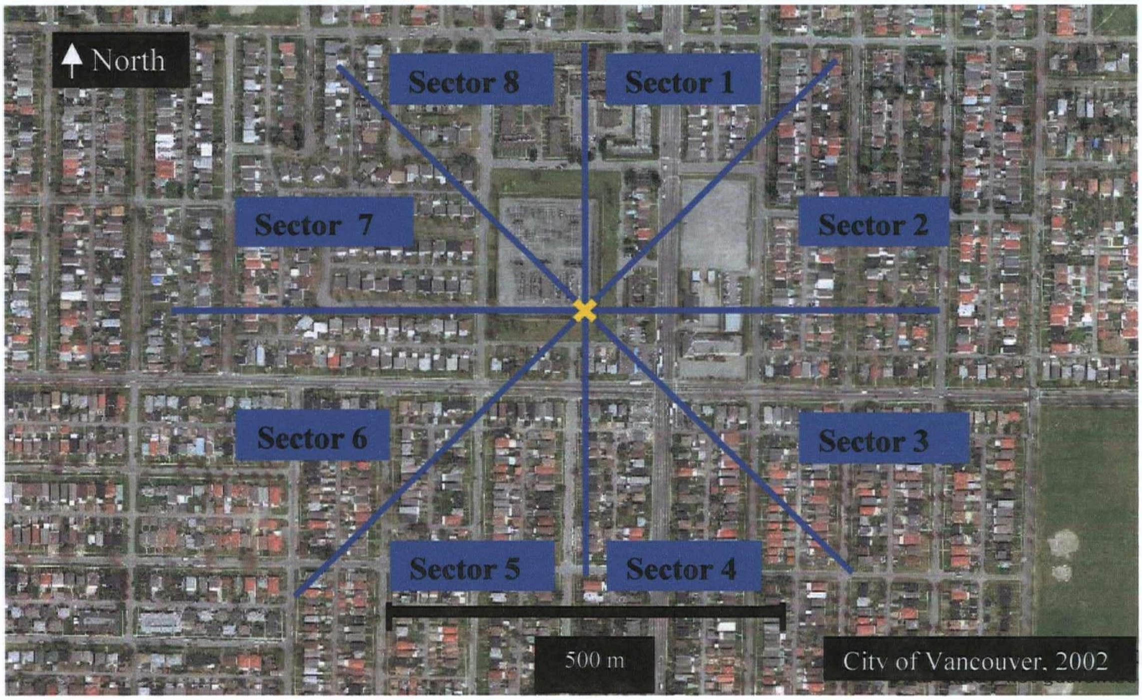

Figure 3 - 23 Wind sectors overlain onto Sunset site airphoto. The Knight Street (running north-south) and 49th Avenue (running east-west) intersection is to the southwest of the tower (marked with a yellow x) and is bisected by Sectors 3 and 4.

The distribution of wind direction (frequency) for the year 2002 is shown in Figure 3 - 24 (a and b). During the day wind is generally from the south-west with the highest frequency of wind direction occurring in Sector 6.

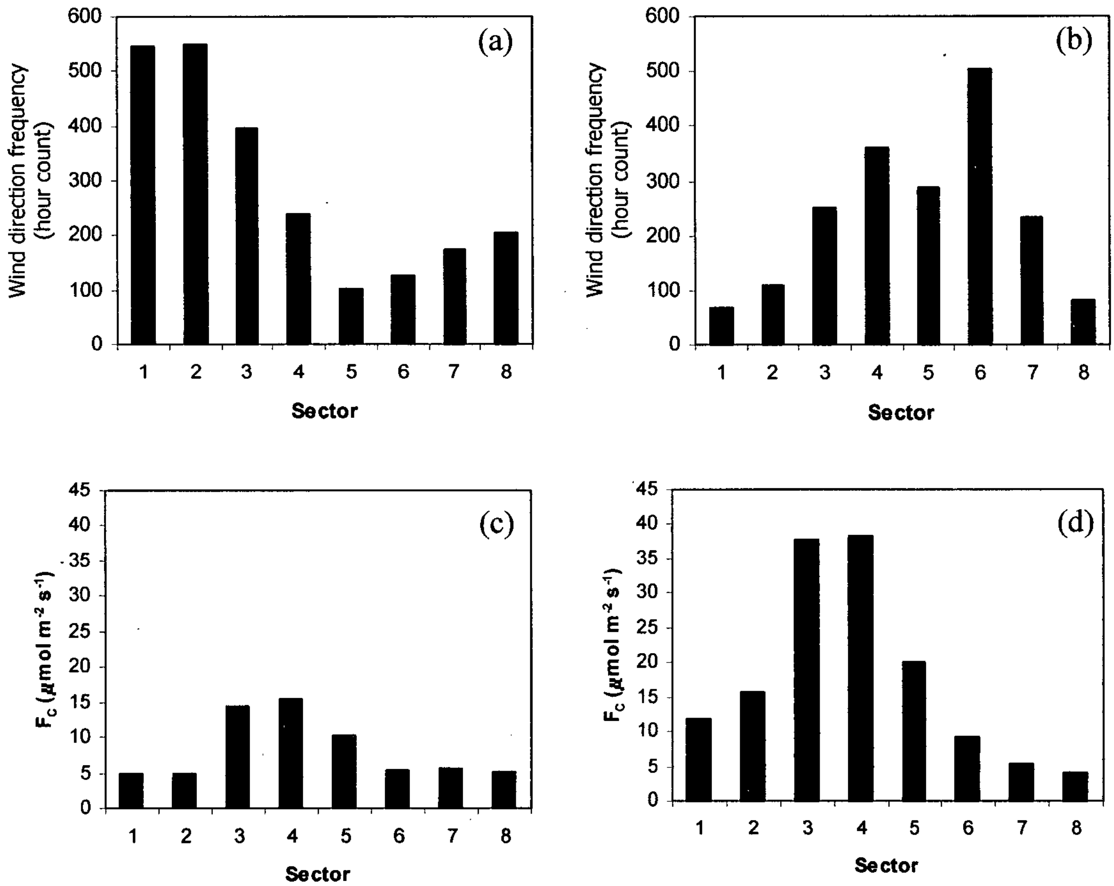

Figure 3 - 24 Frequency of wind direction and magnitude of turbulent CO_2 flux (F_C) from each sector for 2002. (a, c) $Q^*<0$ (night) and (b,d) $Q^*>0$ (day).

A major arterial highway intersection (Knight Street and 49th Avenue) occupies part of the source areas for turbulent fluxes in Sectors 3 and 4 (see Figure 3 - 23). When the wind is from the direction of the intersection, F_C is significantly higher than values from other sectors (Figure 3 - 24 (c, d)). This relationship between wind direction and F_C is seen throughout the year (Figure 3 - 25). Sectors 3 and 4 have higher fluxes in all months except February and March (during which eddy covariance data may not be reliable).

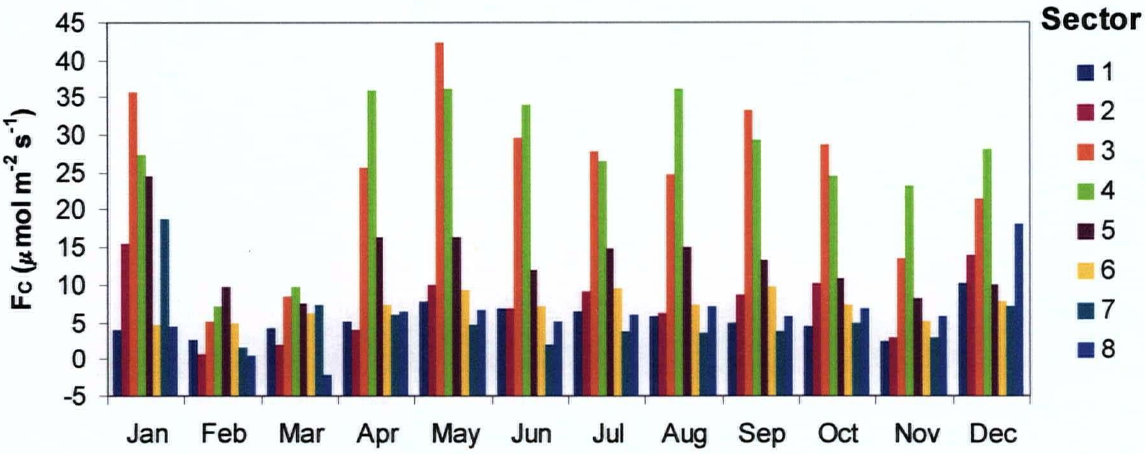

Figure 3 - 25 Monthly average turbulent CO_2 flux (F_C) by sector.

When examining the diurnal trend of F_C a similar directional bias is seen. This is illustrated in Figure 3 - 26. Mid-day fluxes are highest again from Sectors 3 and 4, but similarly low fluxes are seen from all sectors at night because of the stable nocturnal boundary layer. The lowest fluxes are seen from sector 8, which is not surprising due to the grass and gravel surface composition of this sector. The influence of Sectors 3 and 4 is further examined in Figure 3 - 27. When F_C data from Sectors 3 and 4 are excluded the resulting fluxes are approximately cut in half by day.

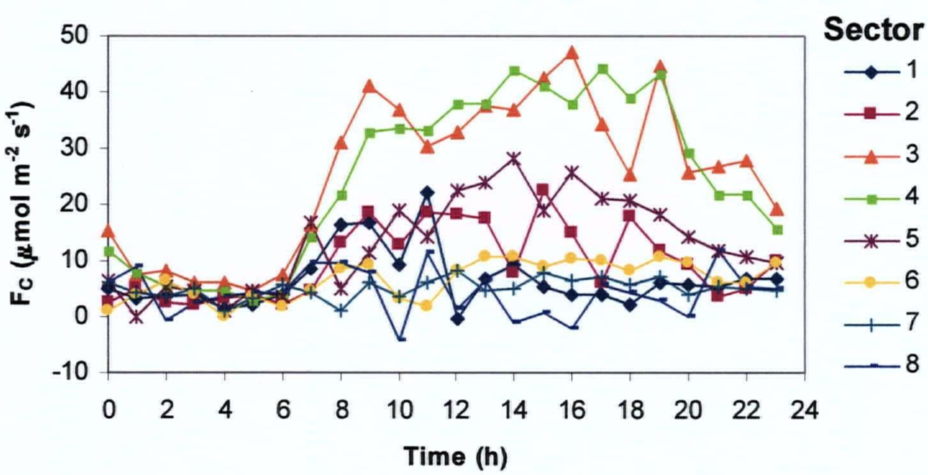

Figure 3 - 26 Diurnal pattern of F_C filtered by wind sector.

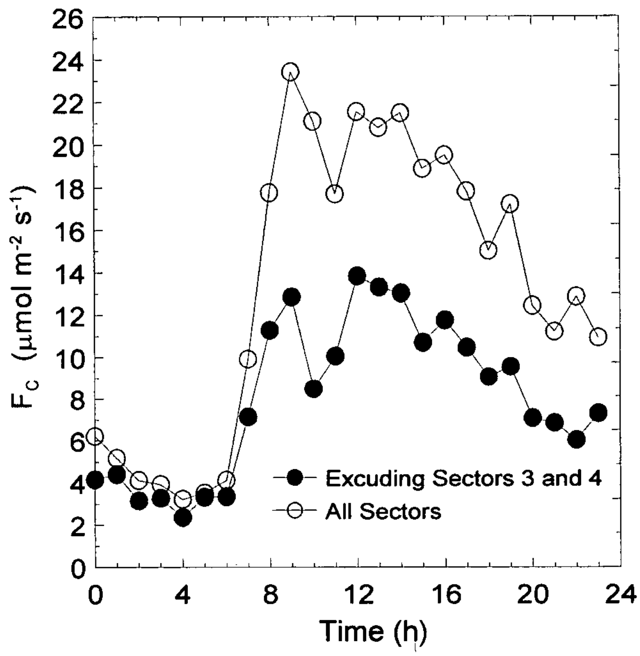

Figure 3 - 27 Diurnal pattern of turbulent CO_2 flux (F_C) for 2002 including and excluding Sectors 3 and 4.

The surface characteristics of the turbulent source areas appear to control the magnitude of F_C. But, is there equivalent dissimilarity in the spatial nature of the source strength distributions for heat and water vapour? Earlier results from this same tower site noted differences in the source distributions of heat and water vapour in that, all urban surfaces are sources of heat, but not necessarily of water, leading to the finding that there is inequality in transfer efficiencies for the two entities (Roth and Oke, 1995). Even so previous results from this site have not noted the existence of sectoral bias in Q_E or Q_H. Normalized values of these fluxes (Q_H/Q^* and Q_E/Q^*) are plotted (Figure 3 - 28 and Figure 3 - 29) to remove any seasonal or diurnal energy cycles. A directional dependence would be present if traces from any of the sectors were either consistently above or consistently below the mean trace for the year. Normalization of Q_H in Figure 3 - 28 indicates there is no significant difference in Q_H based on wind sector. Similar results are present in normalization of Q_E. This indicates that the measurement height for Q_H and Q_E appears to be sufficiently above the roughness sublayer, and hence, these entities are well blended. This illustrates the suitability of the site for measurement of these fluxes.

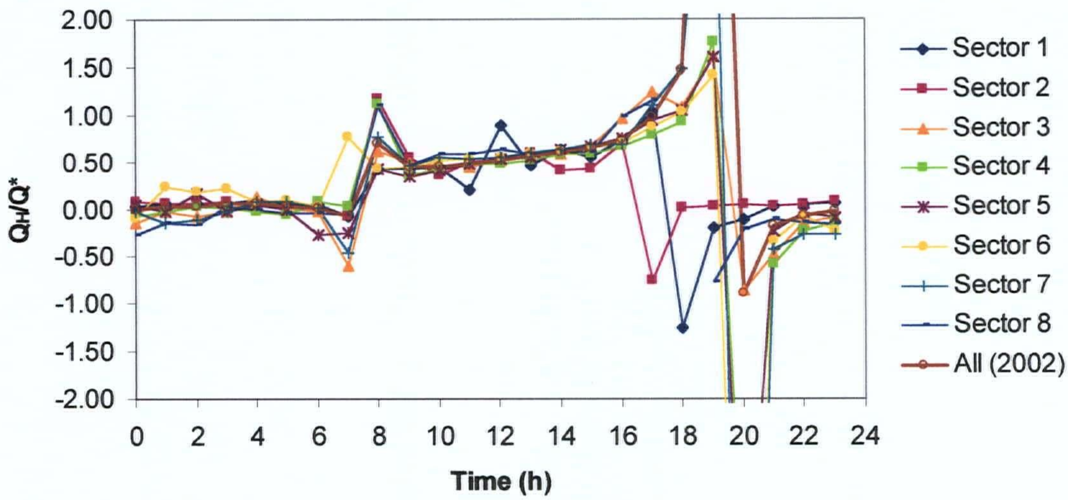

Figure 3 - 28 Normalization of the sensible heat flux (Q_H/Q^*) for each wind sector.

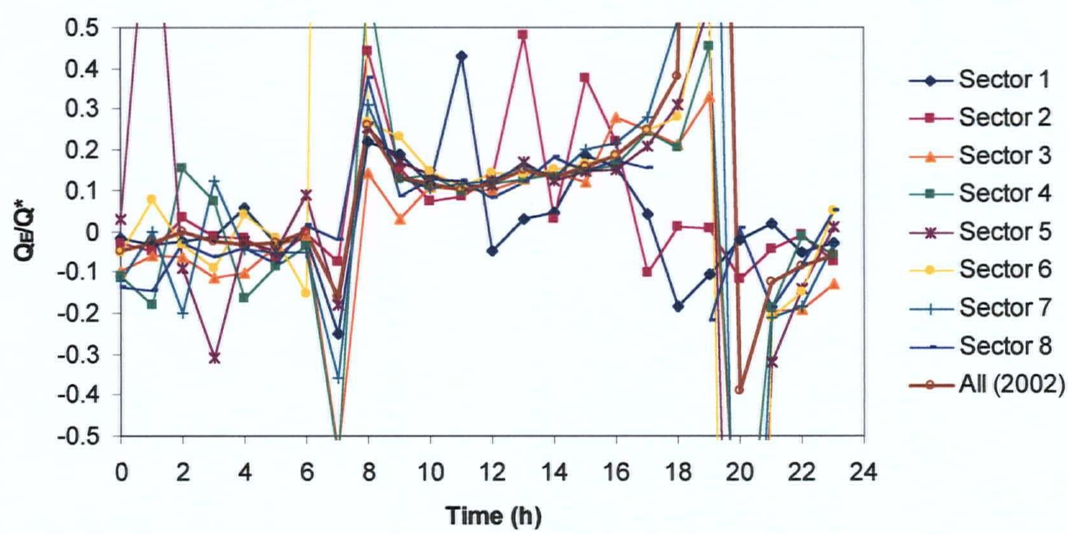

Figure 3 - 29 Normalization of latent heat flux (Q_E/Q^*) for each wind sector.

The sources and sinks of CO_2 are much more uneven than for water and heat, consisting as they do of a mixture of area and line sources and sinks at differing elevations at and above the urban canopy layer. In the present case it appears that the intersection of two major line sources creates a strong directional bias in CO_2 fluxes. The analysis of data from the suburban Sunset site therefore requires special source area considerations not normally necessary in CO_2 studies over natural surfaces.

4 CONCLUSIONS

4.1 Energy and radiation budgets

Radiation budget components followed expected seasonal and diurnal patterns. Energy balance components revealed a peak in Q_E in late spring and a peak in Q_H in mid-summer probably related to the availability of surface water. The year was drier than average and water became limited early in the summer. Energy was channeled into Q_H during the time of water shortage. It was also apparent that the relative role of Q_H in the surface energy balance has increased over the years at the Sunset site. This is because the area surrounding the site has become more built, with impervious, sensible heat rich surface materials replacing natural surfaces such as grass.

Again, it is important to note that Q_E was negatively skewed due to removal of days that had rain events. High Q_E values following rainfall events were not captured due to limitations of the LI-7500 infrared gas analyzer. Overall, there are unavoidable errors and uncertainties in the measurement of urban energy balance components, specifically when using the eddy correlation technique. Nevertheless, the eddy correlation technique is advanced compared to more traditional measurement systems, and it's benefits far outweigh it's weaknesses.

Inclusion of an approximated value of Q_F into the 'observed' surface energy balance proved useful in generating a more reliable and reasonable residual storage term. Further urban studies may benefit from the inclusion of this term.

Comparison of results between urban areas is limited by the use of different measurement techniques, and measurement in areas of differing urban structure. This must be kept in mind before comparisons between urban areas are drawn.

4.2 Carbon Dioxide

Methodological challenges limited interpretation of annual trends in the CO_2 flux data. An annual carbon budget was impossible to calculate due to incomplete data sets, resulting in only a few days of data for many of the winter months. Data gaps were especially apparent when rainfall was frequent. It was therefore extremely difficult to determine monthly or seasonal flux budgets.

In addition, a directional dependence was displayed in the fluxes of CO_2, but was absent in other turbulent fluxes such as Q_E and Q_H. This indicates that the blending height of CO_2 may be higher than that of water or heat. Further studies of CO_2 fluxes in urban areas may benefit from mounting instruments higher in the inertial sublayer to determine if the blending height is indeed elevated for CO_2. Additionally, the availability of several measurement heights may provide valuable information on the mixing height as well as storage of CO_2 in the lower levels of the urban atmosphere.

Unfortunately measurement from one tower site provides only limited knowledge of the dynamics of CO_2 over the entire urban environment. It is not possible to scale these measurements up, and hence is it not possible to determine a spatially representative sample of residential Vancouver. Future research may benefit from vehicle-driven traverses to demonstrate the spatial distribution of CO_2 concentrations. In addition to providing a spatial distribution of

CO_2 sources, it would indicate if the major intersection near the site is typical of other intersections in Vancouver.

Although this study provides a valuable first step in determining the role of CO_2 in urban environments, much more information is necessary to fully understand the complex role of sources and sinks. Further, CO_2 studies may also benefit from determining the emission inventories from a range of surfaces in the urban environment. Incorporation of surface characteristics and CO_2 fluxes and concentrations into a GIS could provide insight into exactly where significant CO_2 sources are located. Additionally, turbulent source areas could be calculated and overlaid into a GIS. Combining turbulent source areas with underlying surface characteristics will provide insight into which surfaces are major sources of CO_2 and on how to analyse flux information to obtain climatologically meaningful statistics and mass budgets.

References

Anderson, D.E. and J. Taggart, (2002): Urban ecosystem-atmosphere exchange of carbon dioxide. Abstract. American Meteorological Society 4th Symposium on the urban environment, American Meteorological Society, Norfolk, VA. May 18-23.

Anderson, D.E., S.B. Verma, and N.J. Rosenberg, (1984): Eddy correlation measurements of CO_2, latent heat and sensible heat fluxes over a crop surface. *Boundary Layer Meteorology,* **29**: 167-183.

Bailey, W.G., T.R. Oke, and W.R. Rouse (editors) (1998): The Surface Climates of Canada. McGill-Queen's University Press, Montreal.

Baldocchi, D.D., J.J. Finnigan, K.W., Wilson, K.T. Paw U, and E. Falge, (2000): On measuring net ecosystem carbon exchange in complex terrain over tall vegetation. *Boundary Layer Meteorology,* **96**: 257-291.

Baldocchi, D.D., E. Flage, L. Gu, R. Olson, D. Hollinger, S. Running, P. Anthoni, C. Bernhofer, K. Davis, R. Evans, J. Fuentes, A. Goldstein, G. Katul, B. Law, X. Lee, Y, Malhi, T. Meyers, W. munger, W. Oechel, K.T. Paw U, K. Pilegaard, H.P. Schmod, R. Valentini, S. Verma, T. Vesala, K. Wilson, S. Wofsy, (2001): FLUXNET: A new tool to study the temporal and spatial variability of ecosystem-scale carbon dioxide, water vapor, and energy flux densities. *Bulletin of the American Meteorological Society,* **82**: 2415-2434.

Berry, R.D. and J.J. Colls, (1990a): Atmospheric carbon dioxide and sulphur dioxide on an urban/rural transect – I. Continuous measurements at the transect ends. *Atmospheric Environment,* **24A**: 2681-2688.

Berry, R.D. and J.J. Colls, (1990b): Atmospheric carbon dioxide and sulphur dioxide on an urban/rural transect – II. Measurements along the transect. *Atmospheric Environment*, **24A**: 2689-2694.

Christen, A., and R. Vogt, (2004). Energy and radiation balance of a central European City. *International Journal of Climatology,* **24**: 1395-1421.

City of Vancouver, (2002): VanMap. (http://www.city.vancouver.bc.ca/vanmap)

Clarke, J.F. and R.B. Faoro, (1966): An evaluation of CO_2 measurements as an indicator of air pollution. *Journal of Air Pollution Control Association*, **16:** 212-218.

Cleugh, H.A., (1990): Development and evaluation of a suburban evaporation model: A study of surface and atmospheric controls on the suburban evaporation regime. Ph. D. Thesis, University of British Columbia.

Cleugh, H.A. and T.R. Oke, (1986): Suburban-rural energy-balance comparisons in summer for Vancouver, BC. *Boundary Layer Meteorology,* **36**: 351-369.

Crane, A.J., (1985): Possible effects of rising CO_2 on climate. *Plant, Cell Environment,* **8**: 371-379.

Dabberdt, W.F., D.H. Lenschow, T.W. Horst, P.R. Zimmerman, S.P. Oncley, and A.C. Delany, (1993): Atmosphere-surface exchange measurements. *Science,* **260**: 1472-1481.

Davenport, A.G., C.S.B. Grimmond, T.R. Oke, and J. Wieringa, (2000): Estimating the roughness of cities and sheltered country. Proceedings of the 12th Conference for Applied Climatology, American Meteorological Society, Boston, pp. 96-99.

Environment Canada, (2004): Climate Normals 1971-2000. National Climate Data and Information Archive. (http://www.climate.weatheroffice.ec.gc.ca/Welcome_e.html)

Falge, E., D. Baldocchi, R. Olsen, P. Anthoni, M. Aubinet, C. Bernhofer, G. Burba, R. Ceulemans, R. Clement, H. Dolman, A Granier, P. Gross, T. Grunwald, D. Hollinger, N.O. Jensen, G. Katul, P. Keronen, A. Kowalski, C.T. Lai, B.E. Law, T. Meyers, H. Moncrieff, E. Moors, J.W. Munger, K. Pilegaard, U. Rannik, C. Rebmann, A. Suyker, J. Tenhunen, K. Tu, S. Verma, T. Vesala, K. Wilson, and S. Wofsy, (2001): Gap filling strategies for defensible annual sums of net ecosystem exchange. *Agricultural and Forest Meteorology,* **107**: 43-69.

Finnigan, J.J., (1999): A comment on the paper by Lee, 1998: "On micrometeorological observations of surface air exchange over tall vegetation." *Agricultural and Forest Meteorology.* **97**: 55-64.

Grimmond, C.S.B., (1992): Midlatitude west-coast city under winter and spring conditions. *International Journal of Climatology,* **12**: 481-497.

Grimmond, C.S.B., (1988): An evaporation-interception model for urban areas. Ph.D. Thesis, University of British Columbia.

Grimmond, C.S.B. and T.R. Oke, (2002): Turbulent heat fluxes in urban areas: observations and a local scale meteorological parameterization scheme (LUMPS). *Journal of American Meteorology*, **41**: 792-810.

Grimmond, C.S.B. and T.R. Oke, (1999a): Heat storage in urban areas: Local scale observations and evaluation of a simple model. *Journal of Applied Meteorology,* **38**: 922-940.

Grimmond, C.S.B. and T.R. Oke, (1999b): Aerodynamic properties of urban areas derived from analysis of surface form. *Journal of Applied Meteorology*, **38**: 1262-92.

Grimmond, C.S.B and T.R. Oke (1991): An evaporation-interception model for urban areas. *Water Resources Research,* **27**: 1739-1755.

Grimmond, C.S.B. and T.R. Oke, (1986): Urban water balance II: Results from a suburb of Vancouver, BC. *Water Resources Research*, **22**: 1404-1412.

Grimmond, C.S.B., B.D. Offerle, J. Hom, and D. Golub, (2002b): Observations of local-scale heat, water, momentum and CO_2 fluxes at Cub Hill, Baltimore. Preprints of the 4th Symposium on the Urban Environment, American Meteorological Society, pp 117-118.

Grimmond, C.S.B., J.A. Salmond, T.R. Oke, B. Offerle and A. Lemonsu, (2004): Flux and turbulence measurements at a dense urban site in Marseille: heat, mass (water, carbon dioxide) and momentum. *Journal of Geophysical Research - Atmospheres*, **109**: 1 - 19.

Grimmond, C.S.B., T.S. King, F.D. Cropley, D.J. Nowak, and C. Souch, (2002a): Local-scale fluxes of carbon dioxide in urban environments: methodological challenges and results from Chicago. *Environmental Pollution,* **116**: S243-S254.

Greater Vancouver Regional District (GVRD), (2002): 2000 Emissions Inventory for the Lower Fraser Valley Airshed. Policy and Planning Department.

Harvey, L.D.D., (1993): A Guide to global warming potentials (GWPS). *Energy Policy,* **21**: 24-34.

Houghton, R.A., (2002): The science of global warming. *Interdisciplinary Science Reviews,* **26**: 247-257.

Houghton, R.A., (1997): Global warming: the complete briefing. Second edition. Cambridge University Press, Cambridge.

Houghton, R.A., E.A Davidson, and G.M. Woodwell (1998): Missing sinks, feedbacks, and understanding the role of terrestrial ecosystems in the global carbon balance. *Global Biogeochemical Cycles,* **12**: 25-34.

Idso, C.D., S.B. Idso, and R.C. Balling, (2001): An intensive two-week study of an urban CO_2 dome in Phoenix, Arizona, USA. *Atmospheric Environment,* **35**: 995-1000.

Idso, C.D., S.B. Idso, and R.C. Balling, (1998): The urban CO_2 dome of Phoenix, Arizona. *Physical Geography,* **19**: 95-108.

International Panel on Climate Change (IPCC), (1995, 2001): Climate Change 2001. Cambridge University Press.

Joiner, D.W., P.M. Lafleur, J.H. McCaughey, P. Bartlett, (1999): Interannual variability in carbon dioxide exchanges at a boreal wetland in the BOREAS northern study area. *Journal of Geophysical Research,* **104**: 27,663-27,672.

Kaimal, J.C. and J.J. Finnigan, (1994): *Atmospheric boundary layer flows: their structure and measurement.* Oxford University Press.

Kalanda, B.D., (1979): Suburban evaporation estimates in Vancouver. M.Sc. Thesis, University of British Columbia.

Kalanda, B.D., T.R. Oke, D.L. Spittlehouse, (1980): Suburban energy-balance estimates for Vancouver, BC, using the Bowen ratio-energy approach. *Journal of Applied Meteorology,* **19**: 791-802.

Keeling D. and T. Worf, (2005): Atmospheric CO_2 concentrations (ppmv) derived from flask and in situ air samples collected at the South Pole. Scripts Institute of Oceanography, University of California. (http://cdiac. ornl.gov/ftp/trends/CO_2/sposio. CO_2).

Keeling, D. and T. Worf, (2002): Increases in carbon dioxide since the industrial revolution. Scripts Institution of Oceanography, University of California. (http://cdiac.ornl.gov/trends/co2/contents.htm)

Koerner, B. and J. Klopatek, (2002): Anthropogenic and natural CO_2 emission sources in an arid urban environment. *Environmental Pollution,* **116**: S45-S51.

Lafleur, P.M., J.H. McCaughey, D.W. Joiner, P.A. Bartlett, and D.E. Jelinski, (1997): Seasonal trends in energy, water, and carbon dioxide fluxes at a northern boreal wetland. *Journal of Geophysical Research,* **102**: 29,009-29,020.

Leahey, D.M., and M.C. Hansen, (1992): Estimates of dark ecosystem respiration of CO_2 from the city of Calgary, Alberta. *Atmospheric Environment,* **26A**: 1725-1733.

Lee, X., (1998): On micrometeorological observations of surface air exchange over tall vegetation. *Agricultural and Forest Meteorology.* **91**: 39-50.

McFadden, J.P., A.A. Widboom, M.E. Bauer, and F. Yuan, (2004): A tall-tower study of carbon exchange from developed land in the U.S. Upper Midwest. American Geophysical Union Fall Meeting, San Francisco, CA.

Mahrt, L., J.I. MacPherson, R. Desjardins, (1994): Observations of fluxes over heterogeneous surfaces. *Boundary Layer Meteorology*, **67**: 345-367.

Mapquest, (2002): Map of Vancouver. *www.mapquest.com.*

Meyers, T.P., (2001): A comparison of summertime water and CO_2 fluxes over rangeland for well-watered and drought conditions. *Agricultural and Forest Meteorology,* **106**: 205-214.

Moriwaki, R., and M. Kanda, (2004): Seasonal and diurnal fluxes of radiation, heat, water vapor and carbon dioxide over a suburban area. *Journal of Applied Meteorology,* **43**: 1700-1710.

Nadelhoffer, K.J., B.A. Emmett, P. Gundersen, O.J. Kjonaas, C.J. Koopmans, P. Schleppi, A. Tietema, and R.F. Wright, (1999): Nitrogen deposition makes a minor contribution to carbon sequestration in temperate forests. *Nature,* **398**: 145-148.

Nemitz, E., K.J. Hargreaves, A.G. McDonald, J.R. Dorsey, and D. Fowler, (2002): Meteorological measurements of the urban heat budget and CO_2 emissions on a city scale. *Environmental Science and Technology, **36***: 3139-3146.

Newton, T.N., (1999): Energy Balance Fluxes in a Subtropical City: Miami, FL. MSc thesis, UBC, Geography.

NOAA, Climate Monitoring and Diagnostics Laboratory (CMDL), (2005): Carbon cycle greenhouse gases figures: co2rug.jpg. (http://www.cmdl.noaa.gov/about/aboutcmdl .html)

Nowak, D.J., (1993): Atmospheric carbon reduction by urban trees. *Journal of Environmental Management* **37**: 207-217.

Offerle, B.D., (2003): The energy balance of an urban area: examining temporal and spatial variability through measurements, remote sensing and modelling. Ph.D Thesis, Indiana University.

Offerle, B.D., C.S.B. Grimmond, K Fortuniak, T.R. Oke, and K. Klysik, (2003): Temporal variability in heat fluxes over Lodz. Proceeding of the 5th International Conference on Urban Climate, Lodz, Poland.

Oke, T.R., (2004): Initial guidance to obtain representative meteorological observations at urban sites, Instruments and Methods of Observation Programme, *IOM Report* No. **81**, WMO/TD No. 1250, World Meteorological Organization, Geneva, 51 pages.

Oke, T. R., (1988): The urban energy balance, *Progress in Physical Geography*, **12**: 471-508.

Oke, T.R., (1987): Boundary Layer Climates. Routledge, London; New York.

Oke, T.R. and J.E. Hay, (1994): The Climate of Vancouver. Geog Series, No. 50, Department of Geography, University of British Columbia, Vancouver.

Pasquill, (1972): Some aspects of boundary layer description. *Quarterly Journal of the Royal Meteorological Society,* **98**: 469-494.

Phillips, O.L., Y. Malhi, N. Higuchi, W.F. Laurance, P.V. Nunez, R.M. Vasquez, S.G. Laurance, L.V. Ferreira, M. Stern, S. Brown, and J. Grace, (1998): Changes in the carbon balance of tropical forests: Evidence from long-term plots. *Science,* **282**: 439-442.

Poisson, A., (1998): Ocean geochemistry – carbon dioxide uptake at sea. *Nature,* **396**: 521-522.

Province of British Columbia, (1995): Clean vehicles and fuels for British Columbia: A policy paper. Ministry of Environment, Lands and Parks.

Reid, K.H., (1995): Observation and simulation of atmospheric carbon dioxide in Vancouver. M.Sc. Thesis, University of British Columbia.

Reid, K.H. and D.G. Steyn, (1997): Diurnal variations of boundary-layer carbon dioxide in a coastal city – Observations and comparison with model results. *Atmospheric Environment,* **31**: 3101-3114.

Reifsnyder, W.E., (1967): Radiation geometry in the measurement and interpretation of the radiation balance. Computer program for the determination of view factors. *Agricultural Meteorology,* **4**: 255-280.

Rohde, H., (1990): A comparison of the contribution of various gases to the greenhouse effect. *Science,* **248**: 1217-1219.

Rotach, M.W., (2000): The siting, choice and operation of surface instrumentation in urban areas. Mixing Heights and Surface Energy Budgets in Urban Areas. Proc. Cost 715 Meeting, Antwerp.

Rotach M.W., (1993): Turbulence close to a rough urban surface .2. Variances and gradients. *Boundary Layer Meteorology,* **66**: 75-92.

Roth M., (2000): Review of atmospheric turbulence over cities. *Quarterly Journal of the Royal Meteorological Society,* **126**: 941-990.

Roth, M., (1991): Turbulent transfer over a suburban surface. Ph.D. Thesis, University of British Columbia.

Roth, M., (1988): Spectral Analysis of Turbulence in an Unstable Suburban Atmosphere, M.Sc. Thesis, University of British Columbia.

Roth, M. and T.R. Oke, (1995): Relative efficiencies of turbulent transfer of heat, mass and momentum over a patchy urban surface. *Journal of the Atmospheric Sciences,* **52**: 1863-1874.

Salmond, J.A., T.R. Oke, C.S.B Grimmond, S. Roberts, and B.D. Offerle, (2005): Venting of heat and carbon dioxide from urban canyons at night. *Journal of Applied Meteorology,* **44**: 1180-1194.

Sarmiento, J.L. and N. Gruber, (2002): Sinks for anthropogenic carbon. *Physics Today,* **55**: 30-36.

Schimel, D.S., (1998): Climate change – The carbon equation. *Nature,* **393**: 208-209.

Schindler D.W., (1999): Carbon cycling – The mysterious missing sink. *Nature,* **398**: 105-107.

Schmid, H.P., H.B. Su, C.S. Vogel, and P.S. Curtis, (2003): Ecosystem-atmosphere exchange of carbon dioxide over a mixed hardwood forest in northern lower Michigan. *Journal of Geophysical Research-Atmospheres,* **108**: 6-1-6-19.

Schmid, H.P., H.A. Cleugh, C.S.B. Grimmond, and T.R. Oke, (1991): Spatial variability of energy fluxes in suburban terrain. *Boundary Layer Meteorology,* **54**: 249-276.

Schmid, H.P., C.S.B. Grimmond, F. Cropley, B. Offerle, and H.B. Su, (2004): Measurements of CO_2 and energy fluxes over a mixed hardwood forest in the mid-western United States. *Agricultural and Forest Meteorology,* **103**: 357-374.

Soegaard, H., (1999): Fluxes of carbon dioxide, water vapour and sensible heat in a boreal agricultural region of Sweden – scaled from canopy to landscape level. *Agricultural and Forest Meteorology,* **98**: 463-478.

Soegaard, H., and L. Moller-Jensen, (2003): Towards a spatial CO_2 budget of a metropolitan region based on textural image classification and flux measurements. *Remote Sensing of Environment,* **87**: 283-294.

Steele P., P. Krummel, and R. Langenfelds, (2002): Atmospheric CO_2 concentrations derived from flask air at Estevan Point, Canada. Commonwealth Scientific and Industrial Research Organization, Aspendale, Victoria, Australia. (http://gaw.kishou.go.jp/wdcgg.html)

Steyn, D.G., (1985): An objective method to achieve closure of overdetermined surface energy budgets. *Boundary Layer Meteorology,* **33**: 303-311.

Steyn, D.G., (1980): Turbulence, diffusion and the daytime mixed layer depth over a coastal city. Ph.D. Thesis, University of British Columbia.

Steyn, D. G. and T. R. Oke, (1980): Effects of a scrub fire on the surface radiation budget, *Weather*, **35**: 212-215.

Takagi, M., K. Gyokusen, A. Saito, (1998): Increase in the CO_2 exchange rate of leaves of Ilex rotunda with elevated atmospheric CO_2 concentration in an urban canyon. *International Journal of Biometeorology,* **42**: 16-21.

Tanaka, M., T. Nakazawa, and S. Aoki, (1985): Atmospheric carbon dioxide variations in the suburbs of Sendai, Japan. *Tellus,* **37B**: 28-34.

Twine, T.E., W.P. Kustas, J.M. Norman, D.R. Cook, P.R. Houser, T.P. Meyers, J.H. Prueger, P.J. Starks, and M.L. Wesely, (2000): Correcting eddy-covariance flux underestimates over a grassland. *Agricultural and Forest Meteorology,* **103**: 279-300.

Ugursal I.V., and A.S. Fung, (1998): Residential carbon dioxide emissions in Canada – impact of efficiency improvements and fuel substitution. *Global Environmental Change,* **8**: 263-273.

Vogt, R., A. Christen, M.W. Rotach, M. Roth, and A.N.V. Satyanarayana, (2004): Fluxes and Profiles of CO_2 in the Urban Roughness Sublayer, *Theoretical and Applied Climatology,* accepted.

Weil, S., N. Martin, M. Levine, L. Price, and J. Sathaye, (1998): The role of building energy efficiency in managing atmospheric carbon dioxide. *Environmental Science and Policy,* **1**: 27-38.

Wentz, E.A., P. Gober, R.C. Balling, Jr., and T.A. Day, (2002): Spatial patterns and determinants of winter atmospheric carbon dioxide concentrations in an urban environment. *Annals of the Association of American Geographers,* **92**: 15-28.

Wofsy, S.C., M.L. Goulden, J.W. Munger, S.M. Fan, P.S., Bakwin, B.C. Daube, S.L. Bassow, and F.A. Bazzaz, (1993): Net exchange of CO_2 in a mid-latitude forest. *Science,* **260**: 1314-1317.

Woods Hole Research Center (WHRC), (2005): Understanding the global carbon cycle. (http://terra.whrc.org/carbon/index.htm)

World Resources, (1996): The Urban Environment. A combined publication of the World Resources Institute, United Nations Environment Programme, United Nations Develpoment Programme, and the World Bank. Oxford University Press, Oxford: 365 pp.

Yap, D. and T.R. Oke, (1974): Sensible heat fluxes over an urban area – Vancouver, BC. *Journal of Applied Meteorology,* **13**: 880-890.